$$\mathrm{Re}\,\hat{\Pi}^{AA}_{\mathrm{had}}(s)=\frac{\alpha}{3\pi}\,s\,\mathrm{Re}\int\limits_{4m_\pi^2}^{\infty}ds'\,\frac{R^{AA}(s')}{s'(s'-s-i\varepsilon)} \tag{8.7}$$

with

$$R^{AA}(s')=\frac{\sigma(e^+e^-\to\gamma^*\to\text{hadrons})}{\sigma(e^+e^-\to\gamma^*\to\mu^+\mu^-)}. \tag{8.8}$$

$R^{AA}(s')$ can be taken from experiment up to some scale s, for larger s perturbative QCD is used. A recent analysis [41] involving data for the energy range below 40 GeV yields for the contribution of the 5 light quarks in the energy region $50\ \mathrm{GeV}<s<200\ \mathrm{GeV}$

$$\begin{aligned}\mathrm{Re}\,\hat{\Pi}^{AA(5)}_{\mathrm{had}}(s)=&-0.0288\pm0.0009\\&-0.002980\left[\log\left(\frac{s}{(92\ \mathrm{GeV})^2}\right)+0.006307\left(\frac{s}{(92\ \mathrm{GeV})^2}-1\right)\right].\end{aligned} \tag{8.9}$$

For energies around the Z-boson mass this can be approximated by (8.4) using the effective quark masses

$$\begin{aligned}&m_u=0.041\ \mathrm{GeV},\quad m_c=1.5\ \mathrm{GeV},\\&m_d=0.041\ \mathrm{GeV},\quad m_s=0.15\ \mathrm{GeV},\quad m_b=4.5\ \mathrm{GeV}.\end{aligned} \tag{8.10}$$

These quark masses, in particular the ones for the three lightest quarks, are effective parameters adjusted to fit the dispersion integral and have no further significance.

In addition to the above parameters we need the strong coupling constant α_s for the QCD corrections. Its value at the scale of the Z-boson mass is given by [5]

$$\alpha_s=0.115\pm0.010. \tag{8.11}$$

For the numerical evaluation we use in the following

$$\alpha_s=0.12. \tag{8.12}$$

The W-mass is determined from the parameters given above through the relation

$$M_W^2\left(1-\frac{M_W^2}{M_Z^2}\right)=\frac{\pi\alpha}{\sqrt{2}G_F}[1+\Delta r]. \tag{8.13}$$

Δr summarizes the radiative corrections to muon decay [26] apart from the QED corrections which coincide with those of the Fermi model. It depends on all parameters of the SM and is given by

$$\begin{aligned}\Delta r=&\Pi^{AA}(0)-\frac{c_W^2}{s_W^2}\left(\frac{\Sigma_T^{ZZ}(M_Z^2)}{M_Z^2}-\frac{\Sigma_T^{W}(M_W^2)}{M_W^2}\right)+\frac{\Sigma_T^{W}(0)-\Sigma_T^{W}(M_W^2)}{M_W^2}\\&+2\,\frac{c_W}{s_W}\,\frac{\Sigma_T^{AZ}(0)}{M_Z^2}+\frac{\alpha}{4\pi s_W^2}\left(6+\frac{7-4s_W^2}{2s_W^2}\log c_W^2\right).\end{aligned} \tag{8.14}$$

The relation (8.13) can be improved by summing the leading higher order reducible corrections. This is done in the next section (eq. 8.23). For the set of parameters specified above we obtain for the W-boson mass

$$M_W = 80.23 \text{ GeV}. \tag{8.15}$$

8.2. Leading higher order contributions

The natural order of magnitude of one-loop radiative corrections is set by the loop expansion parameter $\frac{\alpha}{\pi} \sim 0.0023$. Consequently typical one-loop corrections are of the order of one percent. There are, however, two important types of radiative corrections which are enhanced by large mass ratios. The first type is associated with light fermions the second with a heavy top quark. These corrections can reach several percent. Consequently the corresponding higher loop corrections may become as big as several permill and thus have to be taken into account in predictions for precision experiments.

8.2.1. Leading logarithms from light fermion masses

The first type of enhanced corrections originates from the renormalization of α at zero momentum transfer where the relevant scale is set by the fermion masses. These are much smaller than the relevant scales in high energy experiments. The large ratio of these different scales leads to large logarithms which can be summarized in the universal quantity

$$\Delta\alpha(s) = -\operatorname{Re}\hat{\Pi}^{AA}(s) = \frac{\alpha}{3\pi}\sum_f N_C^f Q_f^2 \log\frac{|s|}{m_f^2} + \ldots = (\Delta\alpha)_{LL} + \ldots, \tag{8.16}$$

where N_C^f is the colour factor of the fermions and the dots indicate nonleading contributions. Renormalization group arguments can be used to show [42] that the leading logarithms $(\Delta\alpha)_{LL}$ are correctly summed to all orders in perturbation theory by the replacement

$$1 + (\Delta\alpha)_{LL} \to \frac{1}{1-(\Delta\alpha)_{LL}}. \tag{8.17}$$

Since not only the leading logarithms but the whole fermionic contribution to $\Delta\alpha$ are gauge invariant we will sum the latter. The gauge dependent bosonic contribution can not be summed, however, because this would violate gauge invariance in higher orders. Thus we arrive at

$$1 + \Delta\alpha = 1 + (\Delta\alpha)_{\text{ferm}} + (\Delta\alpha)_{\text{bos}} \to \frac{1}{1-(\Delta\alpha)_{\text{ferm}}} + (\Delta\alpha)_{\text{bos}}. \tag{8.18}$$

This corresponds to a resummation of the iterated one-loop fermionic vacuum polarization to all orders.

Since the leading logarithms contained in $\Delta\alpha$ originate from the charge renormalization constant δZ_e they are universal, i.e. they appear everywhere where α appears in lowest

order. They can be taken into account by replacing the lowest order α by a running $\alpha(s)$ defined as

$$\alpha = \alpha(0) \to \alpha(s) = \frac{\alpha}{1 - (\Delta\alpha(s))_{\text{ferm}}} . \tag{8.19}$$

$\Delta\alpha(0) = 0$ due to the on-shell renormalization condition for α. Using $\alpha(s)$ instead of α effectively corresponds to renormalize α not at zero momentum transfer but at momentum transfer s. Then the light fermion masses can be neglected everywhere and no large logarithms appear.

There are similar large logarithms associated with external fermion lines. These are related to collinear singularities, arising from the radiation of photons collinear to external particles. They can be consistently treated with the structure function method [43].

8.2.2. Leading m_t^2 contributions

The second type of important corrections is also connected to the fermionic sector. The top quark gives rise to corrections $\propto m_t^2/M_W^2$, which become large if the top quark mass is large compared to the W-boson mass. For $m_t = 200$ GeV they reach several percent. These terms arise from fermion loop contributions to the boson self energies and from the Yukawa couplings of the physical and unphysical Higgs fields, which show up in vertex and fermionic self energy corrections. The latter are process dependent and are therefore not discussed here. The former, however, are universal, they can be traced back to the renormalization of s_W in the on-shell scheme

$$\begin{aligned} \frac{\delta s_W}{s_W} &= -\frac{1}{2}\frac{c_W^2}{s_W^2}\,\widetilde{\text{Re}}\left(\frac{\Sigma_T^W(M_W^2)}{M_W^2} - \frac{\Sigma_T^{ZZ}(M_Z^2)}{M_Z^2}\right) \\ &= \frac{1}{2}\frac{c_W^2}{s_W^2}\frac{\alpha}{4\pi}\frac{3}{4s_W^2}\frac{m_t^2}{M_W^2} + \ldots = \frac{1}{2}\frac{c_W^2}{s_W^2}\Delta\varrho + \ldots \end{aligned} \tag{8.20}$$

where the dots indicate again nonleading contributions.

There is no general principle that determines the resummation of these corrections. The following recipe has been shown to yield the correct leading terms to $O(\alpha^2)$ [44]

$$\begin{aligned} s_W^2 &\to s_W^2 + c_W^2\Delta\bar{\varrho} = \bar{s}_W^2 , \\ c_W^2 &\to c_W^2(1 - \Delta\bar{\varrho}) = \bar{c}_W^2 , \end{aligned} \tag{8.21}$$

where

$$\Delta\bar{\varrho} = \frac{3G_F m_t^2}{8\sqrt{2}\pi^2}\left[1 + \frac{G_F m_t^2}{8\sqrt{2}\pi^2}(19 - 2\pi^2)\right] \tag{8.22}$$

incorporates the result [45] from two-loop irreducible diagrams. Note that α has been replaced by G_F in order to obtain the correct leading $O(\alpha^2)$ terms.

In particular for the relation between M_W and G_F the correct resummation of the leading corrections is given by

$$G_F = \frac{\pi}{M_W^2 \sqrt{2}} \frac{\alpha}{s_W^2} \frac{1}{1-(\Delta\alpha)_{\text{ferm}}} \frac{1}{1+\frac{c_W^2}{s_W^2}\Delta\bar{\varrho}} \left[1+\Delta r-(\Delta\alpha)_{\text{ferm}}+\frac{c_W^2}{s_W^2}\Delta\varrho\right]. \tag{8.23}$$

Note that the two types of leading corrections are summed separately. Inserting $s_W^2 = 1 - M_W^2/M_Z^2$ this relation can be used to determine the W-boson mass M_W including leading higher order contributions.

Neglecting the nonleading contributions and using (8.19) and (8.21) eq. (8.23) can be written as

$$\frac{\pi\alpha(M_W^2)}{\bar{s}_W^2} \approx \sqrt{2} G_F M_W^2. \tag{8.24}$$

With this relation the appearance of G_F in $\Delta\bar{\varrho}$ can be easily understood. All leading universal corrections arise from the renormalization constants of α and s_W. Consequently they can be absorbed by incorporating the leading finite parts of these renormalization constants into the effective parameters $\alpha(s)$ and $\bar{s}_W^2$ (including the leading higher order corrections). Thus one obtains from the lowest order result directly the corresponding result including the leading universal corrections. In particular (8.24) can be obtained in this way. Applying this recipe to $\Delta\varrho$ and using (8.24) introduces naturally G_F.

8.2.3. Recipes for leading universal corrections

From the discussion above we infer that the universal leading higher order contributions can be taken into account by the following replacements

$$\begin{aligned}
\alpha &\longrightarrow \alpha(s), \\
s_W^2 &\longrightarrow \bar{s}_W^2, \quad c_W^2 \longrightarrow \bar{c}_W^2, \\
\frac{e^2}{2s_W^2} &= \frac{2\pi\alpha}{s_W^2} \longrightarrow \frac{2\pi\alpha(s)}{\bar{s}_W^2} \approx 2\sqrt{2} G_F M_W^2, \\
\frac{e^2}{4s_W^2 c_W^2} &= \frac{\pi\alpha}{s_W^2 c_W^2} \longrightarrow \frac{\pi\alpha(s)}{\bar{s}_W^2 \bar{c}_W^2} \approx \sqrt{2} G_F M_Z^2 \frac{1}{1-\Delta\bar{\varrho}}.
\end{aligned} \tag{8.25}$$

Note that this does not include the nonuniversal corrections $\propto \alpha m_t^2/M_W^2$ arising from enhanced Yukawa couplings. These have to be evaluated for each process directly.

9. The Width of the W-Boson

In the coming years the upgrade of the LEP electron positron storage ring to 180–190 GeV CM-energy will allow to study the properties of the W-boson in detail in a model independent way. Besides its mass M_W also its total and partial decay widths are of interest. While the leptonic partial widths allow to test lepton universality the hadronic partial widths can serve to determine the quark mixing matrix elements [46]. The expected accuracy is $\delta M_W \approx 100$ MeV and $\delta\Gamma_W \approx 200$ MeV [47].

An accurate comparison between these experiments and theoretical predictions of the SM requires at least the inclusion of one-loop radiative corrections both for the production and the decay of W-bosons. The W-bosons decay dominantly into fermion-antifermion pairs. The total and partial widths of the W-boson and the corresponding one-loop radiative corrections are discussed in this chapter.

The electroweak and QCD corrections for decays into massless fermions ($m_f \ll M_W$) have been calculated in [48, 49, 50]. The hard bremsstrahlung contribution has been investigated in [52, 53]. The QCD corrections for the decay into a massive top quark and a massless bottom quark were given in [54]. The full one-loop electroweak and QCD corrections together with the complete photonic and gluonic bremsstrahlung were evaluated for arbitrary finite fermion masses in [55].

Since the top quark is probably heavier than the W-boson and since all other quark masses are small compared to the W-boson mass, the fermion mass effects are not of great importance for the W-decay. However, the matrix element for the W-decay into two fermions is directly related via crossing to the one for the decay of the top quark into a W-boson and a bottom quark. In this case the fermion masses are crucial. Since we will discuss top decay in Chap. 10 we give the results for W-decay for finite fermion masses.

9.1. Lowest order

The Born amplitude for the decay $W^+ \to f_i \bar{f}'_j$ was already given in (6.11). For finite fermion masses the following result is obtained for the corresponding partial decay width

$$\Gamma_0^{W f_i f'_j}(M_W, m_{f,i}, m_{f',j}) = N_C^f \frac{\alpha}{12} \frac{1}{2 s_W^2} |V_{ij}|^2 \frac{\kappa(M_W^2, m_{f,i}^2, m_{f',j}^2)}{M_W^3} G_1^-, \tag{9.1}$$

where κ/M_W^3 originates from phase space and

$$G_1^- = \sum_{\text{pol}} \mathcal{M}_1^{-\dagger} \mathcal{M}_1^- = 2 M_W^2 - m_{f,i}^2 - m_{f',j}^2 - \frac{(m_{f,i}^2 - m_{f',j}^2)^2}{M_W^2} \tag{9.2}$$

from the polarization sum of the matrix element squared. The Källén function κ was defined in (4.28). The colour factor N_C^f is given by

$$N_C^f = \begin{cases} 3 & \text{for quarks,} \\ 1 & \text{for leptons.} \end{cases} \tag{9.3}$$

For leptonic decays we have $V_{ij} = \delta_{ij}$. The total width is obtained as a sum over the partial fermionic decay widths with $m_{f,i} + m_{f',j} < M_W$

$$\Gamma_0^W = \sum_{ij} \Gamma_0^{W u_i d_j} + \sum_i \Gamma_0^{W \nu_i l_i}. \tag{9.4}$$

We can write down another possible tree level representation for the partial decay width by eliminating α/s_W^2 in favour of G_F

$$\bar{\Gamma}_0^{W f_i f'_j}(M_W, m_{f,i}, m_{f',j}) = N_C^f \frac{G_F}{12\pi\sqrt{2}} |V_{ij}|^2 \frac{\kappa(M_W^2, m_{f,i}^2, m_{f',j}^2)}{M_W} G_1^-. \tag{9.5}$$

9.2. Electroweak virtual corrections

In our formulation of the on-shell renormalization scheme the invariant matrix element to one-loop order has the following form

$$\mathcal{M}^{W f_i \bar{f}'_j} = -\frac{e}{\sqrt{2}s_W}\left\{V_{ij}\mathcal{M}_1^-\left[1+\delta Z_e-\frac{\delta s_W}{s_W}\right]+\mathcal{M}_1^-\,\delta V_{ij}\right.$$
$$+V_{ij}\mathcal{M}_1^-\frac{1}{2}\delta Z_W+\mathcal{M}_1^-\frac{1}{2}\sum_k\left[\delta Z_{ik}^{f,L\dagger}V_{kj}+V_{ik}\delta Z_{kj}^{f',L}\right]$$
$$\left.+\sum_{a=1}^{2}\sum_{\sigma=\pm}\mathcal{M}_a^\sigma\,\delta F_a^\sigma(M_W, m_{f,i}, m_{f',j})\right\}. \tag{9.6}$$

The standard matrix elements $\mathcal{M}_a^\sigma$ were defined in (5.11). The functions δF_a^σ summarize the loop corrections to the $Wf_i\bar{f}'_j$-vertex. There are no explicit self energy corrections from the external lines. These are all absorbed into the field renormalization constants δZ_W, $\delta Z^{f,L}$ and $\delta Z^{f',L}$. These and the parameter renormalization constants were given in terms of self energies in Sect. 3.3. The explicit forms of the self energies can be found in App. B.

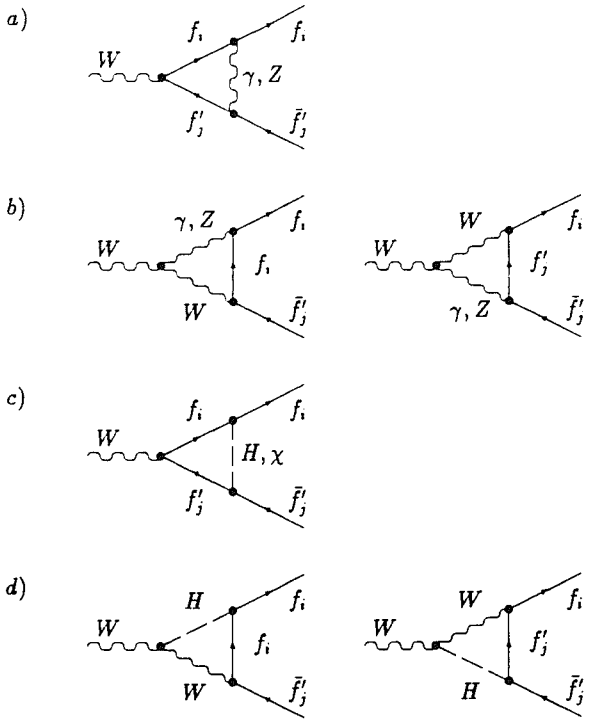

Fig. 9.1. One-loop diagrams for $W \to f_i\bar{f}'_j$

Continuation Figure 9.1.

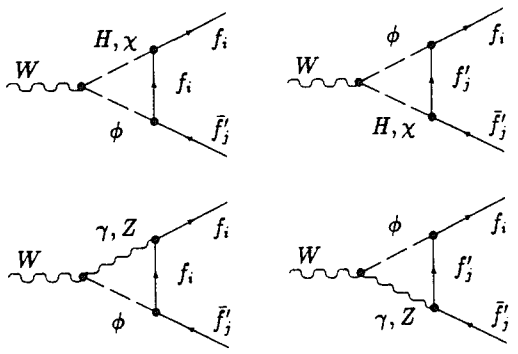

Fig. 9.1. One-loop diagrams for $W \to f_i \bar{f}'_j$

Fig. 9.1 shows the Feynman diagrams contributing to the vertex corrections for massive fermions. They yield the following vertex form factors

$$
\begin{aligned}
\delta F_1^-(M_W, m_1, m_2) = {} & \frac{\alpha}{4\pi} \\
& \times \Bigg\{ Q_f Q_{f'} \mathcal{V}_a(m_1^2, M_W^2, m_2^2, \lambda, m_1, m_2) + g_f^- g_{f'}^- \mathcal{V}_a(m_1^2, M_W^2, m_2^2, M_Z, m_1, m_2) \\
& + \sum_{\sigma=\pm} \Bigg[Q_f \mathcal{V}_b^\sigma(m_1^2, M_W^2, m_2^2, m_1, \lambda, M_W) - Q_{f'} \mathcal{V}_b^\sigma(m_2^2, M_W^2, m_1^2, m_2, \lambda, M_W) \\
& + \frac{c_W}{s_W} g_f^\sigma \mathcal{V}_b^\sigma(m_1^2, M_W^2, m_2^2, m_1, M_Z, M_W) - \frac{c_W}{s_W} g_{f'}^\sigma \mathcal{V}_b^\sigma(m_2^2, M_W^2, m_1^2, m_2, M_Z, M_W) \Bigg] \\
& + \frac{1}{4 s_W^2} \mathcal{V}_c(m_1^2, M_W^2, m_2^2, M_H, m_1, m_2) \\
& + \frac{1}{2 s_W^2} \left[\mathcal{V}_d(m_1^2, M_W^2, m_2^2, m_1, M_H, M_W) + \mathcal{V}_d(m_2^2, M_W^2, m_1^2, m_2, M_H, M_W) \right] \\
& + \frac{1}{2 s_W^2} \left[\mathcal{V}_e(m_1^2, M_W^2, m_2^2, m_1, M_H, M_W) + \mathcal{V}_e(m_2^2, M_W^2, m_1^2, m_2, M_H, M_W) \right. \\
& \left. + \mathcal{V}_e(m_1^2, M_W^2, m_2^2, m_1, M_Z, M_W) + \mathcal{V}_e(m_2^2, M_W^2, m_1^2, m_2, M_Z, M_W) \right] \\
& + \sum_{\sigma=\pm} \Bigg[Q_f \mathcal{V}_f^\sigma(m_1^2, M_W^2, m_2^2, m_1, \lambda, M_W) - Q_{f'} \mathcal{V}_f^\sigma(m_2^2, M_W^2, m_1^2, m_2, \lambda, M_W) \\
& - \frac{s_W}{c_W} g_f^\sigma \mathcal{V}_f^\sigma(m_1^2, M_W^2, m_2^2, m_1, M_Z, M_W) + \frac{s_W}{c_W} g_{f'}^\sigma \mathcal{V}_f^\sigma(m_2^2, M_W^2, m_1^2, m_2, M_Z, M_W) \Bigg] \Bigg\}, \qquad (9.7)
\end{aligned}
$$

$$\delta F_1^+(M_W, m_1, m_2) = \frac{\alpha}{4\pi} m_1, m_2$$

$$\times \Bigg\{ \sum_{\sigma=\pm} \Bigg[Q_f Q_{f'} \mathscr{W}_a^\sigma(m_1^2, M_W^2, m_2^2, \lambda, m_1, m_2) + g_f^\sigma g_{f'}^\sigma \mathscr{W}_a^\sigma(m_1^2, M_W^2, m_2^2, M_Z, m_1, m_2)$$

$$+ Q_f \mathscr{W}_b^\sigma(m_1^2, M_W^2, m_2^2, m_1, \lambda, M_W) - Q_{f'} \mathscr{W}_b^\sigma(m_2^2, M_W^2, m_1^2, m_2, \lambda, M_W)$$

$$+ \frac{c_W}{s_W} g_f^\sigma \mathscr{W}_b^\sigma(m_1^2, M_W^2, m_2^2, m_1, M_Z, M_W) - \frac{c_W}{s_W} g_{f'}^\sigma \mathscr{W}_b^\sigma(m_2^2, M_W^2, m_1^2, m_2, M_Z, M_W) \Bigg]$$

$$+ \frac{1}{4 s_W^2} \Bigg[\sum_{\sigma=\pm} \mathscr{W}_c^\sigma(m_1^2, M_W^2, m_2^2, M_H, m_1, m_2) - \mathscr{W}_c^-(m_1^2, M_W^2, m_2^2, M_Z, m_1, m_2) \Bigg]$$

$$+ \frac{1}{2 s_W^2} \left[\mathscr{W}_d(m_1^2, M_W^2, m_2^2, m_1, M_H, M_W) + \mathscr{W}_d(m_2^2, M_W^2, m_1^2, m_2, M_H, M_W) \right]$$

$$+ \frac{1}{2 s_W^2} \left[\mathscr{W}_e(m_1^2, M_W^2, m_2^2, m_1, M_H, M_W) + \mathscr{W}_e(m_2^2, M_W^2, m_1^2, m_2, M_H, M_W) \right.$$

$$\left. - \mathscr{W}_e(m_1^2, M_W^2, m_2^2, m_1, M_Z, M_W) - \mathscr{W}_e(m_2^2, M_W^2, m_1^2, m_2, M_Z, M_W) \right]$$

$$+ \sum_{\sigma=\pm} \Bigg[Q_f \mathscr{W}_f^\sigma(m_1^2, M_W^2, m_2^2, m_1, \lambda, M_W) - Q_{f'} \mathscr{W}_f^\sigma(m_2^2, M_W^2, m_1^2, m_2, \lambda, M_W)$$

$$- \frac{s_W}{c_W} g_f^\sigma \mathscr{W}_f^\sigma(m_1^2, M_W^2, m_2^2, m_1, M_Z, M_W) + \frac{s_W}{c_W} g_{f'}^\sigma \mathscr{W}_f^\sigma(m_2^2, M_W^2, m_1^2, m_2, M_Z, M_W) \Bigg] \Bigg\}, \quad (9.8)$$

$$\delta F_2^-(M_W, m_1, m_2) = \frac{\alpha}{4\pi} m_1$$

$$\times \Bigg\{ \sum_{\sigma=\pm} \Bigg[Q_f Q_{f'} \mathscr{X}_a^\sigma(m_1^2, M_W^2, m_2^2, \lambda, m_1, m_2) + g_f^\sigma g_{f'}^- \mathscr{X}_a^\sigma(m_1^2, M_W^2, m_2^2, M_Z, m_1, m_2)$$

$$+ Q_f \mathscr{X}_b^\sigma(m_1^2, M_W^2, m_2^2, m_1, \lambda, M_W) + \frac{c_W}{s_W} g_f^\sigma \mathscr{X}_b^\sigma(m_1^2, M_W^2, m_2^2, m_1, M_Z, M_W) \Bigg]$$

$$- Q_{f'} \mathscr{X}_b^-(m_1^2, M_W^2, m_2^2, m_2, M_W, \lambda) - \frac{c_W}{s_W} g_{f'}^- \mathscr{X}_b^-(m_1^2, M_W^2, m_2^2, m_2, M_W, M_Z)$$

$$+ \frac{1}{4 s_W^2} \Bigg[\sum_{\sigma=\pm} \mathscr{X}_c^-(m_1^2, M_W^2, m_2^2, M_H, m_1, m_2) - \mathscr{X}_c^-(m_1^2, M_W^2, m_2^2, M_Z, m_1, m_2) \Bigg]$$

$$+ \frac{1}{2 s_W^2} \mathscr{X}_d(m_1^2, M_W^2, m_2^2, m_1, M_H, M_W) \quad (9.9)$$

Continuation Eq. (9.9)

$$
\begin{aligned}
&-\frac{1}{2s_W^2}\sum_{\sigma=\pm}\Big[\sigma(\mathscr{X}_e^\sigma(m_1^2, M_W^2, m_2^2, m_1, M_H, M_W)-\mathscr{X}_e^\sigma(m_2^2, M_W^2, m_1^2, m_2, M_H, M_W))\\
&-\mathscr{X}_e^\sigma(m_1^2, M_W^2, m_2^2, m_1, M_Z, M_W)-\mathscr{X}_e^\sigma(m_2^2, M_W^2, m_1^2, m_2, M_Z, M_W)\Big]\\
&-\frac{1}{2s_W^2}\frac{m_2^2}{M_W^2}\Big[\mathscr{X}_e^0(m_1^2, M_W^2, m_2^2, m_1, M_H, M_W)-\mathscr{X}_e^0(m_2^2, M_W^2, m_1^2, m_2, M_H, M_W)\\
&-\mathscr{X}_e^0(m_1^2, M_W^2, m_2^2, m_1, M_Z, M_W)-\mathscr{X}_e^0(m_2^2, M_W^2, m_1^2, m_2, M_Z, M_W)\Big]\\
&+Q_f\mathscr{X}_f(m_1^2, M_W^2, m_2^2, m_1, \lambda, M_W)+Q_{f'}\mathscr{X}_f(m_2^2, M_W^2, m_1^2, m_2, \lambda, M_W)\\
&-\frac{s_W}{c_W}\Big[g_f^+\mathscr{X}_f(m_1^2, M_W^2, m_2^2, m_1, M_Z, M_W)+g_{f'}^-\mathscr{X}_f(m_2^2, M_W^2, m_1^2, m_2, M_Z, M_W)\Big]\Big\}. \qquad (9.9)
\end{aligned}
$$

To obtain these results we had to evaluate six generic diagrams labeled by a, b, c, d, e and f in Fig. 9.1. The corresponding invariant functions $\mathscr{V}$, $\mathscr{W}$ and $\mathscr{X}$ are listed in App. C. The formfactor δF_2^+ can be obtained from δF_2^- by the substitutions $m_1 \leftrightarrow m_2$, $Q_f \leftrightarrow -Q_{f'}$, $g_f \leftrightarrow -g_{f'}$.

Squaring the matrix element (9.6), summing over the polarizations of the external particles and multiplying the phase space factor yields the one-loop corrected width

$$
\begin{aligned}
\Gamma_1^{W f_i f_j'} &= N_C^f\frac{\alpha}{12}\frac{1}{2s_W^2}\frac{\kappa(M_W^2, m_{f,i}^2, m_{f',j}^2)}{M_W^3}\\
&\quad\times\left\{|V_{ij}|^2\, G_1^-\left[1+2\delta Z_e-2\frac{\delta s_W}{s_W}+\delta Z_W\right]\right\}\\
&\quad+\frac{1}{2}G_1^-\sum_k\left[(\delta Z_{ik}^{f,L\dagger}+\delta Z_{ik}^{f,L})V_{kj}+V_{ik}(\delta Z_{kj}^{f',L\dagger}+\delta Z_{kj}^{f',L})\right]V_{ij}^\dagger\\
&\quad+2|V_{ij}|^2\sum_{a=1}^{2}\sum_{\sigma=\pm}G_a^\sigma\,\delta F_a^\sigma(M_W, m_{f,i}, m_{f',j})\\
&=\Gamma_0^{W f_i f_j'}(1+\delta_{\text{virt}}^{ew}), \qquad (9.10)
\end{aligned}
$$

where

$$
\begin{aligned}
G_1^+ &= \sum_{\text{pol}}\mathscr{M}_1^{-\dagger}\mathscr{M}_1^+ = 6m_{f,i}m_{f',j},\\
G_2^- &= \sum_{\text{pol}}\mathscr{M}_1^{-\dagger}\mathscr{M}_2^- = -\frac{m_{f,i}}{2}\frac{\kappa^2(M_W^2, m_{f,i}^2, m_{f',j}^2)}{M_W^2},\\
G_2^+ &= \sum_{\text{pol}}\mathscr{M}_1^{-\dagger}\mathscr{M}_2^+ = -\frac{m_{f',j}}{2}\frac{\kappa^2(M_W^2, m_{f,i}^2, m_{f',j}^2)}{M_W^2}, \qquad (9.11)
\end{aligned}
$$

and we have inserted δV_{ij} from (3.23).

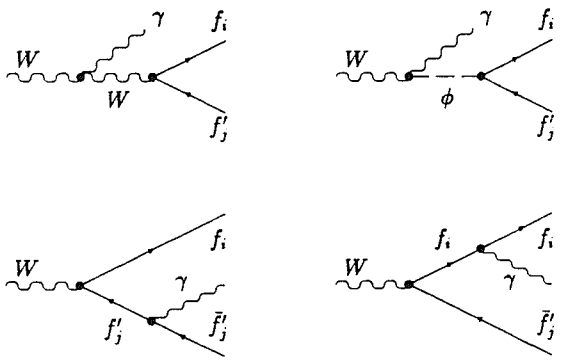

Fig. 9.2. Bremsstrahlung Feynman diagrams for $W \to f_i \bar{f}'_j \gamma$

9.3. Photon bremsstrahlung

Like any one-loop amplitude with external charged particles (9.6) and consequently (9.10) are IR-divergent due to virtual photonic corrections. These singularities are compensated by the the real bremsstrahlung corrections, i.e. the three-body decay

$$W^+(k) \to f_i(p_1)\, \bar{f}'_j(p_2)\gamma(q). \tag{9.12}$$

The corresponding matrix element as given by the Feynman diagrams (Fig. 9.2) is

$$\mathcal{M}_b = V_{ij}\frac{e^2}{\sqrt{2}s_W}\,\bar{u}(p_1)\left\{\frac{-Q_f}{2p_1q}\left[2p_1\eta\not{\varepsilon}+\not{\eta}\not{q}\not{\varepsilon}\right]+\frac{Q_{f'}}{2p_2q}\left[2p_1\eta\not{\varepsilon}+\not{\varepsilon}\not{q}\not{\eta}\right]\right.$$
$$\left.+\frac{(Q_f-Q_{f'})}{-2kq}\left[(q\eta-2k\eta)\not{\varepsilon}+2\varepsilon\eta\not{q}-2q\varepsilon\not{\eta}\right]\right\}\omega_-\, v(p_2), \tag{9.13}$$

where η denotes the polarization vector of the photon. Performing the polarization sum over the square of the amplitude gives

$$\sum_{\text{pol}}|\mathcal{M}_b|^2 = \frac{\alpha^2}{2s_W^2}(64\pi^2)\,|V_{ij}|^2\left\{\frac{Q_fQ_{f'}}{(2p_1q)(2p_2q)}\left[(M_W^2-m_{f,i}^2-m_{f',j}^2)G_1^-\right]\right.$$
$$-\frac{Q_f^2}{(2p_1q)^2}\left[(m_{f,i}^2+2p_1q)G_1^-+\left(1+\frac{m_{f,i}^2+m_{f',j}^2}{2M_W^2}\right)(2p_1q)(-2kq)+(2p_1q)^2\right]$$
$$-\frac{Q_{f'}^2}{(2p_2q)^2}\left[(m_{f',j}^2+2p_2q)G_1^-+\left(1+\frac{m_{f,i}^2+m_{f',j}^2}{2M_W^2}\right)(2p_2q)(-2kq)+(2p_2q)^2\right]$$
$$-\frac{(Q_f-Q_{f'})^2}{(-2kq)^2}\left[(M_W^2-2kq)G_1^-+\frac{m_{f,i}^2+m_{f',j}^2}{2M_W^2}(-2kq)^2-2(2p_1q)(2p_2q)\right]$$
$$-\frac{Q_f(Q_f-Q_{f'})}{-2kq\,2p_1q}\left[(M_W^2+m_{f,i}^2-m_{f',j}^2)G_1^--2(2p_1q)(2p_2q)\right]$$
$$\left.+\frac{Q_{f'}(Q_f-Q_{f'})}{-2kq\,2p_2q}\left[(M_W^2-m_{f,i}^2+m_{f',j}^2)G_1^--2(2p_1q)(2p_2q)\right]\right\}. \tag{9.14}$$

From this the complete bremsstrahlung cross section (including soft and hard photons) is obtained by integrating over the phase space of the photon and the two fermions as

$$\Gamma_b^{Wf_if'_j}(M_W, m_{f,i}, m_{f',j}) = \frac{1}{(2\pi)^5}\frac{N_C^f}{2M_W}\int \frac{d^3q}{2q_0}\frac{d^3p_1}{2p_{10}}\frac{d^3p_2}{2p_{20}}\delta^{(4)}(p_1+p_2+q-k)\frac{1}{3}\sum_{\text{pol}}|\mathscr{M}_b|^2$$
$$= \Gamma_0^{Wf_if'_j}\delta_b^{ew}(M_W, m_{f,i}, m_{f',j}) \tag{9.15}$$

with

$$\begin{aligned}
&\delta_b^{ew}(M_W, m_{f,i}, m_{f',j})\\
&=\left(-\frac{\alpha}{\pi}\right)\frac{4M_W^2}{\kappa(M_W^2, m_{f,i}^2, m_{f',j}^2)}\left\{-Q_fQ_{f'}\left[(M_W^2-m_{f,i}^2-m_{f',j}^2)I_{12}\right]\right.\\
&+Q_f^2\left[(m_{f,i}^2I_{11}+I_1)+\left(1+\frac{m_{f,i}^2+m_{f',j}^2}{2M_W^2}\right)\frac{I_1^0}{G_1^-}+\frac{I}{G_1^-}\right]\\
&+Q_{f'}^2\left[(m_{f',j}^2I_{22}+I_2)+\left(1+\frac{m_{f,i}^2+m_{f',j}^2}{2M_W^2}\right)\frac{I_2^0}{G_1^-}+\frac{I}{G_1^-}\right]\\
&+(Q_f-Q_{f'})^2\left[(M_W^2I_{00}+I_0)+\frac{m_{f,i}^2+m_{f',j}^2}{2M_W^2}\frac{I}{G_1^-}-2\frac{I_{00}^{12}}{G_1^-}\right]\\
&+Q_f(Q_f-Q_{f'})\left[(M_W^2+m_{f,i}^2-m_{f',j}^2)I_{01}-2\frac{I_0^2}{G_1^-}\right]\\
&\left.-Q_{f'}(Q_f-Q_{f'})\left[(M_W^2-m_{f,i}^2+m_{f',j}^2)I_{02}-2\frac{I_0^1}{G_1^-}\right]\right\}.
\end{aligned} \tag{9.16}$$

The bremsstrahlung phase space integrals $I_{\dots}^{\dots} = I_{\dots}^{\dots}(M_W, m_{f,i}, m_{f',j})$ are given in App. D. The IR-singularities contained in the I_{kl} are again regularized by a photon mass λ.

9.4. QCD corrections

Like the electroweak corrections also the QCD corrections consist of virtual and real contributions

$$\delta^{QCD}(M_W, m_{f,i}, m_{f',j}) = \delta_{\text{virt}}^{QCD} + \delta_b^{QCD}, \tag{9.17}$$

which are individually IR-divergent. They are obtained from the electroweak results of the previous sections by keeping only the terms containing Q_f^2, $Q_{f'}^2$ or $Q_fQ_{f'}$, setting $Q_f = Q_{f'} = 1$, replacing α by the strong coupling constant α_s and multiplying an overall colour factor $C_F = \frac{4}{3}$. In particular the virtual QCD-corrections arise only from the diagram of Fig. 9.1a with the photon replaced by a gluon and the corresponding corrections to the fermion wave function renormalization constants. Since this allows many simplifications we give the explicit results

$$\delta_{\text{virt}}^{QCD} = \left(-\frac{\alpha_s}{4\pi}\right) 2 C_F \Big\{ 6 - B_0(M_W^2, m_{f,i}, m_{f',j}) + \frac{1}{2} B_0(0, m_{f,i}, m_{f,i}) + \frac{1}{2} B_0(0, m_{f',j}, m_{f',j}) + 2(M_W^2 - m_{f,i}^2 - m_{f',j}^2)(C_0 + C_1 + C_2) - 2 m_{f,i}^2 C_1 - 2 m_{f',j}^2 C_2 - 2 \log\left(\frac{m_{f,i} m_{f',j}}{\lambda^2}\right) - 2 \frac{G_1^+}{G_1^-} m_{f,i} m_{f',j} [C_1 + C_2] + 4 \frac{G_2^-}{G_1^-} m_{f,i} [C_{11} + C_{12} + C_1] + 4 \frac{G_2^+}{G_1^-} m_{f',j} [C_{22} + C_{12} + C_2] \Big\}. \tag{9.18}$$

The arguments of the three-point functions are $C = C(m_{f,i}^2, M_W^2, m_{f',j}^2, \lambda, m_{f,i}, m_{f',j})$. To the gluonic bremsstrahlung δ_b^{QCD} only the first three terms of (9.16) contribute. For zero fermion masses the total QCD-correction reduces to

$$\delta^{QCD}(M_W, 0, 0) = \frac{\alpha_s}{\pi}. \tag{9.19}$$

9.5. Results and discussion

For numerical evaluation of the previous results we use the parameters listed in Sect. 8.1 including the values for the quark mixing matrix as given by (8.1). The W-mass is determined from the relation (8.23).

In the on-shell scheme the lowest order width is parametrized by α and the particle masses (9.1). In this scheme large electroweak corrections arise due to fermion loop contributions to the renormalization of α and s_W. We can improve the results in this scheme by resumming the corresponding one-loop contributions to all orders as discussed in Sect. 8.2. Thus we obtain for the corrected width

$$\Gamma = \Gamma_0 \left[1 + \delta_1 - (\Delta\alpha)_{\text{ferm}} + \frac{c_W^2}{s_W^2} \Delta\varrho\right] \frac{1}{1 - (\Delta\alpha)_{\text{ferm}}} \frac{1}{1 + \frac{c_W^2}{s_W^2} \Delta\bar{\varrho}} = \Gamma_0 [1 + \delta], \tag{9.20}$$

where

$$\delta_1 = \delta_{\text{virt}}^{ew} + \delta_b^{ew} + \delta_{\text{virt}}^{QCD} + \delta_b^{QCD} \tag{9.21}$$

is the proper one-loop correction without resummation. As in any charged current process we can avoid the large corrections by parametrizing the lowest order decay width with G_F and M_W instead of α and s_W^2 (9.5). Using (8.23) we find the relation between the decay width in both parametrizations

$$\bar{\Gamma}_0 = \Gamma_0 \frac{1}{1 - (\Delta\alpha)_{\text{ferm}}} \frac{1}{1 + \frac{c_W^2}{s_W^2} \Delta\bar{\varrho}} \left[1 + \Delta r - (\Delta\alpha)_{\text{ferm}} + \frac{c_W^2}{s_W^2} \Delta\varrho\right],$$

$$\bar{\Gamma} = \bar{\Gamma}_0 [1 + \delta_1 - \Delta r] = \bar{\Gamma}_0 (1 + \bar{\delta}). \tag{9.22}$$

The large fermionic contributions contained in δ_1 are exactly cancelled by equal contributions in Δr and consequently the remaining corrections $\bar{\delta}$ are small.

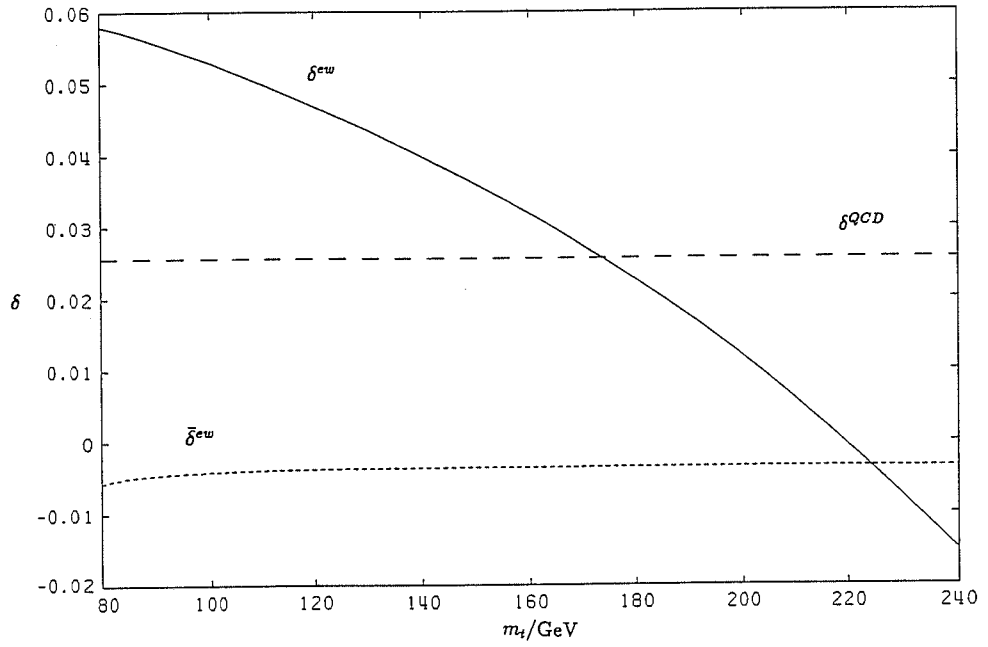

Fig. 9.3. Electroweak radiative corrections δ^{ew} and $\bar{\delta}^{ew}$ and QCD-corrections δ^{QCD} to the total W-width Γ^W versus the top mass

The relative corrections to the total W-boson decay width are shown in Fig. 9.3. They are large and strongly m_t-dependent in the on-shell scheme. This behaviour arises from the fermionic contributions to the renormalization of the weak mixing angle in (9.6) ($\delta s_W^2/s_W^2$) which contain terms $\propto \alpha m_t^2/M_W^2$. In contrast to this in the parametrization with G_F the corrections depend only weakly on m_t and remain below 0.6%. The QCD corrections are practically constant and equal to $2\alpha_s/(3\pi)$, their value for zero fermion masses.

m_t	M_W	Γ_0^W	$\bar{\Gamma}_0^W$	Γ_{ew}^W	$\bar{\Gamma}_{ew}^W$
80.0	79.87	1.8778	2.0056	1.9866	1.9940
100.0	79.99	1.8996	2.0147	2.0002	2.0063
120.0	80.10	1.9211	2.0235	2.0110	2.0158
140.0	80.23	1.9447	2.0330	2.0221	2.0256
160.0	80.37	1.9713	2.0435	2.0340	2.0363
180.0	80.52	2.0018	2.0553	2.0469	2.0481
200.0	80.69	2.0368	2.0684	2.0608	2.0612

Tab. 9.1. W-decay width Γ^W parametrized by α and $\bar{\Gamma}^W$ parametrized by G_F in lowest order and including electroweak corrections. All values are given in GeV.

0,87

Tab. 9.1. shows the lowest order width Γ_0 and the width including electroweak corrections Γ_{ew} in both parametrizations for various values of the top mass. The W-mass obtained from (8.23) is also listed there. While the results for the lowest order width in the two parametrizations differ by several percent, the deviation of the first order expressions is always less than 0.4%.

The analytical results were presented above for finite external fermion masses and with correct renormalization of the quark mixing matrix. However, since the top quark is presumably heavier than the W-boson [57] all relevant actual fermion masses are small compared to the W-boson mass. Therefore in addition to the completely corrected numerical results $\Gamma(M_W, m_{f,i}, m_{f',j})$ for finite fermion masses we also give those for vanishing fermion masses $\Gamma(M_W, 0, 0)$ in Tab. 9.2. The analytical results for vanishing fermion masses were listed in Sect. 6.3. Finally we include an improved Born approximation consisting of the Born widths with zero fermion masses parametrized by G_F and multiplied by the QCD correction factor for zero quark masses

$$\Gamma_{\text{imp}}^{W\nu l} = \frac{G_F M_W^3}{6\sqrt{2}\pi},$$

$$\Gamma_{\text{imp}}^{Wud} = \frac{G_F M_W^3}{2\sqrt{2}\pi} |V_{ij}|^2 \left(1 + \frac{\alpha_s}{\pi}\right),$$

$$\Gamma_{\text{imp}}^{W} = \frac{3 G_F M_W^3}{2\sqrt{2}\pi} \left(1 + \frac{2}{3}\frac{\alpha_s}{\pi}\right), \tag{9.23}$$

for the leptonic partial widths, the hadronic partial widths and for the total width, respectively.

	Born width	complete one-loop	$m_f = 0$ in Γ	improved Born	Branching ratio
$\Gamma(W \to e\nu_e)$	0.2260	0.2252	0.2252	0.2260	0.1084
$\Gamma(W \to \mu\nu_\mu)$	0.2259	0.2252	0.2252	0.2260	0.1084
$\Gamma(W \to \tau\nu_\tau)$	0.2258	0.2250	0.2252	0.2260	0.1083
$\Gamma(W \to \text{lep.})$	0.6777	0.6754	0.6756	0.6778	0.3251
$\Gamma(W \to ud)$	0.6450	0.6672	0.6672	0.6696	0.3211
$\Gamma(W \to us) \times 10$	0.3281	0.3393	0.3393	0.3406	0.0163
$\Gamma(W \to ub) \times 10^4$	0.3306	0.3428	0.3436	0.3448	0.00002
$\Gamma(W \to cd) \times 10$	0.3281	0.3396	0.3396	0.3409	0.0163
$\Gamma(W \to cs)$	0.6432	0.6656	0.6657	0.6682	0.3204
$\Gamma(W \to cb) \times 10^2$	0.1427	0.1480	0.1484	0.1489	0.0007
$\Gamma(W \to \text{had.})$	1.3553	1.4022	1.4023	1.4075	0.6749
$\Gamma(W \to \text{all})$	2.0330	2.0776	2.0779	2.0853	

Tab. 9.2. Partial and total W-decay widths $\bar{\Gamma}$ in different approximations for $m_t = 140$ GeV, $M_H = 100$ GeV and the corresponding W-mass $M_W = 80.23$ GeV.

The numerical values for the partial and total W-widths in these different approximations are given in Tab. 9.2 assuming a top quark mass of 140 GeV and a Higgs boson mass of 100 GeV. The improved Born approximation (9.23) reproduces the exact results up to 0.4% (0.6% for the decays into a b-quark). The effects of the fermion masses are below 0.3%. They are suppressed by m_q^2/s. There are no mass singularities since the width is obtained by integrating over the full phase space of the final state particles [56]. Consequently the exact numerical values of the masses of the external fermions masses are irrelevant[8]). The branching ratios derived from (9.23)

$$\begin{aligned} BR(W \to l\nu) &= \frac{1}{9(1+2\alpha_s/3\pi)}, \\ BR(W \to \text{leptons}) &= \frac{1}{3(1+2\alpha_s/3\pi)}, \\ BR(W \to u_i d_j) &= \frac{|V_{ij}|^2\,(1+\alpha_s/\pi)}{3(1+2\alpha_s/3\pi)}, \\ BR(W \to \text{hadrons}) &= \frac{2(1+\alpha_s/\pi)}{3(1+2\alpha_s/3\pi)} \end{aligned} \tag{9.24}$$

agree numerically within 0.1% with those obtained from the full one loop results. They depend only on α_s and V_{ij}.

The dependence of the W-width on the unknown top and Higgs masses is shown in Tab. 9.3 for Γ^{Wud} and in Tab. 9.4 for $\Gamma^{We\nu}$. A variation of m_t between 80 and 200 GeV affects the partial widths by $\sim 4\%$, a variation of M_H between 50 and 1000 GeV by $\sim 1\%$. This holds as well for the total width as shown in Tab. 9.5. All this is valid for constant α, G_F and M_Z. In this case the top mass dependence is mainly due to the variation of M_W with m_t. Keeping instead M_W, G_F and M_Z fixed the dependence on m_t is

m_t	$M_H = 50$	$M_H = 100$	$M_H = 300$	$M_H = 1000$
80.0	0.2212	0.2209	0.2202	0.2193
100.0	0.2227	0.2224	0.2217	0.2208
120.0	0.2239	0.2236	0.2229	0.2220
140.0	0.2251	0.2248	0.2241	0.2232
160.0	0.2264	0.2261	0.2254	0.2245
180.0	0.2278	0.2276	0.2269	0.2260
200.0	0.2294	0.2291	0.2284	0.2275

Tab. 9.3. Partial W-decay width $\Gamma^{We\nu}$ including first order QCD and electroweak corrections for different values of the top and Higgs masses. All values are given in GeV.

[8]) The values given in Sect. 8.1 are not appropriate for the external quarks. We only use them here to demonstrate the numerical irrelevance of the fermion mass effects.

m_t	$M_H = 50$	$M_H = 100$	$M_H = 300$	$M_H = 1000$
80.0	0.6539	0.6530	0.6509	0.6481
100.0	0.6585	0.6575	0.6554	0.6526
120.0	0.6622	0.6612	0.6591	0.6563
140.0	0.6659	0.6650	0.6629	0.6601
160.0	0.6700	0.6691	0.6670	0.6642
180.0	0.6745	0.6736	0.6715	0.6686
200.0	0.6793	0.6784	0.6763	0.6735

Tab. 9.4. Partial W-decay width Γ^{Wud} including first order QCD and electroweak corrections for different values of the top and Higgs masses. All values are given in GeV.

m_t	$M_H = 50$	$M_H = 100$	$M_H = 300$	$M_H = 1000$
80.0	2.0375	2.0347	2.0283	2.0196
100.0	2.0517	2.0488	2.0423	2.0336
120.0	2.0630	2.0602	2.0537	2.0449
140.0	2.0747	2.0719	2.0654	2.0566
160.0	2.0872	2.0844	2.0780	2.0692
180.0	2.1009	2.0981	2.0917	2.0830
200.0	2.1157	2.1129	2.1066	2.0980

Tab. 9.5. Total W-decay width Γ^W including first order QCD and electroweak corrections for different values of the top and Higgs masses. All values are given in GeV.

considerably smaller. Remember, however, that the prediction for the decay width has the same uncertainty in this parametrization due to the uncertainty of the experimental value for the W-boson mass.

We have compared our results for the partial leptonic width for zero fermion masses to those of JEGERLEHNER [50] and BARDIN et al. [49], who both use the parametrization with G_F. Furthermore Jegerlehner includes two-loop QCD corrections into the boson self energies. If these are switched off the difference between his and our results is less than 0.1 MeV. Performing the same comparison with Bardin et al., our values for the partial widths are 0.7 MeV to 0.8 MeV larger than theirs. Our results for the QCD corrections agree with those obtained by ALVAREZ et al. [54].

10. The Top Width

The present lower limit from CDF data indicates that the top mass is at least 89 GeV [57]. Moreover, LEP data in combination with radiative correction calculations require $m_t = 137 \pm 40$ GeV within the minimal standard model [5, 8] at the 1σ level. Therefore

the top mass lies presumably above the Wb threshold and the dominant decay of the top quark is the one into a W-boson and a bottom quark ($t \to Wb$) and the total width of the top quark can be well described by the partial width $\Gamma^{tWb} = \Gamma(t \to Wb)$.

While the measurement of the top mass will provide a long missing input parameter, the measurement of its width will serve as a consistency check on the standard model. With the operation of LHC, SSC and/or a high energy e^+e^- collider one expects to obtain a sufficiently large number of tops so that both the mass and the width can be measured with good accuracy.

The QCD corrections to the top decay $t \to Wb$ were already evaluated in [58, 59]. The first order electroweak corrections have been calculated by [60, 61].

The electroweak corrections to this decay involve particularly interesting contributions of $O(\alpha m_t^2/M_W^2)$ which are potentially large for large top masses. Those terms arise not only from fermion loop contributions to the boson self energies but also from the Yukawa couplings of the Higgs fields, which show up in vertex and fermionic self energy corrections. As discussed in Sect. 8.2 contributions of the first type can be eliminated if the Born approximation is expressed by G_F and M_W. Surprisingly the effects from strong Yukawa couplings turn out to be small, as will be demonstrated in the following.

We will only consider the decay of free top quarks and sum over the polarizations of the W-bosons. The results are obtained via crossing from the ones for $W \to t\bar{b}$.

10.1. Notation and lowest order decay width

Because we want to use our results for the decay $W^+ \to t\bar{b}$ we consider the decay of an anti-top quark. The corresponding decay width is identical to the one of the top quark because of the CPT theorem.

The lowest order decay of an anti-top quark

$$\bar{t}(p_1) \to W^-(k)\,\bar{b}(p_2) \tag{10.1}$$

is described by the Feynman diagram of Fig. 10.1 yielding the amplitude

$$\mathcal{M}_0 = \frac{-e}{\sqrt{2}s_W} V_{tb}\,\bar{v}(p_1)\not{\omega}_-\,v(p_2). \tag{10.2}$$

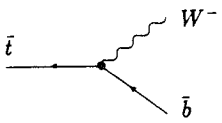

Fig. 10.1. Born diagram for the decay $\bar{t} \to W^-\bar{b}$

It can be obtained from the Born amplitude (6.11) for the decay $W^+ \to t\bar{b}$ by crossing. This amounts to change the signs of p_1 and k and use $u(-p_1) = v(p_1)$ and $\varepsilon(-k) = \varepsilon(k)$. From (10.2) we get the lowest order width

$$\Gamma_0^{tWb}(m_t, M_W, m_b) = \frac{\alpha}{8}\frac{1}{2s_W^2}|V_{tb}|^2\frac{\kappa(m_t^2, M_W^2, m_b^2)}{m_t^3}G_1^-, \tag{10.3}$$

with

$$G_1^- = \left[m_t^2 + m_b^2 - 2M_W^2 + \frac{(m_t^2 - m_b^2)^2}{M_W^2}\right]. \tag{10.4}$$

Eq. (10.3) can directly be derived from (9.1) by substituting $m_i \to m_t$ and $m_j \to m_b$ in G_1^- coming from the matrix element squared, exchanging M_W and m_t in the phase space factors, changing the spin average from 1/3 to 1/2 and supplying a minus sign originating from the different signs of the momenta entering the matrix element squared. This minus sign has been incorporated into the definition of G_1^- which differs from the one in Chap. 9.

Introducing G_F instead of α the lowest order width reads

$$\Gamma_0^{tWb}(m_t, M_W, m_b) = \frac{G_F M_W^2}{8\pi\sqrt{2}} |V_{tb}|^2 \frac{\kappa(m_t^2, M_W^2, m_b^2)}{m_t^3} G_1^- . \tag{10.5}$$

10.2. Virtual corrections

With the four Dirac matrix elements

$$\begin{aligned}
\mathcal{M}_1^- &= \bar{v}(p_1) \not{\varepsilon} \omega_- v(p_2), \\
\mathcal{M}_1^+ &= \bar{v}(p_1) \not{\varepsilon} \omega_+ v(p_2), \\
\mathcal{M}_2^- &= \bar{v}(p_1) \omega_- v(p_2) \varepsilon \cdot p_1, \\
\mathcal{M}_2^+ &= \bar{v}(p_1) \omega_+ v(p_2) \varepsilon \cdot p_1
\end{aligned} \tag{10.6}$$

obtained from (5.11) by setting $p_1 \to -p_1$ the virtual electroweak one-loop corrections take the form of (9.6) with t and b instead of i and j. The corresponding decay width Γ_1^{tWb} follows from (9.10) using the substitutions specified after (10.4).

The QCD corrections can be extracted from the electroweak ones in the same way as in Sect. 9.4.

10.3. Bremsstrahlung

The real photonic contributions of $O(\alpha)$ to the top width arise from the radiative decay

$$\bar{t}(p_1) \to W^-(k)\, \bar{b}(p_2)\, \gamma(q). \tag{10.7}$$

The corresponding amplitude squared, summed over all polarizations, can be derived from (9.14) by replacing the momenta $k \to -k$, $p_1 \to -p_1$ and multiplying an overall factor (-1). From this we get the bremsstrahlung contribution to the top width by integrating over the appropriate phase space

$$\begin{aligned}
\Gamma_0^{tWb}(m_t, M_W, m_b) &= \frac{1}{(2\pi)^5} \frac{1}{2m_t} \int \frac{d^3q}{2q_0} \frac{d^3k}{2k_0} \frac{d^3p_2}{2p_{20}} \delta^{(4)}(p_1 - p_2 - q - k) \frac{1}{2} \sum_{\text{pol}} |\mathcal{M}_b|^2 \\
&= \Gamma_0^{tWb} \delta_b^{ew}(m_t, M_W, m_b).
\end{aligned} \tag{10.8}$$

The correction factor reads

$$\delta_b^{ew}(m_t, M_W, m_b) = \left(-\frac{\alpha}{\pi}\right) \frac{4m_t^2}{\kappa(m_t^2, M_W^2, m_b^2)} \left\{ -Q_t Q_b \left[(M_W^2 - m_t^2 - m_b^2) I_{02} \right] \right.$$
$$+ Q_t^2 \left[(m_t^2 I_{00} + I_0) - \left(1 + \frac{m_t^2 + m_b^2}{2M_W^2}\right) \frac{I_0^1}{G_1^-} - \frac{I}{G_1^-} \right]$$
$$+ Q_b^2 \left[(m_b^2 I_{22} + I_2) - \left(1 + \frac{m_t^2 + m_b^2}{2M_W^2}\right) \frac{I_2^1}{G_1^-} - \frac{I}{G_1^-} \right]$$
$$+ (Q_t - Q_b)^2 \left[(M_W^2 I_{11} + I_1) - \frac{m_t^2 + m_b^2}{2M_W^2} \frac{I}{G_1^-} + 2\frac{I_{11}^{02}}{G_1^-} \right]$$
$$+ Q_t(Q_t - Q_b) \left[(M_W^2 + m_t^2 - m_b^2) I_{01} + 2\frac{I_1^2}{G_1^-} \right]$$
$$\left. - Q_b(Q_t - Q_b) \left[(M_W^2 - m_t^2 + m_b^2) I_{12} + 2\frac{I_1^0}{G_1^-} \right] \right\}. \qquad (10.9)$$

The bremsstrahlung phase space integrals carry the arguments $I^{\cdots} = I^{\cdots}(m_t, M_W, m_b)$. They are given in App. D.

From eq. (10.9) the gluonic bremsstrahlung corrections can be obtained by setting $Q_t = Q_b = 1$, replacing α by the strong coupling constant α_s and multiplying with the colour factor $C_F = \frac{4}{3}$.

10.4. Results and discussion

We again use the parameters listed in Sect. 8.1 as numerical input and calculate the W-mass from the relation (8.23). Unless stated otherwise, we choose for the Higgs mass $M_H = 100$ GeV.

We perform the same summation of the leading higher order corrections as discussed in Sect. 9.5, eq. (9.20), and introduce the parametrization with G_F and M_W as in (9.22). In this parametrization the large corrections arising from the renormalization of α and s_W^2

m_t	M_W	Γ_0^{tWb}	$\bar{\Gamma}_0^{tWb}$	Γ_{ew}^{tWb}	$\bar{\Gamma}_{ew}^{tWb}$
100.0	79.99	0.0887	0.0940	0.0951	0.0951
120.0	80.10	0.3095	0.3260	0.3306	0.3305
140.0	80.23	0.6393	0.6684	0.6788	0.6786
160.0	80.37	1.0850	1.1248	1.1435	1.1433
180.0	80.52	1.6627	1.7071	1.7365	1.7362
200.0	80.69	2.3927	2.4299	2.4724	2.4720
220.0	80.88	3.2989	3.3083	3.3665	3.3661

Tab. 10.1. Top decay width Γ^{tWb} parametrized by α and $\bar{\Gamma}^{tWb}$ by G_F in lowest order and including electroweak corrections. All values are given in GeV.

are absorbed into the lowest order expression. This is not the case for large contributions proportional to $\alpha m_t^2/M_W^2$ arising from vertex and fermion self energy diagrams with enhanced Yukawa couplings.

In Tab. 10.1 we give the lowest order width as well as the width including electroweak corrections in both parametrizations for various values of the top mass together with the W-mass obtained from (8.23). The results for the first order expressions of both parametrizations agree within 0.05%.

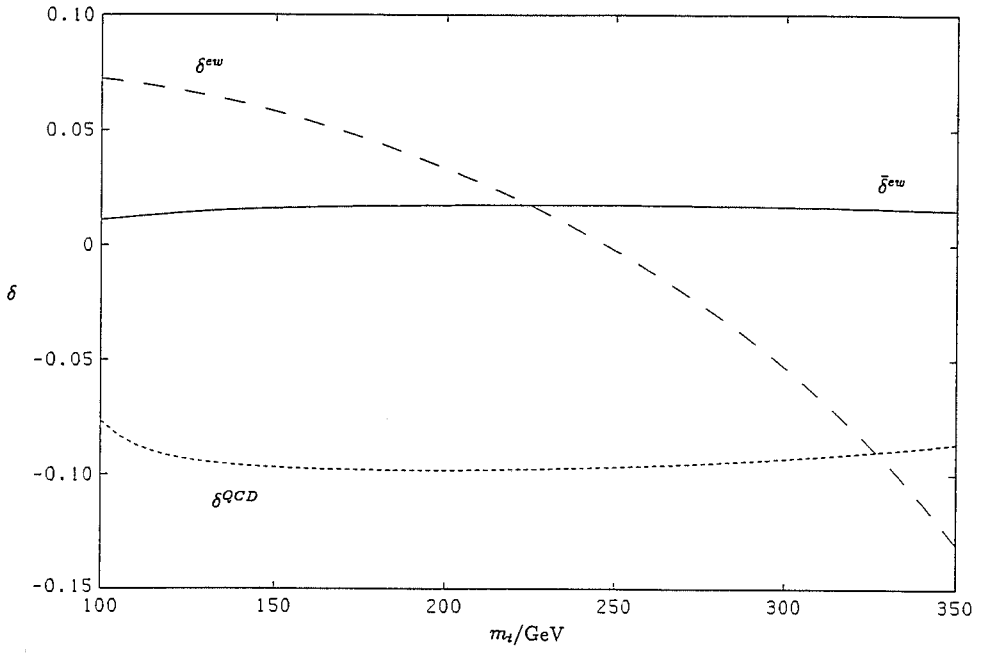

Fig. 10.2. Electroweak radiative corrections δ^{ew} and $\bar{\delta}^{ew}$ and QCD corrections δ^{QCD} to the top decay width versus the top mass.

According to (10.3) the width increases with the top mass approximately like m_t^3/M_W^2. The corresponding relative corrections are shown in Fig. 10.2. The QCD corrections yield about -10% with only a weak dependence on the top mass. In the on-shell scheme we find sizable electroweak corrections which range from $+7\%$ at $m_t = 100$ GeV to -13% at $m_t = 350$ GeV. The large variation arises from terms $\propto \alpha m_t^2/M_W^2$ in the first order corrections. Contrarily in the parametrization with G_F the corrections are only $\approx +1\%$ for $m_t = 100$ GeV and remain almost constant at $\approx +1.7\%$ for $m_t \geqq 160$ GeV. This feature is independent of the Higgs boson mass. However, we expected large corrections $\propto m_t^2$ to arise from the vertex diagrams containing large Yukawa couplings; in the similar case of $Z^0 \to b\bar{b}$ the corresponding contributions are noticeable. The slow variation of the relative correction in this parametrization indicates that the strong Yukawa couplings have no sizable effect on the top width. In order to demonstrate the absence of large corrections the plot in Fig. 10.2 has been extended up to $m_t = 350$ GeV, although this is well above the present upper limits on the top quark mass.

m_t/GeV	200	300	500	1000
leading term	0.023	0.036	0.051	−0.070
next to leading term	−0.043	−0.065	−0.108	−0.217

Tab. 10.2. The two leading terms of the expansion in eq. (10.10) for various values of the top quark mass

Some understanding of this surprising feature can be obtained from the expansion of the relative correction factor in the parametrization with G_F and M_W, $\bar{\delta}^{ew}$, for large top quark masses ($m_t \gg M_W, M_Z, M_H$)

$$\bar{\delta}^{ew} = \delta_1^{ew} - \Delta r \sim \frac{\alpha}{4\pi}\frac{1}{2s_W^2}\frac{m_t^2}{M_W^2}\left\{\left[\frac{17}{4}+\log\left(\frac{M_H^2}{m_t^2}\right)\right]+\left[-\frac{7}{2}\pi\frac{M_H}{m_t}\right]\right.$$
$$\left.+O\left(\log^2\left(\frac{m_t^2}{M_i^2}\right)\right)\right\} \tag{10.10}$$

with $M_i = M_W, M_Z, M_H$. The two leading terms are evaluated in Tab. 10.2 for a wide range of values of the top quark mass and $M_W = 80$ GeV, $M_H = 100$ GeV. For $m_t < 1$ TeV we find the leading term of the expansion to be smaller than the next to leading term. Consequently the expansion is only asymptotic and the contributions $\propto \alpha m_t^2/M_W^2$ are not

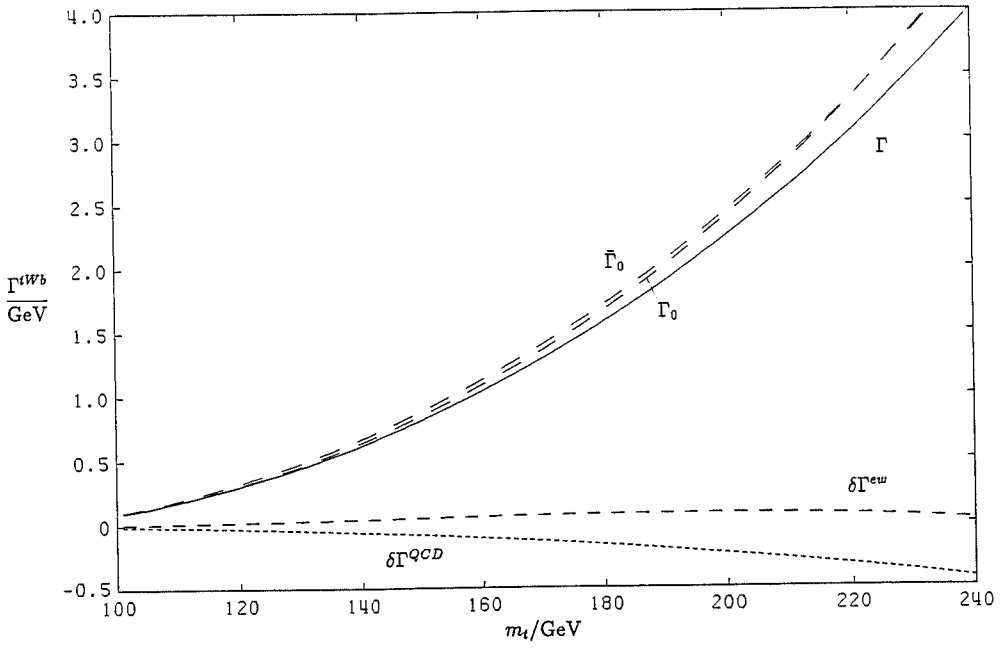

Fig. 10.3. Top decay widht Γ^{tWb} versus the top mass in lowest order Γ_0, $\bar{\Gamma}_0$ including all corrections Γ and the contribution of the electroweak $\delta\Gamma_{ew}$ and QCD corrections $\delta\Gamma_{QCD}$.

dominant unless the top mass has a value of several TeV. In the physically acceptable range of top quark masses, the quadratic terms are numerically compensated by logarithmic contributions. This remains true also for large Higgs masses. The small corrections result from intricate cancellations between leading and nonleading terms.

In Fig. 10.3 we show the lowest order width in both parametrizations Γ_0, $\bar{\Gamma}_0$, the electroweak corrections $\delta\Gamma_{ew}$, the QCD corrections $\delta\Gamma_{QCD}$ as well as the fully corrected width Γ as a function of the top quark mass.

m_t	$M_H = 50$	$M_H = 100$	$M_H = 300$	$M_H = 1000$
100.0	0.0882	0.0883	0.0886	0.0891
120.0	0.3022	0.3021	0.3020	0.3022
140.0	0.6179	0.6174	0.6165	0.6157
160.0	1.0385	1.0377	1.0356	1.0329
180.0	1.5742	1.5734	1.5697	1.5641
200.0	2.2373	2.2376	2.2321	2.2221
220.0	3.0411	3.0438	3.0369	3.0207

Tab. 10.3. Top decay width Γ^{tWb} including first order QCD and electroweak corrections for different values of the Higgs mass. All values are given in GeV.

The dependence of the total width on the Higgs mass is displayed in Tab. 10.3 where this parameter is varied from 50 to 1000 GeV. Although the influence of M_H becomes stronger for large top masses it never exceeds 1%.

We have compared the pure QCD corrections to those obtained in [58] and found complete agreement. Our results for the electroweak corrections agree with those of [61].

11. *W*-Pair Production

One of the predominant aims of LEP200 is the high precision investigation of the properties of the *W*-boson, i.e. its mass, its total and partial widths and its couplings. Probably the most interesting aspect will be the study of the nonabelian gauge interaction which has no direct experimental evidence so far.

The general properties of *W*-pair production at LEP200 have been studied in [62, 63]. While the total cross section of $e^+e^- \to W^+W^-$ is extremely sensitive to deviations from the triple gauge boson couplings of the SM at energies high above the production threshold, the sensitivity to variations of this coupling in the LEP200 energy range is only at the percent level. Consequently theoretical predictions should be better than 1% to obtain reasonable limits on the structure of the gauge boson self interaction.

The *W*-pair production process allows an independent direct measurement of the *W*-boson mass with an expected accuracy of about 100 MeV [47]. Again this requires the knowledge of the total cross section with a precision better than 1%.

Much effort has been made in recent years to obtain such precise theoretical predictions for *W*-pair production. The virtual electroweak and soft photonic corrections were calculated by several authors [64, 65, 66, 67]. The complete analytical results for arbitrary polarizations of the external particles were published in [66]. These will be used for our

evaluations. For the unpolarized case they numerically agree with those of [67] better than 0.3% and essentially also with [64]. The hard photon bremsstrahlung corrections have been evaluated by [68, 14, 69, 70] for definite initial and final state polarizations. The effects arising from the finite width of the W-bosons have been studied in the Born approximation in [71] and including the leading weak corrections in [72]. Recently also the hard bremsstrahlung to the process $e^+e^- \to W^+W^- \to 4$ fermions has been evaluated [73].

In the following we will review and update existing results for the virtual and real electroweak corrections and the finite width effects. We will add some new results on approximate formulae for the W-pair production cross section.

11.1. Notation and amplitudes

We discuss the process

$$e^+(p_1, \sigma_1) + e^-(p_2, \sigma_2) \to W^+(k_1, \lambda_1) + W^-(k_2, \lambda_2). \tag{11.1}$$

The arguments indicate the momenta and helicities of the incoming fermions and outgoing bosons ($\sigma_i = \pm\frac{1}{2}$, $\lambda_i = 1, 0, -1$). We introduce the usual Mandelstam variables

$$\begin{aligned} s &= (p_1 + p_2)^2 = (k_1 + k_2)^2 = 4E^2, \\ t &= (p_1 - k_1)^2 = (p_2 - k_2)^2 = M_W^2 - 2E^2 + 2E^2\beta\cos\vartheta. \end{aligned} \tag{11.2}$$

Here E is the beam energy, ϑ the scattering angle between the e^- and the W^- and $\beta = \sqrt{1 - M_W^2/E^2}$ the velocity of the W-bosons in the center of mass frame. The electron mass has been consistently neglected.

In the approximation of zero electron mass the invariant matrix element vanishes due to chiral symmetry for equal helicities of the e^+ and e^-. Consequently we can write

$$\mathcal{M}(\sigma_1, \sigma_2, \lambda_1, \lambda_2, s, t) = \mathcal{M}(\sigma, \lambda_1, \lambda_2, s, t) \tag{11.3}$$

with $\sigma = \sigma_2 = -\sigma_1$. If we neglect the CP-violating phase in the quark mixing matrix, CP is a symmetry of the process leading to the relation

$$\mathcal{M}(\sigma, \lambda_1, \lambda_2, s, t) = \mathcal{M}(\sigma, -\lambda_2, -\lambda_1, s, t). \tag{11.4}$$

Consequently there are only 12 independent helicity matrix elements instead of 36.

As discussed in Chap. 5 the general matrix element

$$\mathcal{M}(\sigma, \lambda_1, \lambda_2, s, t) = \bar{v}(p_1, -\sigma)\,\mathcal{M}^{\mu\nu}\,u(p_2, \sigma)\,\varepsilon_\mu(k_1, \lambda_1)\,\varepsilon_\nu(k_2, \lambda_2) \tag{11.5}$$

can be decomposed into formfactors and standard matrix elements. Due to the above-mentioned symmetries we do not need all of the (overcomplete) 40 standard matrix elements given in (5.14) for a general process of vector pair production in fermion-antifermion annihilation, but only seven for each fermion helicity

$$\mathcal{M}(\sigma, \lambda_1, \lambda_2, s, t) = \sum_{i=1}^{7} \mathcal{M}_i^\sigma F_i^\sigma(s, t). \tag{11.6}$$

The standard matrix elements $\mathcal{M}_i^\sigma$ are defined in (5.14) together with

$$\begin{aligned}\mathcal{M}_3^\sigma &= \mathcal{M}_{3,1}^\sigma + \mathcal{M}_{3,2}^\sigma,\\ \mathcal{M}_4^\sigma &= \mathcal{M}_{4,1}^\sigma + \mathcal{M}_{4,2}^\sigma,\\ \mathcal{M}_7^\sigma &= \mathcal{M}_{7,1}^\sigma + \mathcal{M}_{7,2}^\sigma.\end{aligned} \tag{11.7}$$

Only six are linear independent. Using (5.15) we can express $\mathcal{M}_7$ by the others

$$\mathcal{M}_7^\sigma = -\frac{s}{2}(\mathcal{M}_1^\sigma + \mathcal{M}_2^\sigma) + \frac{M_W^2 - t}{2}\mathcal{M}_3^\sigma + \frac{s}{2}\mathcal{M}_4^\sigma + \mathcal{M}_5^\sigma. \tag{11.8}$$

Therefore there are only twelve independent formfactors. The standard matrix elements can be calculated with the methods described in Sect. 5.3. The explicit results can be found in [66, 74].

11.2. Born cross section

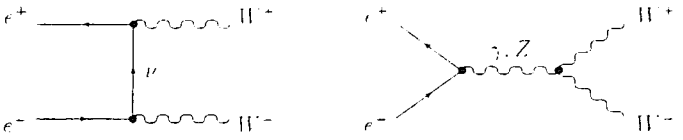

Fig. 11.1. Born diagrams for $e^+e^- \to W^+W^-$

At the Born level three diagrams contribute to W-pair production (Fig. 11.1). We omitted a Higgs-exchange diagram, which is suppressed by a factor m_e/M_W and thus completely negligible. The t-channel ν_e-exchange diagram contributes only for left-handed electrons whereas the s-channel diagrams containing the nonabelian gauge coupling contribute also for right handed electrons. The analytical expressions read

$$\begin{aligned}\mathcal{M}_0(-,\lambda_1,\lambda_2,s,t) &= \mathcal{M}_1^- \frac{e^2}{2s_W^2}\frac{1}{t} + 2(\mathcal{M}_3^- - \mathcal{M}_2^-)\, e^2\left[\frac{1}{s} - \frac{c_W}{s_W} g_e^- \frac{1}{s-M_Z^2}\right]\\ &= \frac{e^2}{2s_W^2}\left[\frac{1}{s}\mathcal{M}_1^- + \frac{2}{s-M_Z^2}(\mathcal{M}_3^- - \mathcal{M}_2^-)\right]\\ &\quad + e^2\left[\frac{1}{s} - \frac{1}{s-M_Z^2}\right]2(\mathcal{M}_3^- - \mathcal{M}_2^-),\\ \mathcal{M}_0(+,\lambda_1,\lambda_2,s,t) &= 2(\mathcal{M}_3^+ - \mathcal{M}_2^+)\, e^2\left[\frac{1}{s} - \frac{c_W}{s_W} g_e^+ \frac{1}{s-M_Z^2}\right]\\ &= e^2\left[\frac{1}{s} - \frac{1}{s-M_Z^2}\right]2(\mathcal{M}_3^+ - \mathcal{M}_2^+),\end{aligned} \tag{11.9}$$

where we have inserted the explicit form of the Z-boson fermion couplings g_e^-, g_e^+ (A.14). The corresponding cross section for arbitrary longitudinal polarizations of the leptons and bosons is given by

$$\left(\frac{d\sigma}{d\Omega}\right)_0 = \frac{\beta}{64\pi^2 s} \sum_{\lambda_1,\lambda_2} \frac{1}{4} (1-2\sigma P^+)(1+2\sigma P^-) |\mathcal{M}_0(\sigma, \lambda_1, \lambda_2, s, t)|^2, \tag{11.10}$$

and $P^\pm$ are the polarization degrees of the leptons ($P^- = \pm 1$ corresponds to purely right- and left-handed electrons, respectively).

The Born cross section determines the main features of W-pair production. We first study the threshold behaviour [75, 76]. For small β the matrix elements behave as

$$\mathcal{M}_2^\sigma, \mathcal{M}_3^\sigma \propto \beta, \qquad \mathcal{M}_1^\sigma \propto 1. \tag{11.11}$$

Consequently the s-channel diagrams vanish at threshold and the t-channel graph dominates in the threshold region. For $\beta \ll 1$ the total cross section is given by

$$\sigma_0(s) \approx \frac{\pi\alpha^2}{s} \frac{1}{4s_W^4} 4\beta + O(\beta^3). \tag{11.12}$$

All terms $\propto \beta^2$ which are present in the differential cross section drop out in the total cross section. s-channel diagrams yield contributions $\propto \beta^3$. In the SM the coefficient of the β^3 term in (11.12) is roughly equal to the one of the leading β term. As long as that coefficient is not enhanced drastically the β^3 term is negligible in the threshold region, i.e. for $2M_W < \sqrt{s} < 2M_W + 10$ GeV (for $\sqrt{s} = 2M_W^2 + 10$ GeV we have $\beta = 0.33$ and $\beta^3 = 0.04$). Consequently the shape of the total cross section close to threshold is completely governed by the linear rise in β and hence by kinematics alone. Any change in the couplings will only affect the coefficient of the β term and thus the normalization of the cross section. Moreover many new physics effects such as anomalous gauge couplings contribute to the s-channel only and thus do not affect the leading term. The inclusion of the finite width of the W-boson smears the threshold considerably (see Sect. 11.5). However, since the next to leading β^3 term becomes only sizable several Γ^W above threshold only the leading term is relevant for the cross section in the region of the nominal threshold.

This fact allows a model independent determination of the W-mass from the W-pair production threshold [75]. The measured cross section up to about 10 GeV above threshold is fitted with a three-parameter curve

$$\sigma(s) = \frac{a}{s} + b\,\sigma_{SM}(M_W, s) \tag{11.13}$$

where a/s accounts for the background, b is a model dependent normalization factor and σ_{SM} the W-pair production cross section in the SM depending on the W-mass. Eq. (11.13) is valid including radiative corrections and finite width effects.

At high energies the W-pair production cross section is subject to large gauge cancellations arising from the contributions of longitudinally polarized W-bosons. For $s \gg M_W^2$ the matrix elements behave as

$$\frac{\mathcal{M}_1^\sigma}{t}, \frac{\mathcal{M}_{2,3}^\sigma}{s} \sim \frac{s}{M_W^2}, \tag{11.14}$$

but

$$\frac{1}{t}\mathcal{M}_1^\sigma + \frac{1}{s-M_Z^2} 2(\mathcal{M}_3^\sigma - \mathcal{M}_2^\sigma) \sim \frac{M_W^2}{t} + O(1),$$

$$\left(\frac{1}{s} - \frac{1}{s-M_Z^2}\right) 2(\mathcal{M}_3^\sigma - \mathcal{M}_2^\sigma) \sim O(1). \tag{11.15}$$

Consequently the Born matrix elements (11.9) have a good high energy behaviour. While the cross sections corresponding to the s-channel or t-channel diagrams alone violate unitarity at high energies

$$\sigma_{0,t}(s) \approx \sigma_{0,s}(s) \approx \frac{\pi\alpha^2}{s} \frac{1}{4s_W^4} \frac{s^2}{24M_W^4}, \tag{11.16}$$

the SM cross section respects it

$$\sigma_0 \approx \frac{\pi\alpha^2}{s} \frac{1}{4s_W^4} \left[2\left(\log\frac{s}{M_W^2} - 1\right) - \frac{1}{2} - \frac{1}{3c_W^2} + \frac{5}{24c_W^4}\right]. \tag{11.17}$$

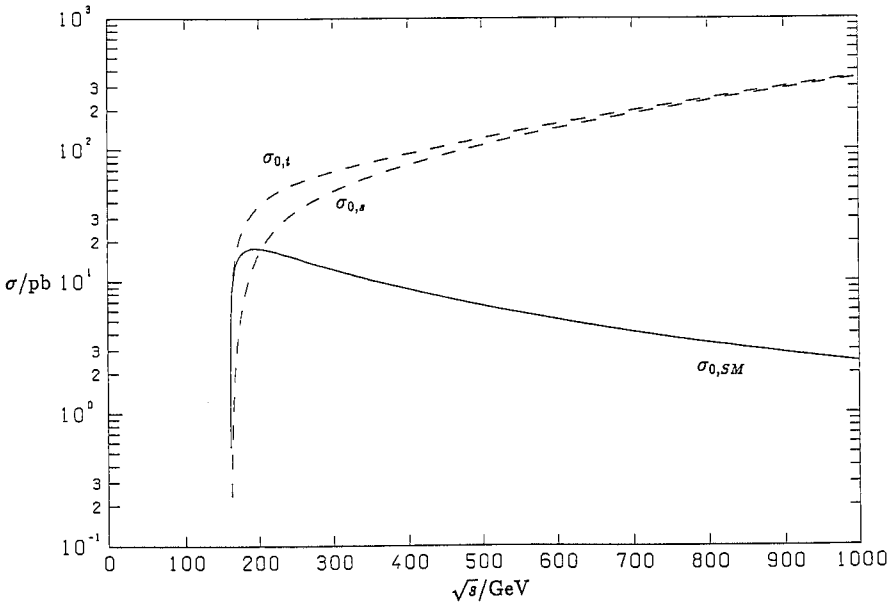

Fig. 11.2. Gauge cancellations in the total cross section for W-pair production. Shown are the Born cross sections arising from the s-channel $\sigma_{0,s}$ and t-channel $\sigma_{0,t}$ diagrams alone and the SM cross section σ_0.

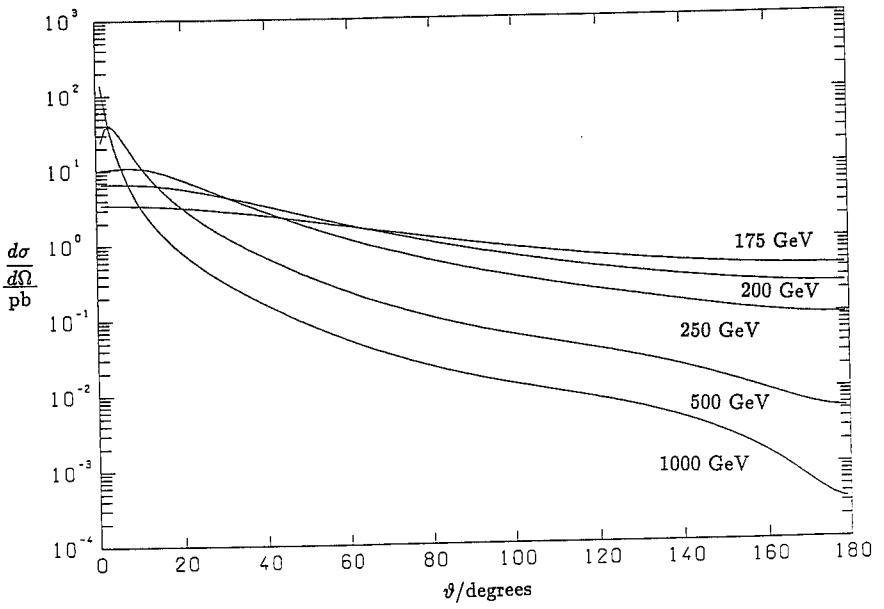

Fig. 11.3. Lowest order differential cross section for the production of unpolarized W-pairs at different center of mass energies

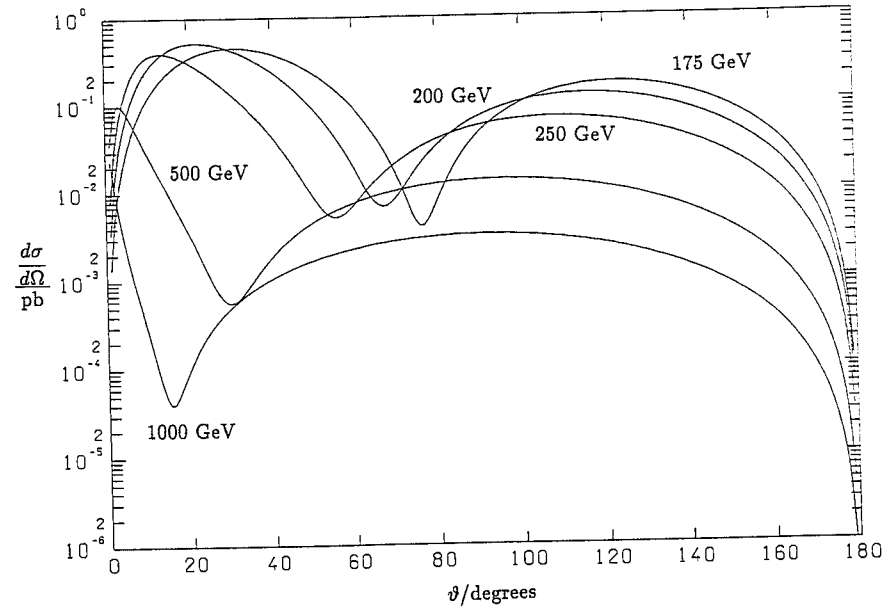

Fig. 11.4. Lowest order differential cross section for the production of longitudinal W-pairs at different center of mass energies

The gauge cancellations are illustrated in Fig. 11.2. They reach one order of magnitude at 400 GeV and two orders at 1 TeV. They only occur for longitudinal W-bosons. After the gauge cancellations the t-channel again dominates the SM cross section. Compared to the t-channel contribution all other contributions to the total cross section are suppressed by $\sim 50 \log(s/M_W^2)$. For example the cross section for right handed electrons is

$$\sigma_0(e_R^- e^+ \to W^+ W^-) \approx \frac{\pi \alpha^2}{s} \frac{1}{12 c_W^4}, \tag{11.18}$$

and the cross section for longitudinal W-bosons

$$\sigma_0(e^- e^+ \to W_L^+ W_L^-) \approx \frac{\pi \alpha^2}{s} \frac{1}{24 c_W^4} \left(\frac{1}{4 s_W^4} + 1 \right). \tag{11.19}$$

We now consider the complete Born expressions for the W-pair production cross section. The differential cross section for the unpolarized case and for longitudinal polarized W-bosons is shown in Fig. 11.3 and 11.4, respectively. Due to the t-channel pole the unpolarized cross section is strongly peaked in forward direction at high energies and drops smoothly with increasing scattering angle. In contrast the differential cross section for longitudinal W-bosons has a minimum for a certain energy dependent finite scattering angle $\neq \pi$.

	σ_0/pb					
$\sqrt{s}$ GeV	unpolarized	e_L^-	e_R^-	$W_T^- W_T^-$	$W_L^+ W_L^-$	$W_T^- W_L^- + W_L^- W_T^-$
165.0	10.761	21.466	0.056	5.254	1.349	4.158
180.0	16.928	33.600	0.256	9.397	1.743	5.788
200.0	17.709	35.070	0.348	11.189	1.428	5.092
250.0	15.011	29.745	0.277	11.487	0.731	2.793
500.0	6.534	13.019	0.050	6.178	0.113	0.244
1000.0	2.439	4.867	0.010	2.395	0.027	0.017

Tab. 11.1. Integrated lowest order cross section for different polarizations and different center of mass energies and $M_W = 80.23$ GeV

In order to show the importance of the separate contributions we give in Tab. 11.1 the integrated cross section for different center of mass energies and different polarizations of the leptons and W-bosons.

The gauge cancellations depend crucially on the values of the SM couplings. Any deviations from these values can lead to sizable effects at higher energies since they are enhanced by a factor $\beta s/M_W^2$. This fact concerns especially anomalous three gauge boson couplings which have been studied by many authors [77]. The sensitivity to these effects is best at high energies and large scattering angles where the t-channel pole is not dominant. Nevertheless one hopes to determine the anomalous couplings up to 20% at LEP200 [6].

Using right-handed electrons one could study a pure triple gauge coupling process, but this would require longitudinally polarized electron beams. Furthermore the right-handed cross section is suppressed by two orders of magnitude compared to the dominant left-handed mode, mainly because there is no t-channel contribution. On the other hand, nonstandard couplings or other new physics can enhance it drastically exactly for this reason.

11.3. Virtual and soft photonic corrections

The radiative corrections can be naturally divided into three classes, the virtual corrections, the soft photonic, and the hard photonic corrections. Since the process $e^+e^- \to W^+W^-$ involves the charged current, the radiative corrections cannot be separated into electromagnetic and weak ones in a gauge invariant way. We first discuss the virtual and soft photonic corrections.

11.3.1. Virtual corrections

The virtual corrections get contributions from the ν_e-, γ- and Z-self energies, the γ-Z-mixing energy, from the vertex corrections to the $ee\gamma$-, eeZ-, $e\nu_e W$-, $WW\gamma$- and WWZ-vertices and from box diagrams. The necessary counterterms involve in addition the e- and W-self energies. Altogether one has to calculate more than 200 individual diagrams. These can be treated using the methods described in the first part of this review. The number of generic diagrams to be evaluated is about 30. The results can be expressed in terms of the formfactors defined in (11.6)

$$\delta\mathcal{M}_1(\sigma, \lambda_1, \lambda_2, s, t) = \sum_{i=1}^{7} \mathcal{M}_i^{\sigma}\, \delta F_i^{\sigma}. \tag{11.20}$$

The formfactors δF_i^{σ} can be evaluated for every CP-invariant set of diagrams separately. For CP-violating diagrams we need in addition the standard matrix elements $\mathcal{M}_{3,1}^{\sigma} - \mathcal{M}_{3,2}^{\sigma}$, $\mathcal{M}_{4,1}^{\sigma} - \mathcal{M}_{4,2}^{\sigma}$ and $\mathcal{M}_{7,1}^{\sigma} - \mathcal{M}_{7,2}^{\sigma}$. These drop out in CP-invariant combinations. The explicit analytical results for the formfactors are given in terms of the scalar coefficients of tensor integrals in [66, 74]. The reduction to scalar integrals and their evaluation is done numerically using the formulae given in Chap. 4. The contribution of the virtual corrections to the cross section is given by

$$\delta\left(\frac{d\sigma}{d\Omega}\right)_V = \frac{\beta}{64\pi^2 s} \sum_{\lambda_1,\lambda_2} \frac{1}{4} (1-2\sigma P^+)(1+2\sigma P^-)\, 2\,\mathrm{Re}(\mathcal{M}_0^{*}\, \delta\mathcal{M}_1). \tag{11.21}$$

The cancellations already present at the Born level occur as well at the level of radiative corrections. These cancellations only work for gauge invariant quantities. Consequently the inclusion of the leading higher order contributions must be done such that gauge invariance is respected. Otherwise one may introduce sizable unphysical corrections. This will be discussed in more detail in Sect. 11.3.3

The presence of these cancellations enforces very careful tests of the numerical stability of the computer programs. The reliability of the results is founded on agreement between independent calculations [66, 67].

11.3.2. Soft photonic corrections

The soft photonic corrections can be easily obtained using the results of Chap. 7. The soft photon matrix element reads (k is the photon momentum)

$$\mathcal{M}_s = e\mathcal{M}_0 \left[\frac{\varepsilon p_2}{k p_2} - \frac{\varepsilon p_1}{k p_1} + \frac{\varepsilon k_1}{k k_1} - \frac{\varepsilon k_2}{k k_2} \right]. \tag{11.22}$$

This yields the soft photon cross section as

$$\left(\frac{d\sigma}{d\Omega}\right)_s = \left(\frac{d\sigma}{d\Omega}\right)_0 \delta_s \tag{11.23}$$

with

$$\begin{aligned}
\delta_s = & -\frac{\alpha}{2\pi^2} \int_{|\mathbf{k}|<\Delta E} \frac{d^3k}{2\omega_k} \left\{ \frac{p_1^2}{(p_1 k)^2} + \frac{p_2^2}{(p_2 k)^2} - \frac{2 p_1 p_2}{(p_1 k)(p_2 k)} \right. \\
& + \frac{k_1^2}{(k_1 k)^2} + \frac{k_2^2}{(k_2 k)^2} - \frac{2 k_1 k_2}{(k_1 k)(k_2 k)} \\
& \left. - \frac{2 p_1 k_1}{(p_1 k)(k_1 k)} - \frac{2 p_2 k_2}{(p_2 k)(k_2 k)} + \frac{2 p_1 k_2}{(p_1 k)(k_2 k)} + \frac{2 p_2 k_1}{(p_2 k)(k_1 k)} \right\} \\
= & -\frac{\alpha}{\pi} \left\{ 4 \log \frac{2\Delta E}{\lambda} - 2 \log \frac{2\Delta E}{\lambda} \log \frac{s}{m_e^2} + 4 \log \frac{2\Delta E}{\lambda} \log \frac{M_W^2 - u}{M_W^2 - t} \right. \\
& + \frac{1+\beta^2}{\beta} \log \frac{2\Delta E}{\lambda} \log \left(\frac{1-\beta}{1+\beta} \right) \\
& + \log \frac{m_e^2}{s} + \frac{1}{\beta} \log \left(\frac{1-\beta}{1+\beta} \right) + \frac{\pi^2}{3} + \frac{1}{2} \log^2 \frac{m_e^2}{s} \\
& + \frac{1+\beta^2}{\beta} \left[\mathrm{Li}_2 \left(\frac{2\beta}{1+\beta} \right) + \frac{1}{4} \log^2 \left(\frac{1-\beta}{1+\beta} \right) \right] \\
& + 2 \left[\mathrm{Li}_2 \left(1 - \frac{s(1-\beta)}{2(M_W^2 - t)} \right) + \mathrm{Li}_2 \left(1 - \frac{s(1+\beta)}{2(M_W^2 - t)} \right) \right. \\
& \left. \left. - \mathrm{Li}_2 \left(1 - \frac{s(1-\beta)}{2(M_W^2 - u)} \right) - \mathrm{Li}_2 \left(1 - \frac{s(1+\beta)}{2(M_W^2 - u)} \right) \right] \right\}.
\end{aligned} \tag{11.24}$$

Adding the soft photon cross section to the contribution of the virtual corrections (11.21) the IR-singularities cancel. Moreover also the large Sudakov double logarithms $\log^2(m_e^2/s)$ drop out.

11.3.3. Leading weak corrections

In order to set up improved Born approximations which are often very handy the first step is to extract the leading corrections [78]. The universal corrections involving $\Delta\alpha$ and $\Delta\varrho$ can be easily obtained from (8.25) including the leading $O(\alpha^2)$ contributions. There are no nonuniversal corrections $\propto \alpha m_t^2/M_W^2$ to the W-pair production cross section for not too high energies, i.e. as long as the unitarity cancellations are not sizeable. In the LEP200 energy region also terms involving $\log m_t^2$ or $\log M_H^2$ may become important. These have been evaluated in the limit $M_H^2, m_t^2 \gg s$. In addition close to threshold apart from the large bremsstrahlung corrections which will be discussed in the next section there is a sizable effect of the Coulomb singularity. This can be simply obtained from general considerations or to $O(\alpha)$ directly from the loop diagrams involving photons exchanged between the final state W-bosons. Altogether this yields the following approximation

$$
\begin{aligned}
\mathcal{M}_a^- &= \frac{e^2}{2s_W^2}\left[\frac{1}{t}\mathcal{M}_1^- + \frac{1}{s-M_Z^2}2(\mathcal{M}_3^- - \mathcal{M}_2^-)\frac{1}{1-\Delta\alpha}\frac{1}{1+\frac{c_W^2}{s_W^2}\Delta\varrho}\right.\\
&\quad \left. + \frac{\alpha}{4\pi}\frac{1}{2s_W^2}\left(\frac{1}{3}-\frac{c_W^2}{s_W^2}\right)\log\frac{m_t^2}{M_W^2} + \frac{\alpha}{4\pi}\frac{11}{6}\frac{1}{2s_W^2}\log\frac{M_H^2}{M_W^2} + \frac{\alpha\pi}{4\beta}\right]\\
&\quad + e^2\left(\frac{1}{s}-\frac{1}{s-M_Z^2}\right)2(\mathcal{M}_3^- - \mathcal{M}_2^-)\left[\frac{1}{1-\Delta\alpha}+\frac{\alpha\pi}{4\beta}\right]\\
&\quad + e^2\frac{\alpha}{4\pi}\frac{1}{s-M_Z^2}2(\mathcal{M}_3^- - \mathcal{M}_2^-)\left[\frac{4s_W^2-3}{12c_W^2s_W^4}\log\frac{m_t^2}{M_W^2} - \frac{1}{48c_W^2s_W^4}\log\frac{M_H^2}{M_W^2}\right],\\
\mathcal{M}_a^+ &= e^2\left(\frac{1}{s}-\frac{1}{s-M_Z^2}\right)2(\mathcal{M}_3^+ - \mathcal{M}_2^+)\left[\frac{1}{1-\Delta\alpha}+\frac{\alpha\pi}{4\beta}\right]\\
&\quad + e^2\frac{\alpha}{4\pi}\frac{1}{s-M_Z^2}2(\mathcal{M}_3^+ - \mathcal{M}_2^+)\frac{1}{6s_W^2c_W^2}\left[\log\frac{m_t^2}{M_W^2} - \frac{1}{4}\log\frac{M_H^2}{M_W^2}\right].
\end{aligned}
\tag{11.25}
$$

All terms in (11.25) respect the high energy cancellations apart from those involving $\log m_t^2$ and $\log M_H^2$. However, these were obtained for $M_H^2, m_t^2 \gg s$, whereas the unitarity cancellations work for $s \gg M_H^2, m_t^2$. In this limit the terms containing $\log m_t^2$ and $\log M_H^2$ are absent. These may, however, cause large effects for small energies and large top quark or Higgs boson masses. This phenomenon was called delayed unitary cancellation in [79]. Introducing G_F instead of e^2/s_W^2 and the running $\alpha(s)$ we obtain

$$
\begin{aligned}
\mathcal{M}_a^- &= 2\sqrt{2}G_F M_W^2\left[\frac{1}{t}\mathcal{M}_1^- + \frac{1}{s-M_Z^2}2(\mathcal{M}_3^- - \mathcal{M}_2^-)\right]\left[1+\frac{\alpha\pi}{4\beta}+C_1^-(s,t)\right]\\
&\quad + 4\pi\alpha(s)\left(\frac{1}{s}-\frac{1}{s-M_Z^2}\right)2(\mathcal{M}_3^- - \mathcal{M}_2^-)\left[1+\frac{\alpha\pi}{4\beta}+C_2^-(s,t)\right]\\
&\quad + e^2\frac{\alpha}{4\pi}\frac{1}{s-M_Z^2}2(\mathcal{M}_3^- - \mathcal{M}_2^-)\left[\frac{4s_W^2-3}{12c_W^2s_W^4}\log\frac{m_t^2}{M_Z^2} - \frac{1}{48c_W^2s_W^4}\log\frac{M_H^2}{s}\right],
\end{aligned}
$$

Continuation Eq. (11.26)

$$\mathcal{M}_a^+ = 4\pi\alpha(s)\left(\frac{1}{s}-\frac{1}{s-M_Z^2}\right)2(\mathcal{M}_3^+-\mathcal{M}_2^+)\left[1+\frac{\alpha\pi}{4\beta}+C_2^+(s,t)\right]$$
$$+2\sqrt{2}\,G_F M_W^2\left[\frac{1}{t}\mathcal{M}_1^+ + \frac{1}{s-M_Z^2}2(\mathcal{M}_3^+-\mathcal{M}_2^+)\right]C_1^+(s,t)$$
$$+e^2\frac{\alpha}{4\pi}\frac{1}{s-M_Z^2}2(\mathcal{M}_3^+-\mathcal{M}_2^+)\frac{1}{6s_W^2c_W^2}\left[\log\frac{m_t^2}{M_Z^2}-\frac{1}{4}\log\frac{M_H^2}{s}\right]. \qquad (11.26)$$

We have included four functions $C_i(s,t)$, $i=1,2$, $\sigma=\pm$ in this approximation. These are necessary to describe the angular dependence of the differential cross section. The complete one-loop invariant matrix element for W-pair production involves 12 form-factors F_i^σ. It turns out, however, that only four of them namely the C_i^σ are relevant in the LEP200 energy region. For higher energies even C_1^+ can be omitted. The functions C_i^σ have been determined such that they reproduce the corresponding exact one-loop form-factors sufficiently well in the LEP200 energy region [78].

We want to stress that the naive summation of the Dyson series of the self energies may lead to incorrect results, i.e. a wrong high energy behaviour. This happens because the leading corrections are not only contained in the self energies but also in the vertex corrections. The actual place of their appearance depends on the choice of the field renormalization.

11.3.4. Numerical results for the virtual and soft photonic corrections

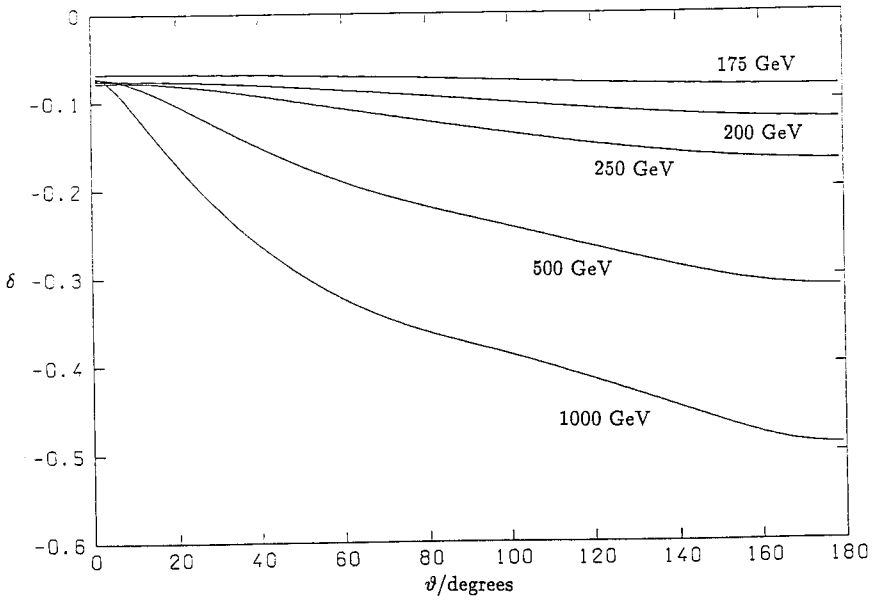

Fig. 11.5. Radiative corrections to the differential cross section relative to lowest order for the unpolarized case at various center of mass energies

We now present some numerical results for the radiative corrections in the soft photon approximation. The numerical input parameters are defined in Sect. 8.1. The soft photon cutoff is chosen as $\Delta E/E = 0.1$. Different choices of $\Delta E/E$ uniformly shift the absolute value of the corrections but do not influence their angular dependence very much. Fig. 11.5 shows the relative correction factor δ defined through

$$\frac{d\sigma}{d\Omega} = \left(\frac{d\sigma}{d\Omega}\right)_0 (1+\delta_s) + \delta\left(\frac{d\sigma}{d\Omega}\right)_V = \left(\frac{d\sigma}{d\Omega}\right)_0 (1+\delta) \tag{11.27}$$

for the unpolarized case. While the variation with the scattering angle is relatively flat for LEP200 energies it becomes stronger with increasing energy. In the forward direction where the Born cross section is dominated by the t-channel pole the energy dependence is very weak. In the backward direction, however, the percentage correction varies strongly with energy and reaches large negative values up to -50% at 1 TeV. Nevertheless since the absolute cross section is small for large scattering angles (see Fig. 11.3), the relative corrections to the integrated cross section stay below 20% up to 1 TeV. Note that the one-loop corrections are large exactly in that region where the sensitivity to new physics is highest.

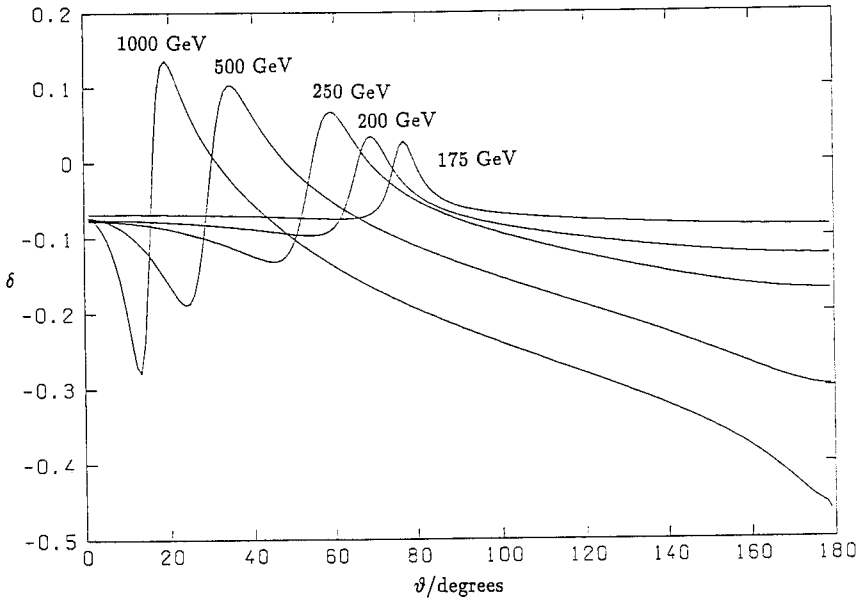

Fig. 11.6. Radiative corrections to the differential cross section relative to lowest order for purely longitudinal W-bosons at various center of mass energies

The behaviour of the corrections for purely transverse W-bosons is similar to the unpolarized case. In contrast to this the corrections for purely longitudinal bosons (Fig. 11.6) exhibit a strong angular dependence arising from the minima in the lowest order cross section (Fig. 11.4).

m_t/GeV =	80	120	160	200
M_W/GeV =	79.87	80.10	80.37	80.69
$\sqrt{s}$/GeV	σ/pb			
165.0	10.120	9.743	9.218	8.461
180.0	15.521	15.620	15.646	15.626
200.0	15.944	16.112	16.220	16.301
500.0	5.689	5.760	5.807	5.847
1000.0	2.064	2.088	2.103	2.113

Tab. 11.2. Total unpolarized cross section for $e^+e^- \to W^+W^-$ including virtual and soft photonic corrections for different to quark masses at various center of mass energies

M_H/GeV =	50	100	300	1000
M_W/GeV =	80.26	80.23	80.16	80.06
$\sqrt{s}$/GeV	σ/pb			
165.0	9.488	9.503	9.614	9.793
180.0	15.654	15.638	15.612	15.598
200.0	16.168	16.168	16.143	16.105
500.0	5.785	5.785	5.776	5.764
1000.0	2.097	2.096	2.093	2.088

Tab. 11.3. Total unpolarized cross section for $e^+e^- \to W^+W^-$ including virtual and soft photonic corrections for different Higgs boson masses at various center of mass energies

The sensitivity of the total unpolarized cross section on the unknown masses of the Higgs boson and top quark is illustrated in Tab. 11.2 and Tab. 11.3. A change of m_t from 80 to 200 GeV affects the cross section by less than 3% apart from the region very close to threshold. The large effect close to threshold is due to the variation of M_W and thus the variation of the threshold with m_t. A variation of M_H between 50 and 1000 GeV influences the total cross section by less than 0.5%, again with the exception of the threshold region. Note that this is valid for constant α, G_F and M_Z. Fixing instead G_F, M_W and M_Z the dependence on m_t is much weaker. This allows to determine M_W from the cross section practically independently on m_t and M_H as pointed out by JEGERLEHNER [80]. These results for the top and Higgs mass dependence remain valid if we include hard photonic corrections.

Using the functions C_i^q given in [78] the improved Born approximation (11.26) agrees with the full one-loop order result within 0.5% for $\sqrt{s} < 200$ GeV and within 1% for $\sqrt{s} < 270$ GeV in the case of the total cross section. For the differential cross section the deviation is at most 1% for $\sqrt{s} < 210$ GeV. The largest difference occurs for large scattering angles, i.e. where the cross section is small.

11.4. Hard photon bremsstrahlung

11.4.1. Complete calculations

The complete hard photonic bremsstrahlung to $e^+e^- \to W^+W^-$ was determined in [68, 70]. The polarized amplitudes for the process $e^+e^- \to W^+W^-\gamma$ were calculated using three different methods. The first one, described in detail in [69] uses the Weyl representation for Dirac matrices and spinors and results in expressions for the amplitudes in terms of the components of momentum and polarization vectors in the center of mass frame of the incoming leptons. The second method used in [14] is based on the Weyl-van der Waerden formalism. It yields concise analytical formulae for the amplitude which are manifestly Lorentz invariant. The relative numerical difference between both results was found to be less than 10^{-6} for the amplitude squared. In [70] the amplitudes were calculated numerically.

From this the total cross section is obtained as

$$\sigma(s) = \frac{1}{(2\pi)^5}\frac{1}{2s}\int \frac{d^3k_1}{2k_{10}}\frac{d^3k_2}{2k_{20}}\frac{d^3k}{2k_0}\frac{1}{4}\sum_{\text{pol}}|\mathcal{M}|^2\,\delta^{(4)}(p_1+p_2-k_1-k_2-k)$$

$$= \frac{1}{2s}\frac{1}{8(2\pi)^4}\int d\cos\vartheta_2\, d\cos\vartheta\, d\phi\, dk_0 \left|\frac{k_0|\mathbf{k}_2|^2}{|\mathbf{k}_2|(\sqrt{s}-k_0)+k_0k_{20}c_{20}}\right| \frac{1}{4}\sum_{\text{pol}}|\mathcal{M}|^2, \tag{11.28}$$

where ϑ_2, ϑ are the polar angles of the W^--boson and the photon. ϕ is the azimuthal angle of the photon with respect to the incoming electron and

$$c_{20} = \sin\vartheta_2\sin\vartheta\cos\phi + \cos\vartheta_2\cos\vartheta. \tag{11.29}$$

The nontrivial phase space integrations are performed using Monte Carlo routines. Thus experimental cuts can be easily implemented.

Eq. (11.28) contains the soft photon poles. These are eliminated by a cut $k_0 > \Delta E$ on the photon energy. After combining soft and hard photonic corrections the cut dependence drops out. This has been checked numerically for $\Delta E/E$ between 10^{-3} and 10^{-6}.

11.4.2. Leading logarithmic approximation

The leading logarithmic (LL) QED correction to the W-pair production cross section were already calculated in [43]. The resulting cross section is given by [68]

$$\sigma_{LL}(s) = \int_{4M_W^2/s}^{1} dz\,\phi(z)\,\hat{\sigma}_0(zs), \tag{11.30}$$

where $\hat{\sigma}_0(zs)$ denotes the (improved) Born cross section at the reduced CMS energy squared zs. The flux $\phi(z)$ reads

$$\phi(z)=\delta(1-z)$$
$$+\frac{\alpha}{\pi}(L-1)\left[\delta(1-z)\,2\log\varepsilon+\theta(1-\varepsilon-z)\,\frac{2}{1-z}\right]$$
$$+\frac{\alpha}{\pi}L\left[\delta(1-z)\,\frac{3}{2}-\theta(1-\varepsilon-z)\,(1+z)\right]$$
$$+\left(\frac{\alpha}{\pi}L\right)^2\left\{\delta(1-z)\left(2\log^2\varepsilon+3\log\varepsilon+\frac{9}{8}-\frac{\pi^2}{3}\right)\right.$$
$$\left.+\theta(1-\varepsilon-z)\left[\frac{1+z^2}{1-z}\left(2\log(1-z)-\log z+\frac{3}{2}\right)+\frac{1}{2}(1+z)\log z-(1-z)\right]\right\} \tag{11.31}$$

where $L=\log(Q^2/m_e^2)$ is the leading logarithm and $\varepsilon=\Delta E/E$ the soft photon cutoff. $\phi(z)$ is given including $O(\alpha^2)$ LL-contributions. Furthermore some nonleading terms are incorporated taking into account the fact that the residue of the soft photon pole is proportional to $L-1$ rather than L for the initial state radiation. The scale Q^2 is a free parameter. It can only be determined through higher order calculations. In [68] the integral in (11.30) was performed numerically. Neglecting the $O(\alpha^2)$ leading logarithms and the nonlogarithmic terms it has been evaluated analytically [78].

11.4.3. Numerical results

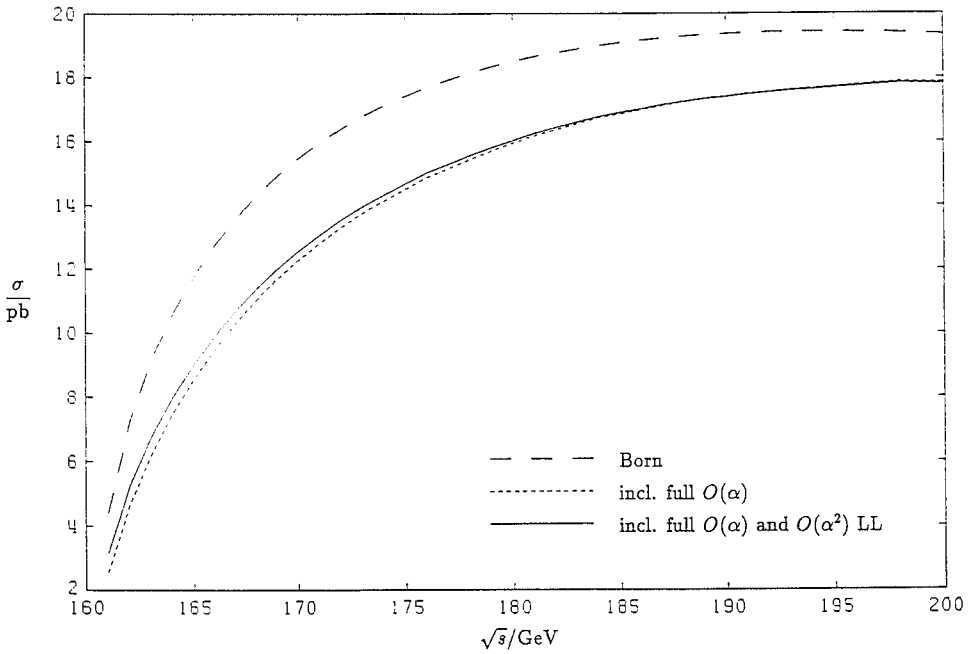

Fig. 11.7. Total cross section for W-pair production including hard photonic corrections

The results presented in this section were calculated by [68, 81]. The parameters are the same as in Sect. 8.1. In the Born cross section $\hat{\sigma}_0$, entering the LL approximation, α has been replaced by G_F everywhere. Thus the large fermionic corrections are absorbed at least in the dominant t-channel contributions.

The total cross section is plotted in Fig. 11.7 in the LEP200 energy range. Shown are the Born cross section with α replaced by G_F, the cross section including the full $O(\alpha)$ corrections and including in addition the $O(\alpha^2)$ LL corrections. The corresponding numbers are given in Tab. 11.4 for various CMS energies. The uncertainty of the full $O(\alpha)$ result is due to the Monte Carlo integration of the hard bremsstrahlung corrections. This error refers also to the last column of Tab. 11.4. The $O(\alpha)$ LL results were evaluated for two scale choices

$$Q^2 = s$$

$$Q^2 = -t_{\min} = -M_W^2 + \frac{s}{2}(1-\beta). \tag{11.32}$$

The second one is motivated by the fact that the total cross section is dominated by the t-channel pole. It reproduces the exact $O(\alpha)$ results better. The difference is found to be less than 2% for $\sqrt{s} > 165$ GeV. Choosing the scale $Q^2 = s$ the deviation from the exact $O(\alpha)$ result is about 5% at 165 GeV. Also at higher energies the scale choice $Q^2 = -t_{\min}$ turns out to be preferable. It reproduces the complete $O(\alpha)$ result including hard photon bremsstrahlung within 1% for $170\ \text{GeV} < \sqrt{s} < 500$ GeV. The effect of the $O(\alpha^2)$ LL contribution is demonstrated in the last column of Tab. 11.4. It reaches about 5% at 165 GeV, decreases with increasing energy and is small for $\sqrt{s} > 190$ GeV. A practically identical result is obtained by soft photon exponentiation.

$\sqrt{s}$ GeV	Born (G_F)	incl. $O(\alpha)$ LL $Q^2 = s$	incl. $O(\alpha)$ LL $Q^2 = -t_{\min}$	incl. $O(\alpha)$ exact	incl. $O(\alpha)$ exact + $O(\alpha^2)$ LL
161.0	4.411	2.003	2.158	2.556 ± 0.002	3.255
165.0	11.761	8.141	8.429	8.553 ± 0.006	9.089
170.0	15.465	11.967	12.285	12.264 ± 0.010	12.606
175.0	17.413	14.264	14.578	14.484 ± 0.013	14.690
180.0	18.501	15.730	16.028	15.920 ± 0.014	16.033
190.0	19.361	17.272	17.525	17.373 ± 0.016	17.375
200.0	19.354	17.810	18.015	17.796 ± 0.017	17.742
250.0	16.406	16.223	16.257	16.033 ± 0.023	15.937
300.0	13.473	13.734	13.682	13.543 ± 0.026	13.470
500.0	7.142	7.664	7.519	7.449 ± 0.019	7.430

Tab. 11.4. Total cross section for $e^+e^- \to W^+W^-$ in pb including hard photonic corrections

The large deviation between $O(\alpha)$ LL and the exact result close to threshold is due to the Coulomb singularity (see Sect. 11.3.3). It amounts to about 10% at 1 GeV above threshold and is not included in the $O(\alpha)$ LL result. Note also the large $O(\alpha^2)$ correction close to threshold (28% at 161 GeV).

11.5. Finite widths effects

Realistic calculations for W-pair production must include the decays of the W-bosons into fermions. These are especially important around threshold.

In real experiments one observes the reaction

$$e^+e^- \to W^+W^- \to \text{final states}. \tag{11.33}$$

The W-bosons give rise to peaks in the invariant mass distributions of the final state particles. Therefore one has to calculate the cross section for $e^+e^- \to f_1\bar{f}_2 f_3\bar{f}_4(\gamma, g)$. This task has been attacked but not completed so far [83]. Above the W-pair production threshold the dominant contributions come from Feynman diagrams containing resonant W-propagators. The cross section for W-pair production is obtained by calculating all diagrams containing two resonant W-propagators. Diagrams contributing to the same final state but without two resonant propagators are considered as background. They are suppressed by a factor $M_W/\Gamma^W \approx 40$ if the full range of invariant masses $\sqrt{s_i}$ of the final state particles is included. If $\sqrt{s_i}$ is restricted by a cut Δ

$$M_W - \Delta < \sqrt{s_i} < M_W + \Delta, \tag{11.34}$$

the suppression is even $M_W^2/(\Gamma^W\Delta) \approx 300$ for $\Delta \approx 10$ GeV. Explicit calculations show that the background contributions are below 1% for $\sqrt{s} \geqq 2M_W$ [83]. It becomes, however, more relevant below the nominal threshold. But even above threshold nonresonant Born contributions to $e^+e^- \to f_1\bar{f}_2 f_3\bar{f}_4(\gamma, g)$ must be taken into account to obtain an accuracy of better than 1%.

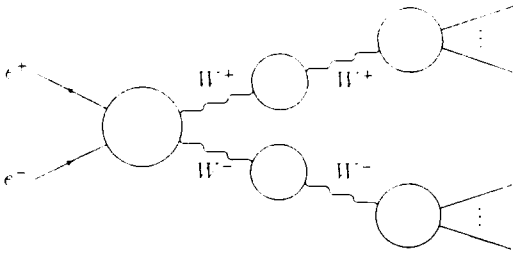

Fig. 11.8. General structure of diagrams containing two resonant W-propagators

There are three types of diagrams which may give resonant contributions. The most important ones are factorizable diagrams with the structure shown in Fig. 11.8 which evidently contain two resonant W-propagators. The corresponding cross section is given by

$$\sigma(s)=\int_{M_W-\Delta}^{M_W+\Delta} ds_1\, ds_2\, \sigma^*(s, s_1, s_2)\, \varrho(s_1)\, \varrho(s_2)\, \theta(\sqrt{s}-\sqrt{s_1}-\sqrt{s_2}), \tag{11.35}$$

where $\sigma^*(s, s_1, s_2)$ is the "cross section" for the production of two off-shell W-bosons and

$$\varrho(s)=\frac{1}{\pi}\,\frac{\sqrt{s}\,\Gamma^W(s)}{(s-M_W^2)^2+s(\Gamma^W(s))^2}, \tag{11.36}$$

with the "decay width" $\Gamma^W(s)$ for an off-shell W-boson. Note that

$$\varrho(s)\to\delta(s-M_W^2) \quad \text{for} \quad \Gamma^W\to 0. \tag{11.37}$$

The off-shell quantities $\sigma^*(s, s_1, s_2)$ and $\Gamma^W(s)$ are not gauge invariant. However, the leading resonant contributions to $\sigma(s)$ are. Eq. (11.35) closely resembles a Breit-Wigner approximation for the unstable W-bosons. In the threshold region $\sigma^*(s, s_1, s_2)$ depends strongly on s_1 and s_2. Consequently $\sigma(s)$ deviates considerably from $\sigma^*(s, M_W^2, M_W^2)$, the

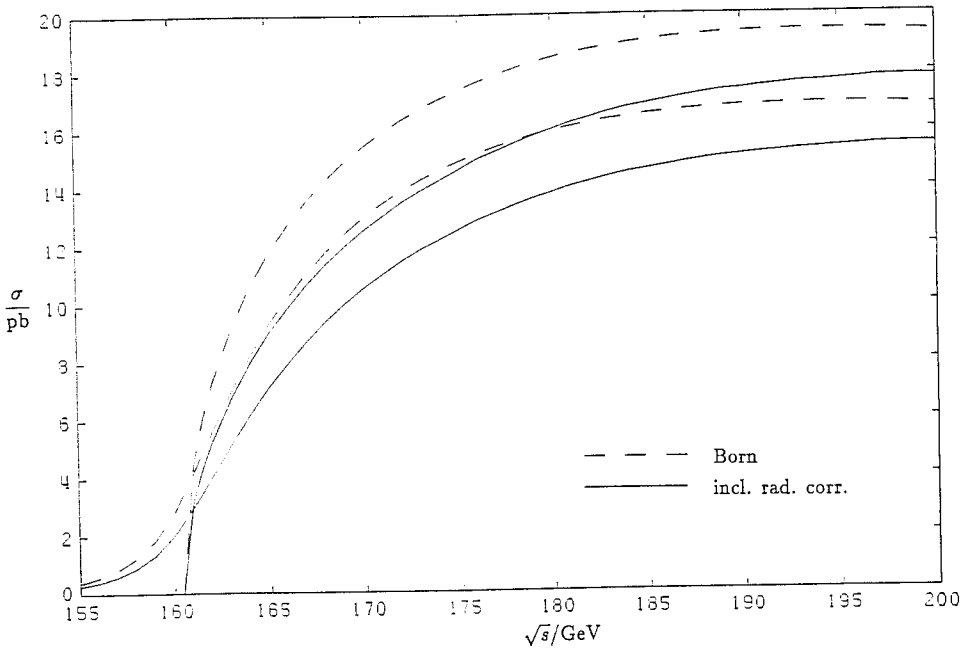

Fig. 11.9. Total cross section for W-pair production in lowest order and including the full $O(\alpha)$ corrections with and without finite width effects

cross section for on-shell stable W's. Fig. 11.9 [81] shows this effect in lowest order and with the full $O(\alpha)$ corrections to σ^* and $\Gamma^W(s)$ included. This dependence is mainly due to the threshold factor $\kappa^{1/2}(s, s_1, s_2)$ contained in $\sigma^*(s, s_1, s_2)$. Extracting this factor, $\sigma^*/\kappa^{1/2}$ depends only weakly on s_1 and s_2. This is also the case for $\Gamma^W(s)/\sqrt{s}$ with respect to s. Replacing these quantities by their on-shell values we find the following approximation

$$\sigma(s) \approx \frac{\sigma^*(s, M_W^2, M_W^2)}{\kappa^{1/2}(s, M_W^2, M_W^2)} \int_{M_W-\Delta}^{M_W+\Delta} ds_1\, ds_2\, \kappa^{1/2}(s, s_1, s_2)\, \tilde{\varrho}(s_1)\, \tilde{\varrho}(s_2)\, \theta(\sqrt{s}-\sqrt{s_1}-\sqrt{s_2}) \tag{11.38}$$

with

$$\tilde{\varrho}(s) = \frac{1}{\pi} \frac{s\Gamma^W(M_W^2)}{(s-M_W^2)^2 + s^2(\Gamma^W(M_W^2))^2}\,. \tag{11.39}$$

This approximation is gauge invariant because $\sigma^*(s, M_W^2, M_W^2)$ and $\Gamma^W(M_W^2)$ are physical on-shell quantities. It is particulary useful above the nominal threshold, whereas it gets worse below threshold because there at least one of the W-bosons has to be off-shell.

For high energies ($s \gg M_W^2$) also $\kappa(s, s_1, s_2)$ varies only weakly with s_1 and s_2 in the resonance region $s_1 \approx s_2 \approx M_W^2$. Replacing it by its on-shell value we can perform the integrations and obtain

$$\sigma(s) \approx \sigma^*(s, M_W^2, M_W^2), \quad \text{for} \quad s \gg M_W \quad \text{and} \quad \Delta \gg \Gamma^W. \tag{11.40}$$

Eq. (11.35) incorporates all resonant lowest order contributions and all one-loop corrections associated either with the production of W-pairs or the decay of the W-bosons (given in Chap. 9). This includes in particular all self energy and vertex corrections and thus all leading corrections. A more thorough analysis of this kind has been carried through for the case of Z-pair production [82].

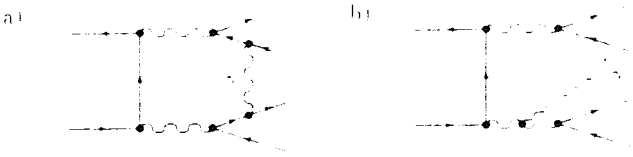

Fig. 11.10. Examples for additional diagrams leading to resonant contributions

Feynman diagrams which do not fit into the structure shown in Fig. 11.8 give non-resonant contributions and can thus be neglected with the exception of two classes. Both originate from photonic corrections. The first type results from virtual photons exchanged between the external lines connected to different blobs in Fig. 11.8. An example is shown in Fig. 11.10a. These diagrams give rise to resonant contributions coming from photons which are nearly on-shell. From similar cases in μ-pair production we know that these are cancelled by the corresponding bremsstrahlung diagrams if one integrates over the whole photon phase space. For stringent cuts, however, resonant contributions survive.

The second type of diagrams consists of those where a real photon is emitted from the internal W-boson line (Fig. 11.10b). There are three W-propagators in the diagram. If the photon is hard the corresponding resonances appear in three different regions of phase space. Therefore these diagrams seem not to fit into the simple Breit-Wigner-like picture discussed above.

In order to take into account these resonant contributions properly one has to calculate the virtual and real photonic corrections to $e^+e^- \to 4$ fermions. This has been done for real photon radiation [73]. Evaluation of the virtual photonic corrections is under way [83].

12. Conclusion

With the electroweak standard model (SM) we have a theory that describes all known experimental facts about the electroweak interaction. It has succesfully survived all precision experiments at low energies and at LEP100. The upcoming experiments at LEP200, HERA and the planned hadron colliders will allow to investigate sectors of the SM which were not directly accessible so far. For a conclusive confrontation of future experimental results with the SM precise predictions are mandatory.

For the adequate theoretical description of the experiments at LEP100 the calculation of radiative corrections was inevitable. Although experiments outside the Z-region will not profit from the presence of a resonance, the expected experimental accuracy will be such that radiative corrections will be indispensable. Moreover radiative corrections allow to obtain information on otherwise not accessible quantities such as the mass of the top quark or the Higgs boson.

One of the next important classes of experiments will be the investigation of the W-boson and its nonabelian couplings at LEP200. We have presented the relevant formulae necessary for the corresponding higher order calculations. Together with [66, 14] these cover the complete analytical expressions for processes with on-shell W-bosons. The one-loop virtual corrections are settled for the polarized differential and total cross section. Also hard bremsstrahlung has been calculated by several authors. We have given an improved Born approximation including the leading two-loop contributions for the total and differential cross section. The effects of the finite width of the W-bosons have been discussed for the lowest order cross section and the cross section including radiative corrections. While the inclusion of the non-photonic corrections is simple the correct simultaneous treatment of photonic corrections and finite width effects involves nonfactorizable box diagrams. These contributions are under consideration.

We have discussed the total and partial W-decay widths including all one-loop and leading two-loop corrections. Because the W-boson decays only into light fermions the widths can be described by a very simple expression with an accuracy better than 0.6%.

Furthermore we have given results on the t-quark decay width. Also in this case the electroweak corrections can be incorporated into a simple approximation valid for a top mass below 250 GeV with an accuracy of about 1.7%.

Apart from giving these explicit results we have discussed many techniques needed for the calculation of one-loop corrections. We have compiled a comprehensive set of formulae which are relevant for the calculation of one-loop radiative corrections within and outside the standard model. We have listed the complete set of Feynman rules for the electroweak standard model including the counter terms. These were expressed by the self energies of the physical particles in terms of two-point functions. We have given explicit results for the scalar N-point functions for $N = 1, \ldots, 4$ and the relevant formulae for the reduction of the higher scalar functions and the tensor functions to those. Furthermore we have outlined a general strategy for the calculation of one-loop diagrams. Finally we have given the general expressions for the soft photonic corrections.

If the SM will prove to describe the upcoming experimental results succesfully, further precision checks will become necessary and a lot more calculations of radiative corrections will be required. These calculations will be even more involved than the existing ones because the structure of the corresponding physical processes will in general be more complicated. The techniques and formulae presented in this review are general enough to serve as a basis for the evaluation of radiative corrections to reactions which will be studied at future colliders such as gauge boson scattering processes ($W^+W^- \to W^+W^-$), electron photon reactions ($e\gamma \to \nu_e W$), reactions with three or more final state particles and so on.

The methods described here have been implemented in the computer algebra package *FeynCalc*. Many of the quoted formulae are included in this package. We hope that this compilation together with the packages *FeynCalc* and *FeynArts* can serve as a useful tool, facilitating future calculations of radiative corrections.

Acknowledgements

I would like to thank M. Böhm for his support and permanent encouragement during the past years. Many of the results presented here were calculated together with T. Sack who also provided some of the figures and tables. The results on W-pair-production were obtained in a fruitful collaboration with W. Beenakker, F. A. Berends, H. Kuijf, M. Böhm and T. Sack. I have profited from many stimulating and clarifying discussions with the people mentioned above and H. Spiesberger, W. Hollik, J. H. Kühn, F. Jegerlehner and W. L. van Neerven. I am grateful to R. Mertig, J. Küblbeck, R. Guth, H. Eck, R. Scharf, U. Nierste and S. Dittmaier for their assistance. I am indebted to my wife R. Denner for typing parts of the manuscript and in particular for her patience.

A. Feynman Rules

In this appendix we list the Feynman rules of the SM in the 't Hooft-Feynman gauge including the counterterms in a way appropriate for the concept of generic diagrams. I.e. we write down generic Feynman rules and give the possible actual insertions. We omit any field renormalization constants for the unphysical fields. For brevity we introduce the shorthand notation

$$c = c_W, \quad s = s_W. \tag{A.1}$$

In the vertices all momenta are considered as incoming.

Propagators:
for gauge bosons $V = \gamma, Z, W$ in the 't Hooft Feynman gauge ($\xi_i = 1$)

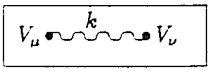

$$= \frac{-ig_{\mu\nu}}{k^2 - M_V^2},$$

for Faddeev-Popov ghosts $G = u^\gamma, u^Z, u^W$

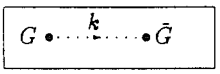

$$= \frac{i}{k^2 - M_G^2},$$

for scalar fields $S = H, \chi, \phi$

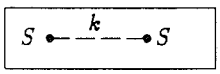

$$= \frac{i}{k^2 - M_S^2},$$

and for fermion fields $F = f_i$

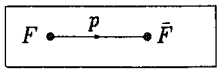

$$= \frac{i(\not{p} + m_F)}{p^2 - m_F^2}.$$

In the 't Hooft-Feynman gauge we have the following relations:

$$M_{u^0} = 0, \quad M_{u^Z} = M_\chi = M_Z, \quad M_{u^+} = M_\phi = M_W. \tag{A.2}$$

Tadpole:

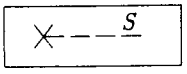

$$= i\delta t.$$

VV-counterterm:

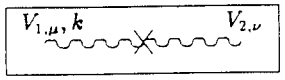

$$= -ig_{\mu\nu}[C_1 k^2 - C_2]$$

with the actual values of V_1, V_2 and C_1, C_2

$$\begin{aligned}
&W^+W^- : C_1 = \delta Z_W, && C_2 = M_W^2 \delta Z_W + \delta M_W^2,\\
&ZZ \quad\;\; : C_1 = \delta Z_{ZZ}, && C_2 = M_Z^2 \delta Z_{ZZ} + \delta M_Z^2,\\
&AZ \quad\;\; : C_1 = \tfrac{1}{2}\delta Z_{AZ} + \tfrac{1}{2}\delta Z_{ZA}, && C_2 = M_Z^2 \tfrac{1}{2}\delta Z_{ZA},\\
&AA \quad\;\; : C_1 = \delta Z_{AA}, && C_2 = 0.
\end{aligned} \tag{A.3}$$

SS-counterterm:

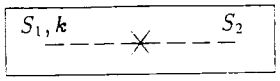

$$= i[C_1 k^2 - C_2]$$

with the actual values of S_1, S_2 and C_1, C_2

$$HH : C_1 = \delta Z_H, \quad C_2 = M_H^2 \delta Z_H + \delta M_H^2. \tag{A.4}$$

FF-counterterm:

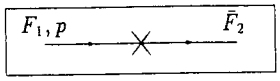

$$= i[C_L \not{p} \omega_- + C_R \not{p} \omega_+ - C_S^- \omega_- - C_S^+ \omega_+]$$

with the actual values of F_1, $\bar{F}_2$ and C_L, C_R, C_S^-, C_S^+

$$f_j \bar{f}_i : \begin{cases} C_L = \frac{1}{2}(\delta Z_{ij}^{f,L} + \delta Z_{ij}^{f,L\dagger}), \quad C_R = \frac{1}{2}(\delta Z_{ij}^{f,R} + \delta Z_{ij}^{f,R\dagger}), \\ C_S^- = m_{f,i} \frac{1}{2}\delta Z_{ij}^{f,L} + m_{f,j} \frac{1}{2}\delta Z_{ij}^{f,R\dagger} + \delta_{ij}\delta m_{f,i}, \\ C_S^+ = m_{f,i} \frac{1}{2}\delta Z_{ij}^{f,R} + m_{f,j} \frac{1}{2}\delta Z_{ij}^{f,L\dagger} + \delta_{ij}\delta m_{f,i}. \end{cases} \tag{A.5}$$

VVVV-coupling:

(A.2)

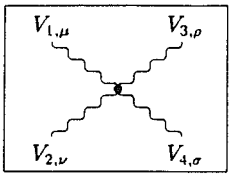

$$= ie^2 C[2g_{\mu\nu}g_{\sigma\varrho} - g_{\nu\varrho}g_{\mu\sigma} - g_{\varrho\mu}g_{\nu\sigma}]$$

with the actual values of V_1, V_2, V_3, V_4 and C

$$\begin{aligned}
&W^+W^+W^-W^- &&: C = \tfrac{1}{s^2}[1 + 2\delta Z_e - 2\tfrac{\delta s}{s} + 2\delta Z_W],\\
&W^+W^-ZZ &&: C = -\tfrac{c^2}{s^2}[1 + 2\delta Z_e - 2\tfrac{1}{c^2}\tfrac{\delta s}{s} + \delta Z_W + \delta Z_{ZZ}] + \tfrac{1}{2}\tfrac{c}{s}\delta Z_{AZ},\\
&W^+W^-AZ &&: \begin{cases} C = \tfrac{c}{s}[1 + 2\delta Z_e - \tfrac{1}{c^2}\tfrac{\delta s}{s} + \delta Z_W + \tfrac{1}{2}\delta Z_{ZZ} + \tfrac{1}{2}\delta Z_{AA}], \\ \quad -\tfrac{1}{2}\delta Z_{AZ} - \tfrac{1}{2}\tfrac{c^2}{s^2}\delta Z_{ZA} \end{cases}\\
&W^+W^-AA &&: C = -[1 + 2\delta Z_e + \delta Z_W + \delta Z_{AA}] + \tfrac{1}{2}\tfrac{c}{s}\delta Z_{ZA}.
\end{aligned} \tag{A.6}$$

VVV-coupling:

(A.3)

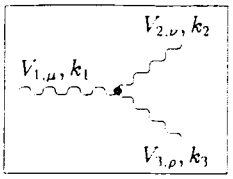

$$= -ieC[g_{\mu\nu}(k_2 - k_1)_\varrho + g_{\nu\varrho}(k_3 - k_2)_\mu + g_{\varrho\mu}(k_1 - k_3)_\nu]$$

with the actual values of V_1, V_2, V_3 and C

(A.4)

$$\begin{aligned}
&AW^+W^- &&: C = 1 + \delta Z_e + \delta Z_W + \tfrac{1}{2}\delta Z_{AA} - \tfrac{1}{2}\tfrac{c}{s}\delta Z_{ZA},\\
&ZW^+W^- &&: C = -\tfrac{c}{s}(1 + \delta Z_e - \tfrac{1}{c^2}\tfrac{\delta s}{s} + \delta Z_W + \tfrac{1}{2}\delta Z_{ZZ}) + \tfrac{1}{2}\delta Z_{AZ}.
\end{aligned} \tag{A.7}$$

SSSS-coupling:

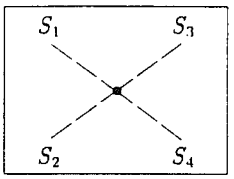

$$= ie^2 C$$

(A.5)

with the actual values of S_1, S_2, S_3, S_4 and C

$$
\begin{aligned}
&HHHH : C = -\tfrac{3}{4s^2}\tfrac{M_H^2}{M_W^2}\Big[1+2\delta Z_e - 2\tfrac{\delta s}{s} + \tfrac{\delta M_H^2}{M_H^2} - \tfrac{\delta M_W^2}{M_W^2} + 2\delta Z_H\Big],\\
&\left.\begin{matrix} HH\chi\chi \\ HH\phi\phi \end{matrix}\right\} : C = -\tfrac{1}{4s^2}\tfrac{M_H^2}{M_W^2}\Big[1+2\delta Z_e - 2\tfrac{\delta s}{s} + \tfrac{\delta M_H^2}{M_H^2} - \tfrac{\delta M_W^2}{M_W^2} + \delta Z_H\Big],\\
&\chi\chi\chi\chi \quad : C = -\tfrac{3}{4s^2}\tfrac{M_H^2}{M_W^2}\Big[1+2\delta Z_e - 2\tfrac{\delta s}{s} + \tfrac{\delta M_H^2}{M_H^2} - \tfrac{\delta M_W^2}{M_W^2}\Big],\\
&\chi\chi\phi\phi \quad : C = -\tfrac{1}{4s^2}\tfrac{M_H^2}{M_W^2}\Big[1+2\delta Z_e - 2\tfrac{\delta s}{s} + \tfrac{\delta M_H^2}{M_H^2} - \tfrac{\delta M_W^2}{M_W^2}\Big],\\
&\phi\phi\phi\phi \quad : C = -\tfrac{1}{2s^2}\tfrac{M_H^2}{M_W^2}\Big[1+2\delta Z_e - 2\tfrac{\delta s}{s} + \tfrac{\delta M_H^2}{M_H^2} - \tfrac{\delta M_W^2}{M_W^2}\Big].
\end{aligned}
\tag{A.8}
$$

SSS-coupling:

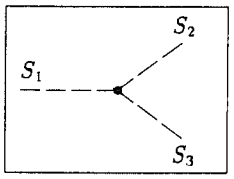

$= ieC$

with the actual values of S_1, S_2, S_3 and C

$$
\begin{aligned}
&HHH : C = -\tfrac{3}{2s}\tfrac{M_H^2}{M_W}\Big[1+\delta Z_e - \tfrac{\delta s}{s} + \tfrac{\delta M_H^2}{M_H^2} - \tfrac{1}{2}\tfrac{\delta M_W^2}{M_W^2} + \tfrac{3}{2}\delta Z_H\Big],\\
&\left.\begin{matrix} H\chi\chi \\ H\phi\phi \end{matrix}\right\} : C = -\tfrac{1}{2s}\tfrac{M_H^2}{M_W}\Big[1+\delta Z_e - \tfrac{\delta s}{s} + \tfrac{\delta M_H^2}{M_H^2} - \tfrac{1}{2}\tfrac{\delta M_W^2}{M_W^2} + \tfrac{1}{2}\delta Z_H\Big].
\end{aligned}
\tag{A.9}
$$

VVSS-coupling:

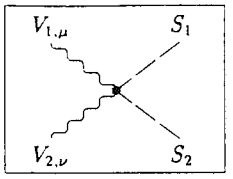

$= ie^2 g_{\mu\nu} C$

with the actual values of V_1, V_2, S_1, S_2 and C

$$
\begin{aligned}
&W^+W^-HH \quad : C = \tfrac{1}{2s^2}\Big[1+2\delta Z_e - 2\tfrac{\delta s}{s} + \delta Z_W + \delta Z_H\Big],\\
&\left.\begin{matrix} W^+W^-\chi\chi \\ W^+W^-\phi^+\phi^- \end{matrix}\right\} : C = \tfrac{1}{2s^2}\Big[1+2\delta Z_e - 2\tfrac{\delta s}{s} + \delta Z_W\Big],\\
&ZZ\phi^+\phi^- \quad : C = \tfrac{(s^2-c^2)^2}{2s^2c^2}\Big[1+2\delta Z_e + \tfrac{2}{(s^2-c^2)c^2}\tfrac{\delta s}{s} + \delta Z_{ZZ}\Big] + \tfrac{s^2-c^2}{sc}\tfrac{1}{2}\delta Z_{AZ},\\
&ZA\phi^+\phi^- \quad : \begin{cases} C = \tfrac{s^2-c^2}{sc}\Big[1+2\delta Z_e + \tfrac{1}{(s^2-c^2)c^2}\tfrac{\delta s}{s} + \tfrac{1}{2}\delta Z_{ZZ} + \tfrac{1}{2}\delta Z_{AA}\Big] \\ \quad + \tfrac{(s^2-c^2)^2}{2s^2c^2}\tfrac{1}{2}\delta Z_{ZA} + \delta Z_{AZ}, \end{cases}
\end{aligned}
\tag{A.10}
$$

Continuation Eq. (A.10)

$$
\begin{aligned}
&AA\phi^+\phi^- && : C = 2\left[1+2\delta Z_e+\delta Z_{AA}\right]+\tfrac{s^2-c^2}{sc}\,\tfrac{1}{2}\delta Z_{ZA},\\
&ZZHH && : C = \tfrac{1}{2s^2c^2}\left[1+2\delta Z_e+2\tfrac{s^2-c^2}{c^2}\,\tfrac{\delta s}{s}+\delta Z_{ZZ}+\delta Z_H\right],\\
&ZZ\chi\chi && : C = \tfrac{1}{2s^2c^2}\left[1+2\delta Z_e+2\tfrac{s^2-c^2}{c^2}\,\tfrac{\delta s}{s}+\delta Z_{ZZ}\right],\\
&\left.\begin{matrix}ZAHH\\ ZA\chi\chi\end{matrix}\right\} && : C = \tfrac{1}{2s^2c^2}\,\tfrac{1}{2}\delta Z_{ZA},\\
&W^\pm Z\phi^\mp H && : C = -\tfrac{1}{2c}\left[1+2\delta Z_e-\tfrac{\delta c}{c}+\tfrac{1}{2}\delta Z_W+\tfrac{1}{2}\delta Z_H+\tfrac{1}{2}\delta Z_{ZZ}\right]-\tfrac{1}{2s}\,\tfrac{1}{2}\delta Z_{AZ},\\
&W^\pm A\phi^\mp H && : C = -\tfrac{1}{2s}\left[1+2\delta Z_e-\tfrac{\delta s}{s}+\tfrac{1}{2}\delta Z_W+\tfrac{1}{2}\delta Z_H+\tfrac{1}{2}\delta Z_{AA}\right]-\tfrac{1}{2c}\,\tfrac{1}{2}\delta Z_{ZA},\\
&W^\pm Z\phi^\mp\chi && : C = \mp\tfrac{i}{2c}\left[1+2\delta Z_e-\tfrac{\delta c}{c}+\tfrac{1}{2}\delta Z_W+\tfrac{1}{2}\delta Z_{ZZ}\right]\mp\tfrac{i}{2s}\,\tfrac{1}{2}\delta Z_{AZ},\\
&W^\pm A\phi^\mp\chi && : C = \mp\tfrac{i}{2s}\left[1+2\delta Z_e-\tfrac{\delta s}{s}+\tfrac{1}{2}\delta Z_W+\tfrac{1}{2}\delta Z_{AA}\right]\mp\tfrac{i}{2c}\,\tfrac{1}{2}\delta Z_{ZA}. \qquad \text{(A.10)}
\end{aligned}
$$

(A.8)

VSS-coupling:

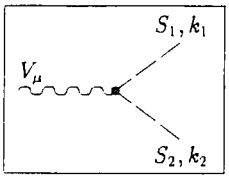

$$= ieC(k_1-k_2)_\mu \qquad \text{(A.9)}$$

with the actual values of V, S_1, S_2 and C

$$
\begin{aligned}
&A\chi H && : C = -\tfrac{i}{2cs}\,\tfrac{1}{2}\delta Z_{ZA},\\
&Z\chi H && : C = -\tfrac{i}{2cs}\left[1+\delta Z_e+\tfrac{s^2-c^2}{c^2}\,\tfrac{\delta s}{s}+\tfrac{1}{2}\delta Z_H+\tfrac{1}{2}\delta Z_{ZZ}\right],\\
&A\phi^+\phi^- && : C = -\left[1+\delta Z_e+\tfrac{1}{2}\delta Z_{AA}+\tfrac{s^2-c^2}{2sc}\,\tfrac{1}{2}\delta Z_{ZA}\right],\\
&Z\phi^+\phi^- && : C = -\tfrac{s^2-c^2}{2sc}\left[1+\delta Z_e+\tfrac{1}{(s^2-c^2)c^2}\,\tfrac{\delta s}{s}+\tfrac{1}{2}\delta Z_{ZZ}\right]-\tfrac{1}{2}\delta Z_{AZ},\\
&W^\pm\phi^\mp H && : C = \mp\tfrac{1}{2s}\left[1+\delta Z_e-\tfrac{\delta s}{s}+\tfrac{1}{2}\delta Z_W+\tfrac{1}{2}\delta Z_H\right],\\
&W^\pm\phi^\mp\chi && : C = -\tfrac{i}{2s}\left[1+\delta Z_e-\tfrac{\delta s}{s}+\tfrac{1}{2}\delta Z_W\right]. \qquad \text{(A.11)}
\end{aligned}
$$

SVV-coupling:

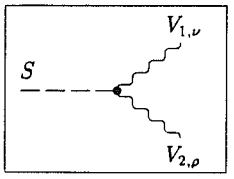

$$= ieg_{\mu\nu}C$$

with the actual values of S, V_1, V_2 and C

$$
\begin{aligned}
HW^+W^- &: C = M_W \tfrac{1}{s}\Big[1+\delta Z_e - \tfrac{\delta s}{s} + \tfrac{1}{2}\tfrac{\delta M_W^2}{M_W^2} + \tfrac{1}{2}\delta Z_H + \delta Z_W\Big],\\
HZZ &: C = M_W \tfrac{1}{sc^2}\Big[1+\delta Z_e + \tfrac{2s^2-c^2}{c^2}\tfrac{\delta s}{s} + \tfrac{1}{2}\tfrac{\delta M_W^2}{M_W^2} + \tfrac{1}{2}\delta Z_H + \delta Z_{ZZ}\Big],\\
HZA &: C = M_W \tfrac{1}{sc^2}\tfrac{1}{2}\delta Z_{ZA},\\
\phi^\pm W^\mp Z &: C = -M_W \tfrac{s}{c}\Big[1+\delta Z_e + \tfrac{1}{c^2}\tfrac{\delta s}{s} + \tfrac{1}{2}\tfrac{\delta M_W^2}{M_W^2} + \tfrac{1}{2}\delta Z_W + \tfrac{1}{2}\delta Z_{ZZ}\Big] - M_W \tfrac{1}{2}\delta Z_{AZ},\\
\phi^\pm W^\mp A &: C = -M_W\Big[1+\delta Z_e + \tfrac{1}{2}\tfrac{\delta M_W^2}{M_W^2} + \tfrac{1}{2}\delta Z_W + \tfrac{1}{2}\delta Z_{AA}\Big] - M_W \tfrac{s}{c}\tfrac{1}{2}\delta Z_{ZA}. \qquad \text{(A.12)}
\end{aligned}
$$

VFF-coupling:

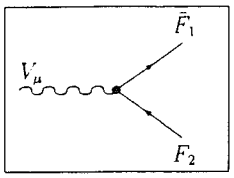

$$= ie\gamma_\mu(C^-\omega_- + C^+\omega_+)$$

with the actual values of V, $\bar{F}_1$, F_2 and C^+, C^-

$$
\gamma \bar{f}_i f_j \quad : \begin{cases} C^+ = -Q_f\big[\delta_{ij}(1+\delta Z_e + \tfrac{1}{2}\delta Z_{AA}) + \tfrac{1}{2}(\delta Z_{ij}^{f,R} + \delta Z_{ij}^{f,R\dagger})\big] + \delta_{ij} g_f^+ \tfrac{1}{2}\delta Z_{ZA},\\ C^- = -Q_f\big[\delta_{ij}(1+\delta Z_e + \tfrac{1}{2}\delta Z_{AA}) + \tfrac{1}{2}(\delta Z_{ij}^{f,L} + \delta Z_{ij}^{f,L\dagger})\big] + \delta_{ij} g_f^- \tfrac{1}{2}\delta Z_{ZA}, \end{cases}
$$

$$
Z \bar{f}_i f_j \quad : \begin{cases} C^+ = g_f^+\big[\delta_{ij}(1+\tfrac{\delta g_f^+}{g_f^+} + \tfrac{1}{2}\delta Z_{ZZ}) + \tfrac{1}{2}(\delta Z_{ij}^{f,R} + \delta Z_{ij}^{f,R\dagger})\big] - \delta_{ij} Q_f \tfrac{1}{2}\delta Z_{AZ},\\ C^- = g_f^-\big[\delta_{ij}(1+\tfrac{\delta g_f^-}{g_f^-} + \tfrac{1}{2}\delta Z_{ZZ}) + \tfrac{1}{2}(\delta Z_{ij}^{f,L} + \delta Z_{ij}^{f,L\dagger})\big] - \delta_{ij} Q_f \tfrac{1}{2}\delta Z_{AZ}, \end{cases}
$$

$$
W^+ \bar{u}_i d_j : \begin{cases} C^+ = 0, \quad C^- = \tfrac{1}{\sqrt{2}s}\big[V_{ij}(1+\delta Z_e - \tfrac{\delta s}{s} + \tfrac{1}{2}\delta Z_W) + \delta V_{ij}\\ \qquad\qquad + \tfrac{1}{2}\Sigma_k(\delta Z_{ik}^{u,L\dagger} V_{kj} + V_{ik}\delta Z_{kj}^{d,L})\big], \end{cases}
$$

$$
W^- \bar{d}_j u_i : \begin{cases} C^+ = 0, \quad C^- = \tfrac{1}{\sqrt{2}s}\big[V_{ji}^\dagger(1+\delta Z_e - \tfrac{\delta s}{s} + \tfrac{1}{2}\delta Z_W) + \delta V_{ji}^\dagger\\ \qquad\qquad + \tfrac{1}{2}\Sigma_k(\delta Z_{jk}^{d,L\dagger} V_{ki}^\dagger + V_{jk}^\dagger \delta Z_{ki}^{u,L})\big], \end{cases}
$$

$$
W^+ \bar{\nu}_i l_j : C^+ = 0, \quad C^- = \tfrac{1}{\sqrt{2}s}\delta_{ij}\big[1+\delta Z_e - \tfrac{\delta s}{s} + \tfrac{1}{2}\delta Z_W + \tfrac{1}{2}(\delta Z_{ii}^{\nu,L\dagger} + \delta Z_{ii}^{l,L})\big],
$$

$$
W^- \bar{l}_j \nu_i : C^+ = 0, \quad C^- = \tfrac{1}{\sqrt{2}s}\delta_{ij}\big[1+\delta Z_e - \tfrac{\delta s}{s} + \tfrac{1}{2}\delta Z_W + \tfrac{1}{2}(\delta Z_{ii}^{l,L\dagger} + \delta Z_{ii}^{\nu,L})\big], \qquad \text{(A.13)}
$$

where

$$
\begin{aligned}
g_f^+ &= -\tfrac{s}{c}Q_f, \qquad \delta g_f^+ = -\tfrac{s}{c}Q_f\big[\delta Z_e + \tfrac{1}{c^2}\tfrac{\delta s}{s}\big],\\
g_f^- &= \tfrac{I_{W,f}^3 - s^2 Q_f}{sc}, \quad \delta g_f^- = \tfrac{I_{W,f}^3}{sc}\big[\delta Z_e + \tfrac{s^2-c^2}{c^2}\tfrac{\delta s}{s}\big] + \delta g_f^+. \qquad \text{(A.14)}
\end{aligned}
$$

The vector and axial vector couplings of the Z-boson are given by

$$v_f = \tfrac{1}{2}(g_f^- + g_f^+) = \frac{I^3_{W,f} - 2s^2 Q_f}{2sc}, \quad a_f = \tfrac{1}{2}(g_f^- - g_f^+) = \frac{I^3_{W,f}}{2sc}. \tag{A.15}$$

SFF-coupling:

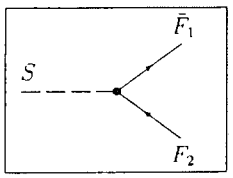

$$= ie(C^- \omega_- + C^+ \omega_+)$$

with the actual values of S, $\bar{F}_1$, F_2 and C^+, C^-

$$H\bar{f}_i f_j \;:\begin{cases} C^+ = -\frac{1}{2s}\frac{m_{f,i}}{M_W}\big[\delta_{ij}(1+\delta Z_e - \frac{\delta s}{s} + \frac{\delta m_{f,i}}{m_{f,i}} - \frac{\delta M_W}{M_W} + \frac{1}{2}\delta Z_H) \\ \qquad + \frac{1}{2}(\delta Z_{ij}^{f,R} + \delta Z_{ij}^{f,R\dagger})\big], \\ C^- = -\frac{1}{2s}\frac{m_{f,i}}{M_W}\big[\delta_{ij}(1+\delta Z_e - \frac{\delta s}{s} + \frac{\delta m_{f,i}}{m_{f,i}} - \frac{\delta M_W}{M_W} + \frac{1}{2}\delta Z_H) \\ \qquad + \frac{1}{2}(\delta Z_{ij}^{f,L} + \delta Z_{ij}^{f,L\dagger})\big], \end{cases}$$

$$\chi\bar{f}_i f_j \;:\begin{cases} C^+ = i\,\frac{1}{2s}\,2I^3_{W,f}\frac{m_{f,i}}{M_W}\big[\delta_{ij}(1+\delta Z_e - \frac{\delta s}{s} + \frac{\delta m_{f,i}}{m_{f,i}} - \frac{\delta M_W}{M_W}) + \frac{1}{2}(\delta Z_{ij}^{f,R} + \delta Z_{ij}^{f,R\dagger})\big], \\ C^- = -i\,\frac{1}{2s}\,2I^3_{W,f}\frac{m_{f,i}}{M_W}\big[\delta_{ij}(1+\delta Z_e - \frac{\delta s}{s} + \frac{\delta m_{f,i}}{m_{f,i}} - \frac{\delta M_W}{M_W}) + \frac{1}{2}(\delta Z_{ij}^{f,L} + \delta Z_{ij}^{f,L\dagger})\big], \end{cases}$$

$$\phi^+ \bar{u}_i d_j : \begin{cases} C^+ = -\frac{1}{\sqrt{2}s}\frac{m_{d,j}}{M_W}\big[V_{ij}(1+\delta Z_e - \frac{\delta s}{s} + \frac{\delta m_{d,j}}{m_{d,j}} - \frac{\delta M_W}{M_W}) + \delta V_{ij} \\ \qquad + \frac{1}{2}\Sigma_k(\delta Z_{ik}^{u,R\dagger} V_{kj} + V_{ik}\delta Z_{kj}^{d,R})\big], \\ C^- = \frac{1}{\sqrt{2}s}\frac{m_{u,i}}{M_W}\big[V_{ij}(1+\delta Z_e - \frac{\delta s}{s} + \frac{\delta m_{u,i}}{m_{u,i}} - \frac{\delta M_W}{M_W}) + \delta V_{ij} \\ \qquad + \frac{1}{2}\Sigma_k(\delta Z_{ik}^{u,L\dagger} V_{kj} + V_{ik}\delta Z_{kj}^{d,L})\big], \end{cases}$$

$$\phi^- \bar{d}_j u_i : \begin{cases} C^+ = \frac{1}{\sqrt{2}s}\frac{m_{u,i}}{M_W}\big[V_{ji}^\dagger(1+\delta Z_e - \frac{\delta s}{s} + \frac{\delta m_{u,i}}{m_{u,i}} - \frac{\delta M_W}{M_W}) + \delta V_{ji}^\dagger \\ \qquad + \frac{1}{2}\Sigma_k(\delta Z_{jk}^{d,R\dagger} V_{ki}^\dagger + V_{jk}^\dagger \delta Z_{ki}^{u,R})\big], \\ C^- = -\frac{1}{\sqrt{2}s}\frac{m_{d,j}}{M_W}\big[V_{ji}^\dagger(1+\delta Z_e - \frac{\delta s}{s} + \frac{\delta m_{d,j}}{m_{d,j}} - \frac{\delta M_W}{M_W}) + \delta V_{ji}^\dagger \\ \qquad + \frac{1}{2}\Sigma_k(\delta Z_{jk}^{d,L\dagger} V_{ki}^\dagger + V_{jk}^\dagger \delta Z_{ki}^{u,L})\big], \end{cases}$$

(A.13)

$$\phi^+ \bar{\nu}_i l_j \;:\begin{cases} C^+ = -\frac{1}{\sqrt{2}s}\frac{m_{l,j}}{M_W}\delta_{ij}\big[1+\delta Z_e - \frac{\delta s}{s} + \frac{\delta m_{l,j}}{m_{l,j}} - \frac{\delta M_W}{M_W} + \frac{1}{2}(\delta Z_{ii}^{\nu,R\dagger} + \delta Z_{ii}^{l,R})\big], \\ C^- = 0, \end{cases}$$

$$\phi^- \bar{l}_j \nu_i \;:\begin{cases} C^+ = 0, \\ C^- = -\frac{1}{\sqrt{2}s}\frac{m_{l,j}}{M_W}\delta_{ij}\big[1+\delta Z_e - \frac{\delta s}{s} + \frac{\delta m_{l,j}}{m_{l,j}} - \frac{\delta M_W}{M_W} + \frac{1}{2}(\delta Z_{ii}^{l,L\dagger} + \delta Z_{ii}^{\nu,L})\big]. \end{cases} \tag{A.16}$$

(A.14)

VGG-coupling:

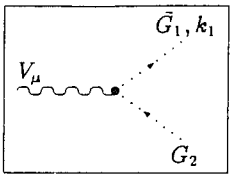

$$= ie k_{1,\mu} C$$

with the actual values of V, $\bar{G}_1$, G_2 and C

$$\begin{aligned}
&A\bar{u}^{\pm}u^{\pm} &&: C = \pm\left[1+\delta Z_e+\tfrac{1}{2}\delta Z_{AA}\right]\mp\tfrac{c}{s}\tfrac{1}{2}\delta Z_{ZA},\\
&Z\bar{u}^{\pm}u^{\pm} &&: C = \mp\tfrac{c}{s}\left[1+\delta Z_e-\tfrac{1}{c^2}\tfrac{\delta s}{s}+\tfrac{1}{2}\delta Z_{ZZ}\right]\pm\tfrac{1}{2}\delta Z_{AZ},\\
&W^{\pm}\bar{u}^{\pm}u^{Z} &&: C = \pm\tfrac{c}{s}\left[1+\delta Z_e-\tfrac{1}{c^2}\tfrac{\delta s}{s}+\tfrac{1}{2}\delta Z_W\right],\\
&W^{\pm}\bar{u}^{Z}u^{\mp} &&: C = \mp\tfrac{c}{s}\left[1+\delta Z_e-\tfrac{1}{c^2}\tfrac{\delta s}{s}+\tfrac{1}{2}\delta Z_W\right],\\
&W^{\pm}\bar{u}^{\pm}u^{\gamma} &&: C = \mp\left[1+\delta Z_e+\tfrac{1}{2}\delta Z_W\right],\\
&W^{\pm}\bar{u}^{\gamma}u^{\mp} &&: C = \pm\left[1+\delta Z_e+\tfrac{1}{2}\delta Z_W\right].
\end{aligned} \qquad \text{(A.17)}$$

SGG-coupling:

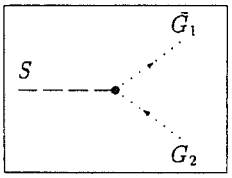

$$= ieC$$

with the actual values of S, $\bar{G}_1$, G_2 and C

$$\begin{aligned}
&H\bar{u}^{Z}u^{Z} &&: C = -\tfrac{1}{2sc^2}M_W\left[1+\delta Z_e+\tfrac{2s^2-c^2}{c^2}\tfrac{\delta s}{s}+\tfrac{1}{2}\tfrac{\delta M_W^2}{M_W^2}+\tfrac{1}{2}\delta Z_H\right],\\
&H\bar{u}^{\pm}u^{\pm} &&: C = -\tfrac{1}{2s}M_W\left[1+\delta Z_e-\tfrac{\delta s}{s}+\tfrac{1}{2}\tfrac{\delta M_W^2}{M_W^2}+\tfrac{1}{2}\delta Z_H\right],\\
&\chi\bar{u}^{\pm}u^{\pm} &&: C = \mp i\tfrac{1}{2s}M_W\left[1+\delta Z_e-\tfrac{\delta s}{s}+\tfrac{1}{2}\tfrac{\delta M_W^2}{M_W^2}\right],\\
&\phi^{\pm}\bar{u}^{Z}u^{\mp} &&: C = \tfrac{1}{2sc}M_W\left[1+\delta Z_e+\tfrac{s^2-c^2}{c^2}\tfrac{\delta s}{s}+\tfrac{1}{2}\tfrac{\delta M_W^2}{M_W^2}\right],\\
&\phi^{\pm}\bar{u}^{\pm}u^{Z} &&: C = \tfrac{s^2-c^2}{2sc}M_W\left[1+\delta Z_e+\tfrac{1}{(s^2-c^2)c^2}\tfrac{\delta s}{s}+\tfrac{1}{2}\tfrac{\delta M_W^2}{M_W^2}\right],\\
&\phi^{\pm}\bar{u}^{\pm}u^{\gamma} &&: C = M_W\left[1+\delta Z_e+\tfrac{1}{2}\tfrac{\delta M_W^2}{M_W^2}\right].
\end{aligned} \qquad \text{(A.18)}$$

B. Self Energies

In this appendix we list all self energies of the physical fields.

The gauge boson self energies read

$$\Sigma_T^{AA}(k^2) = -\frac{\alpha}{4\pi}\left\{\frac{2}{3}\sum_{f,i} N_C^f\, 2Q_f^2\left[-(k^2+2m_{f,i}^2)\, B_0(k^2, m_{f,i}, m_{f,i})\right.\right.$$
$$\left. + 2m_{f,i}^2\, B_0(0, m_{f,i}, m_{f,i}) + \frac{1}{3}k^2\right]$$
$$\left. + \{[3k^2+4M_W^2]\, B_0(k^2, M_W, M_W) - 4M_W^2\, B_0(0, M_W, M_W)\}\right\}, \tag{B.1}$$

$$\Sigma_T^{AZ}(k^2) = -\frac{\alpha}{4\pi}\left\{\frac{2}{3}\sum_{f,i} N_C^f(-Q_f)\,(g_f^+ + g_f^-)\left[-(k^2+2m_{f,i}^2)\, B_0(k^2, m_{f,i}, m_{f,i})\right.\right.$$
$$\left. + 2m_{f,i}^2\, B_0(0, m_{f,i}, m_{f,i}) + \frac{1}{3}k^2\right]$$
$$-\frac{1}{3s_W c_W}\left\{\left[\left(9c_W^2+\frac{1}{2}\right)k^2 + (12c_W^2+4)M_W^2\right] B_0(k^2, M_W, M_W)\right.$$
$$\left.\left. -(12c_W^2-2)M_W^2\, B_0(0, M_W, M_W) + \frac{1}{3}k^2\right\}\right\}, \tag{B.2}$$

$$\Sigma_T^{ZZ}(k^2) = -\frac{\alpha}{4\pi}\left\{\frac{2}{3}\sum_{f,i} N_C^f\left\{((g_f^+)^2 + (g_f^-)^2)\left[-(k^2+2m_{f,i}^2)\, B_0(k^2, m_{f,i}, m_{f,i})\right.\right.\right.$$
$$\left.\left. + 2m_{f,i}^2\, B_0(0, m_{f,i}, m_{f,i}) + \frac{1}{3}k^2\right] + \frac{3}{4s_W^2 c_W^2}\, m_{f,i}^2\, B_0(k^2, m_{f,i}, m_{f,i})\right\}$$
$$+\frac{1}{6s_W^2 c_W^2}\left\{\left[\left(18\,c_W^4 + 2c_W^2 - \frac{1}{2}\right)k^2 + (24c_W^4 + 16c_W^2 - 10)M_W^2\right] B_0(k^2, M_W, M_W)\right.$$
$$\left. -(24c_W^4 - 8c_W^2 + 2)M_W^2\, B_0(0, M_W, M_W) + (4c_W^2 - 1)\frac{1}{3}k^2\right\}$$
$$+\frac{1}{12s_W^2 c_W^2}\left\{(2M_H^2 - 10M_Z^2 - k^2)\, B_0(k^2, M_Z, M_H)\right.$$
$$-2M_Z^2\, B_0(0, M_Z, M_Z) - 2M_H^2\, B_0(0, M_H, M_H)$$
$$\left.\left. -\frac{(M_Z^2 - M_H^2)^2}{k^2}\,(B_0(k^2, M_Z, M_H) - B_0(0, M_Z, M_H)) - \frac{2}{3}k^2\right\}\right\}, \tag{B.3}$$

$$\Sigma_T^W(k^2) = -\frac{\alpha}{4\pi}\left\{\frac{2}{3}\frac{1}{2s_W^2}\sum_i\left[-\left(k^2-\frac{m_{l,i}^2}{2}\right)B_0(k^2,0,m_{l,i})+\frac{1}{3}k^2\right.\right.$$
$$\left.+m_{l,i}^2\,B_0(0,m_{l,i},m_{l,i})+\frac{m_{l,i}^4}{2k^2}\left(B_0(k^2,0,m_{l,i})-B_0(0,0,m_{l,i})\right)\right]$$
$$+\frac{2}{3}\frac{1}{2s_W^2}3\sum_{ij}|V_{ij}|^2\left[-\left(k^2-\frac{m_{u,i}^2+m_{d,j}^2}{2}\right)B_0(k^2,m_{u,i},m_{d,j})+\frac{1}{3}k^2\right.$$
$$+m_{u,i}^2\,B_0(0,m_{u,i},m_{u,i})+m_{d,j}^2\,B_0(0,m_{d,j},m_{d,j})$$
$$\left.+\frac{(m_{u,i}^2-m_{d,j}^2)^2}{2k^2}\left(B_0(k^2,m_{u,i},m_{d,j})-B_0(0,m_{u,i},m_{d,j})\right)\right]$$
$$+\frac{2}{3}\left\{(2M_W^2+5k^2)\,B_0(k^2,M_W,\lambda)-2M_W^2\,B_0(0,M_W,M_W)\right.$$
$$\left.-\frac{M_W^4}{k^2}\left(B_0(k^2,M_W,\lambda)-B_0(0,M_W,\lambda)\right)+\frac{1}{3}k^2\right\}$$
$$+\frac{1}{12s_W^2}\left\{\left[(40c_W^2-1)k^2+(16c_W^2+54-10c_W^{-2})M_W^2\right]B_0(k^2,M_W,M_Z)\right.$$
$$-(16c_W^2+2)\left[M_W^2\,B_0(0,M_W,M_W)+M_Z^2\,B_0(0,M_Z,M_Z)\right]+(4c_W^2-1)\frac{2}{3}k^2$$
$$\left.-(8c_W^2+1)\frac{(M_W^2-M_Z^2)^2}{k^2}\left(B_0(k^2,M_W,M_Z)-B_0(0,M_W,M_Z)\right)\right\}$$
$$+\frac{1}{12s_W^2}\left\{(2M_H^2-10M_W^2-k^2)\,B_0(k^2,M_W,M_H)\right.$$
$$-2M_W^2\,B_0(0,M_W,M_W)-2M_H^2\,B_0(0,M_H,M_H)$$
$$\left.\left.-\frac{(M_W^2-M_H^2)^2}{k^2}\left(B_0(k^2,M_W,M_H)-B_0(0,M_W,M_H)\right)-\frac{2}{3}k^2\right\}\right\}. \tag{B.4}$$

For the self energy of the physical Higgs boson we obtain

$$\Sigma_T^H(k^2) = -\frac{\alpha}{4\pi}\left\{\sum_{f,i}N_C^f\frac{m_{f,i}^2}{2s_W^2M_W^2}\left[2A_0(m_{f,i})+(4m_{f,i}^2-k^2)\,B_0(k^2,m_{f,i},m_{f,i})\right]\right.$$
$$-\frac{1}{2s_W^2}\left[\left(6M_W^2-2k^2+\frac{M_H^4}{2M_W^2}\right)B_0(k^2,M_W,M_W)+\left(3+\frac{M_H^2}{2M_W^2}\right)A_0(M_W)-6M_W^2\right]$$
$$-\frac{1}{4s_W^2c_W^2}\left[\left(6M_Z^2-2k^2+\frac{M_H^4}{2M_Z^2}\right)B_0(k^2,M_Z,M_Z)+\left(3+\frac{M_H^2}{2M_Z^2}\right)A_0(M_Z)-6M_Z^2\right]$$
$$\left.-\frac{3}{8s_W^2}\left[3\frac{M_H^4}{M_W^2}B_0(k^2,M_H,M_H)+\frac{M_H^2}{M_W^2}A_0(M_H)\right\}\right]. \tag{B.5}$$

The fermion self energies are given by

$$\Sigma_{ij}^{f,L}(p^2) = -\frac{\alpha}{4\pi}\left\{\delta_{ij}Q_f^2\left[2B_1(p^2, m_{f,i}, \lambda)+1\right]\right.$$
$$+\delta_{ij}(g_f^-)^2\left[2B_1(p^2, m_{f,i}, M_Z)+1\right]$$
$$+\delta_{ij}\frac{1}{2s_W^2}\frac{1}{2}\frac{m_{f,i}^2}{M_W^2}\left[B_1(p^2, m_{f,i}, M_Z)+B_1(p^2, m_{f,i}, M_H)\right]$$
$$\left.+\frac{1}{2s_W^2}\sum_k V_{ik}V_{kj}^{\dagger}\left[\left(2+\frac{m_{f',k}^2}{M_W^2}\right)B_1(p^2, m_{f',k}, M_Z)+1\right]\right\}, \tag{B.6}$$

$$\Sigma_{ij}^{f,R}(p^2) = -\frac{\alpha}{4\pi}\left\{\delta_{ij}Q_f^2\left[2B_1(p^2, m_{f,i}, \lambda)+1\right]\right.$$
$$+\delta_{ij}(g_f^+)^2\left[2B_1(p^2, m_{f,i}, M_Z)+1\right]$$
$$+\delta_{ij}\frac{1}{2s_W^2}\frac{1}{2}\frac{m_{f,i}^2}{M_W^2}\left[B_1(p^2, m_{f,i}, M_Z)+B_1(p^2, m_{f,i}, M_H)\right]$$
$$\left.+\frac{1}{2s_W^2}\frac{m_{f,i}m_{f,j}}{M_W^2}\sum_k V_{ik}V_{kj}^{\dagger}B_1(p^2, m_{f',k}, M_W)\right\}, \tag{B.7}$$

$$\Sigma_{ij}^{f,S}(p^2) = -\frac{\alpha}{4\pi}\left\{\delta_{ij}Q_f^2\left[4B_0(p^2, m_{f,i}, \lambda)-2\right]\right.$$
$$+\delta_{ij}g_f^+g_f^-\left[4B_0(p^2, m_{f,i}, M_Z)-2\right]$$
$$+\delta_{ij}\frac{1}{2s_W^2}\frac{1}{2}\frac{m_{f,i}^2}{M_W^2}\left[B_0(p^2, m_{f,i}, M_Z)-B_0(p^2, m_{f,i}, M_H)\right]$$
$$\left.+\frac{1}{2s_W^2}\sum_k V_{ik}V_{kj}^{\dagger}\frac{m_{f',k}^2}{M_W^2}B_0(p^2, m_{f',k}, M_W)\right\}, \tag{B.8}$$

f' is the isospin partner of the fermion f and N_C^f the colour factor. i, j, k run over the fermion generations. For down-type quarks $V_{ik}V_{kj}^{\dagger}$ has to be replaced by $V_{ik}^{\dagger}V_{kj}$.

The two-point function B_0 was given in Sect. 4.3. For B_1 we find

$$B_1(p^2, m_0, m_1) = \frac{m_1^2-m_0^2}{2p^2}\left(B_0(p^2, m_0, m_1)-B_0(0, m_0, m_1)\right)$$
$$-\tfrac{1}{2}B_0(p^2, m_0, m_1). \tag{B.9}$$

For the field renormalization constants one needs in addition the derivatives of the self energies with respect to k^2 or p^2, respectively. These are easily obtained from the expressions above. $\frac{\partial B_0}{\partial p^2}$ was given in Sect. 4.3, $\frac{\partial B_1}{\partial p^2}$ can be calculated from (B.9) as

$$\frac{\partial}{\partial p^2} B_1(p^2, m_0, m_1) = -\frac{m_1^2 - m_0^2}{2p^4} (B_0(p^2, m_0, m_1) - B_0(0, m_0, m_1)) + \frac{m_1^2 - m_0^2 - p^2}{2p^2} \frac{\partial}{\partial p^2} B_0(p^2, m_0, m_1). \tag{B.10}$$

These derivatives become IR-singular for $m_0^2 = p^2$ and $m_1^2 = 0$ or vice versa. This leads to IR-singular contributions in the field renormalization constants of charged particles arising from photonic corrections to the corresponding self energies. Because these reduce to very simple expressions we give the photonic contributions to the field renormalization constants of the W-boson and the charged fermions explicitly

$$\delta Z_W|_{\text{photonic}} = -\frac{\alpha}{\pi} \log \frac{\lambda}{M_W} + \frac{\alpha}{6\pi} \left(\frac{1}{3} + 5 \left(\Delta + 1 - \log \frac{M_W^2}{\mu^2} \right) \right), \tag{B.11}$$

$$\delta Z_{ii}^{f,L}|_{\text{photonic}} = \delta Z_{ii}^{f,R}|_{\text{photonic}} = -\frac{\alpha}{4\pi} Q_f^2 \left[\Delta - \log \frac{m_{f,i}^2}{\mu^2} + 4 + 4 \log \frac{\lambda}{m_{f,i}} \right]. \tag{B.12}$$

C. Vertex Formfactors

The vertex formfactors $\mathcal{V}$, $\mathcal{W}$, $\mathcal{X}$, can be expressed by the scalar one-loop integrals $B_0(m_0^2, M_1, M_2)$, $C_0(m_1^2, m_0^2, m_2^2, M_0, M_1, M_2)$ and the scalar coefficients of the vector and tensor integrals $B_1(m_0^2, M_1, M_2)$, $C_{i(j)}(m_1^2, m_0^2, m_2^2, M_0, M_1, M_2)$

$$\mathcal{V}_a(m_1^2, m_0^2, m_2^2, M_0, M_1, M_2) = B_0(m_0^2, M_1, M_2) - 2 - (M_0^2 - m_1^2 - M_1^2) C_1 - (M_0^2 - m_2^2 - M_2^2) C_2 - 2(m_0^2 - m_1^2 - m_2^2)(C_1 + C_2 + C_0), \tag{C.1}$$

$$\mathcal{V}_b^-(m_1^2, m_0^2, m_2^2, M_0, M_1, M_2) = 3B_0(m_0^2, M_1, M_2) + 4M_0^2 C_0 + (4m_1^2 + 2m_2^2 - 2m_0^2 + M_0^2 - M_1^2) C_1 + (4m_2^2 + 2m_1^2 - 2m_0^2 + M_0^2 - M_2^2) C_2, \tag{C.2}$$

$$\mathcal{V}_b^+(m_1^2, m_0^2, m_2^2, M_0, M_1, M_2) = 3m_1^2 C_0, \tag{C.3}$$

$$\mathcal{V}_c(m_1^2, m_0^2, m_2^2, M_0, M_1, M_2) = -2 \frac{m_1^2 m_2^2}{M_W^2} (C_1 + C_2 + 2C_0), \tag{C.4}$$

$$\mathcal{V}_d(m_1^2, m_0^2, m_2^2, M_0, M_1, M_2) = m_1^2 (C_1 - C_0), \tag{C.5}$$

$$\mathcal{V}_e(m_1^2, m_0^2, m_2^2, M_0, M_1, M_2) = \frac{m_1^2}{M_W^2} C_{00}, \tag{C.6}$$

$$\mathcal{V}_f^-(m_1^2, m_0^2, m_2^2, M_0, M_1, M_2) = m_1^2 C_0 + m_2^2 C_2, \tag{C.7}$$

$$\mathcal{V}_f^+(m_1^2, m_0^2, m_2^2, M_0, M_1, M_2) = m_1^2 C_1, \tag{C.8}$$

$$\mathscr{W}_a^-(m_1^2, m_0^2, m_2^2, M_0, M_1, M_2) = 2(C_1 + C_2 + C_0), \tag{C.9}$$

$$\mathscr{W}_a^+(m_1^2, m_0^2, m_2^2, M_0, M_1, M_2) = -2C_0, \tag{C.10}$$

$$\mathscr{W}_b^-(m_1^2, m_0^2, m_2^2, M_0, M_1, M_2) = 3(C_1 + C_2), \tag{C.11}$$

$$\mathscr{W}_b^+(m_1^2, m_0^2, m_2^2, M_0, M_1, M_2) = 3C_0, \tag{C.12}$$

$$\mathscr{W}_c^-(m_1^2, m_0^2, m_2^2, M_0, M_1, M_2) = \frac{1}{2M_W^2}\left[B_0(m_0^2, M_1, M_2) - 1 - M_0^2(C_1 + C_2)\right], \tag{C.13}$$

$$\mathscr{W}_c^+(m_1^2, m_0^2, m_2^2, M_0, M_1, M_2) = \frac{2}{M_W^2}\left[m_1^2 C_1 + m_2^2 C_2\right], \tag{C.14}$$

$$\mathscr{W}_d(m_1^2, m_0^2, m_2^2, M_0, M_1, M_2) = -C_2, \tag{C.15}$$

$$\mathscr{W}_e(m_1^2, m_0^2, m_2^2, M_0, M_1, M_2) = \frac{-1}{M_W^2} C_{00}, \tag{C.16}$$

$$\mathscr{W}_f^-(m_1^2, m_0^2, m_2^2, M_0, M_1, M_2) = -C_1, \tag{C.17}$$

$$\mathscr{W}_f^+(m_1^2, m_0^2, m_2^2, M_0, M_1, M_2) = -C_2 - C_0, \tag{C.18}$$

$$\mathscr{X}_a^-(m_1^2, m_0^2, m_2^2, M_0, M_1, M_2) = -4[C_{11} + C_{12} + 2C_1 + C_2 + C_0], \tag{C.19}$$

$$\mathscr{X}_a^+(m_1^2, m_0^2, m_2^2, M_0, M_1, M_2) = 4[C_1 + C_2 + C_0], \tag{C.20}$$

$$\mathscr{X}_b^-(m_1^2, m_0^2, m_2^2, M_0, M_1, M_2) = 2[2C_{11} + 2C_{12} - C_2], \tag{C.21}$$

$$\mathscr{X}_b^+(m_1^2, m_0^2, m_2^2, M_0, M_1, M_2) = 6[C_1 + C_2], \tag{C.22}$$

$$\mathscr{X}_c^-(m_1^2, m_0^2, m_2^2, M_0, M_1, M_2) = -2\frac{m_2^2}{M_W^2}[C_{22} + C_{12}], \tag{C.23}$$

$$\mathscr{X}_c^+(m_1^2, m_0^2, m_2^2, M_0, M_1, M_2) = -4\frac{m_2^2}{M_W^2} C_2, \tag{C.24}$$

$$\mathscr{X}_d(m_1^2, m_0^2, m_2^2, M_0, M_1, M_2) = 2C_2, \tag{C.25}$$

$$\mathscr{X}_e^-(m_1^2, m_0^2, m_2^2, M_0, M_1, M_2) = \frac{m_1^2}{M_W^2}[C_{11} + C_{12} + C_1], \tag{C.26}$$

$$\mathscr{X}_e^0(m_1^2, m_0^2, m_2^2, M_0, M_1, M_2) = [C_{22} + C_{12} + C_2], \tag{C.27}$$

$$\mathscr{X}_e^+(m_1^2, m_0^2, m_2^2, M_0, M_1, M_2) = \frac{m_1^2}{M_W^2}[C_1 + C_2 + C_0], \tag{C.28}$$

$$\mathscr{X}_f(m_1^2, m_0^2, m_2^2, M_0, M_1, M_2) = -2C_1. \tag{C.29}$$

Using the reduction methods described in Chap. 4 the vector and tensor coefficients can be expressed by scalar integrals. For illustration we give the explicit reduction formulae.

The vertex function is defined as

$$C_{\dots} = C_{\dots}(p_1, p_2, M_0, M_1, M_2) = C_{\dots}(m_1^2, m_0^2, m_2^2, M_0, M_1, M_2)$$
$$= \frac{(2\pi\mu)^{4-D}}{i\pi^2} \int d^D q \, \frac{\dots}{[q^2 - M_0^2]\,[(q+p_1)^2 - M_1^2]\,[(q+p_2)^2 - M_2^2]} \tag{C.30}$$

with

$$p_1^2 = m_1^2, \quad p_2^2 = m_2^2, \quad p_1 p_2 = -\frac{1}{2}(m_0^2 - m_1^2 - m_2^2). \tag{C.31}$$

For the three-point vector functions (4.18) yields ($P = 1$, $M = N - 1 = 2$)

$$C_k = T_k^3 = (X_2^{-1})_{kk'} R^{3,k'} \tag{C.32}$$

with $k, k' = 1, 2$ and

$$X_2 = \begin{pmatrix} m_1^2 & \frac{1}{2}(m_1^2 + m_2^2 - m_0^2) \\ \frac{1}{2}(m_1^2 + m_2^2 - m_0^2) & m_2^2 \end{pmatrix}. \tag{C.33}$$

Evaluating X_2^{-1} this gives

$$C_1 = -\frac{4}{\kappa^2}\left[m_2^2 R^{3,1} + \frac{1}{2}(m_0^2 - m_1^2 - m_2^2) R^{3,2}\right],$$
$$C_2 = -\frac{4}{\kappa^2}\left[\frac{1}{2}(m_0^2 - m_1^2 - m_2^2) R^{3,1} + m_1^2 R^{3,2}\right], \tag{C.34}$$

where

$$\kappa = \kappa(m_0^2, m_1^2, m_2^2), \tag{C.35}$$

from (4.28). The R's are obtained from (4.19) as

$$R^{3,1} = \frac{1}{2}\left[B_0(m_2^2, M_0, M_2) - (m_1^2 - M_1^2 + M_0^2) C_0 - B_0(m_0^2, M_2, M_1)\right],$$
$$R^{3,2} = \frac{1}{2}\left[B_0(m_1^2, M_0, M_1) - (m_2^2 - M_2^2 + M_0^2) C_0 - B_0(m_0^2, M_2, M_1)\right]. \tag{C.36}$$

The tensor coefficients are evaluated analogously as ($P=2$, $M=2$)

$$C_{00} = \frac{1}{D-2}\,[R^{3,00} - R_1^{3,1} - R_2^{3,2}]$$

$$C_{ki} = T_{ki}^3 = (X_2^{-1})_{kk'}\,[R_i^{3,k'} - \delta_i^{k'}\,C_{00}] \tag{C.37}$$

or more explicitly

$$C_{00} = \frac{1}{4}\,[B_0(m_0^2, M_2, M_1) + (M_0^2 - M_1^2 + m_1^2)\,C_1$$
$$+ (M_0^2 - M_2^2 + m_2^2)\,C_2 + 1 + 2\,M_0^2\,C_0], \tag{C.30}$$

$$C_{11} = -\frac{4}{\kappa^2}\left[m_2^2(R_1^{3,1} - C_{00}) + \frac{1}{2}\,(m_0^2 - m_1^2 - m_2^2)\,R_1^{3,2}\right], \tag{C.31}$$

$$C_{21} = -\frac{4}{\kappa^2}\left[\frac{1}{2}\,(m_0^2 - m_1^2 - m_2^2)\,(R_1^{3,1} - C_{00}) + m_1^2\,R_1^{3,2}\right], \tag{C.32}$$

$$C_{12} = -\frac{4}{\kappa^2}\left[m_2^2\,R_2^{3,1} + \frac{1}{2}\,(m_0^2 - m_1^2 - m_2^2)\,(R_2^{3,2} - C_{00})\right], \tag{C.33}$$

$$C_{22} = -\frac{4}{\kappa^2}\left[\frac{1}{2}\,(m_0^2 - m_1^2 - m_2^2)\,R_2^{3,1} + m_1^2(R_2^{3,2} - C_{00})\right] \tag{C.38}$$

with

$$R^{3,00} = M_0^2\,C_0 + B_0(m_0^2, M_2, M_1),$$

$$R_1^{3,1} = \frac{1}{2}\,[\qquad\qquad -(m_1^2 - M_1^2 + M_0^2)\,C_1 - B_1(m_0^2, M_2, M_1)], \tag{C.34}$$

$$R_2^{3,1} = \frac{1}{2}\,[B_1(m_2^2, M_0, M_2) - (m_1^2 - M_1^2 + M_0^2)\,C_2 + (B_0 + B_1)\,(m_0^2, M_2, M_1)],$$

$$R_1^{3,2} = \frac{1}{2}\,[B_1(m_1^2, M_0, M_1) - (m_2^2 - M_2^2 + M_0^2)\,C_1 - B_1(m_0^2, M_2, M_1)], \tag{C.35}$$

$$R_2^{3,2} = \frac{1}{2}\,[\qquad\qquad -(m_2^2 - M_2^2 + M_0^2)\,C_2 + (B_0 + B_1)\,(m_0^2, M_2, M_1)]. \tag{C.39}$$

Note that $C_{12} = C_{21}$ can be calculated in two different ways. In the evaluation of C_{00} we used (4.55).

B_1 was given in (B.9). The results for the scalar integrals can again be found in Sect. 4.3. (C.36)

D. Bremsstrahlung Integrals

For tl

For the decay width of a massive particle with momentum p_0 and mass m_0 into two massive particles with momenta p_1, p_2 and masses m_1, m_2 and a photon with momentum q and mass λ we need the following phase space integrals

$$I^{j_1,\dots,j_m}_{i_1,\dots,i_n}(m_0, m_1, m_2) = \frac{1}{\pi^2}\int \frac{d^3p_1}{2p_{10}}\frac{d^3p_2}{2p_{20}}\frac{d^3q}{2q_0}\,\delta(p_0-p_1-p_2-q)\,\frac{(\pm 2qp_{j_1})\cdots(\pm 2qp_{j_m})}{(\pm 2qp_{i_1})\cdots(\pm 2qp_{i_n})}. \tag{D.1}$$

Here j_k, $i_l = 0, 1, 2$ and the plus signs belongs to p_1, p_2, the minus signs to p_0.

Introducing the abbreviations

$$\kappa = \kappa(m_0^2, m_1^2, m_2^2), \tag{D.2}$$

as defined in (4.28) and

$$\beta_0 = \frac{m_0^2-m_1^2-m_2^2+\kappa}{2m_1m_2},$$

$$\beta_1 = \frac{m_0^2-m_1^2+m_2^2-\kappa}{2m_0m_2}, \quad \beta_2 = \frac{m_0^2+m_1^2-m_2^2-\kappa}{2m_0m_1}, \tag{D.3}$$

with

$$\beta_0\beta_1\beta_2 = 1, \tag{D.4}$$

we get compact expressions for the final results. From (D.1) it is evident that the integrals with the indices 1 and 2 interchanged are obtained by interchanging m_1 and m_2. We list only the independent integrals. The IR-singular ones are given by

$$I_{00} = \frac{1}{4m_0^4}\left[\kappa\log\left(\frac{\kappa^2}{\lambda m_0m_1m_2}\right)-\kappa-(m_1^2-m_2^2)\log\left(\frac{\beta_1}{\beta_2}\right)-m_0^2\log(\beta_0)\right], \tag{D.5}$$

$$I_{11} = \frac{1}{4m_1^2m_0^2}\left[\kappa\log\left(\frac{\kappa^2}{\lambda m_0m_1m_2}\right)-\kappa-(m_0^2-m_2^2)\log\left(\frac{\beta_0}{\beta_2}\right)-m_1^2\log(\beta_1)\right], \tag{D.6}$$

$$I_{01} = \frac{1}{4m_0^2}\left[-2\log\left(\frac{\lambda m_0m_1m_2}{\kappa^2}\right)\log(\beta_2)+2\log^2(\beta_2)-\log^2(\beta_0)-\log^2(\beta_1) + 2Sp(1-\beta_2^2)-Sp(1-\beta_0^2)-Sp(1-\beta_1^2)\right], \tag{D.7}$$

$$I_{12} = -I_{01}-I_{02} = \frac{1}{4m_0^2}\left[-2\log\left(\frac{\lambda m_0m_1m_2}{\kappa^2}\right)\log(\beta_0)+2\log^2(\beta_0)-\log^2(\beta_1)-\log^2(\beta_2) + 2Sp(1-\beta_0^2)-Sp(1-\beta_1^2)-Sp(1-\beta_2^2)\right]. \tag{D.8}$$

Note

For the IR finite integrals we obtain

$$I = \frac{1}{4m_0^2}\left[\frac{\kappa}{2}(m_0^2+m_1^2+m_2^2)+2m_0^2m_1^2\log(\beta_2)+2m_0^2m_2^2\log(\beta_1)+2m_1^2m_2^2\log(\beta_0)\right], \tag{D.9}$$

$$I_0 = \frac{1}{4m_0^2}\left[-2m_1^2\log(\beta_2)-2m_2^2\log(\beta_1)-\kappa\right], \tag{D.10}$$

$$I_0^1 = \frac{1}{4m_0^2}\left[m_0^4\log(\beta_2)-m_2^2(2m_0^2-2m_1^2+m_2^2)\log(\beta_1) - \frac{\kappa}{4}(m_0^2-3m_1^2+5m_2^2)\right], \tag{D.11}$$

$$I_1^0 = \frac{1}{4m_0^2}\left[m_1^4\log(\beta_2)-m_2^2(2m_1^2-2m_0^2+m_2^2)\log(\beta_0) - \frac{\kappa}{4}(m_1^2-3m_0^2+5m_2^2)\right], \tag{D.12}$$

$$\begin{aligned} I_2^1 &= -I-I_2^0 \\ &= \frac{1}{4m_0^2}\left[m_1^4\log(\beta_0)-m_0^2(2m_2^2-2m_1^2+m_0^2)\log(\beta_1) - \frac{\kappa}{4}(m_2^2-3m_1^2+5m_0^2)\right], \end{aligned} \tag{D.13}$$

$$I_{00}^{12} = -\frac{1}{4m_0^2}\left[m_1^4\log(\beta_2)+m_2^4\log(\beta_1)+\frac{\kappa^3}{6m_0^2}+\frac{\kappa}{4}(3m_1^2+3m_2^2-m_0^2)\right], \tag{D.14}$$

$$I_{11}^{02} = -\frac{1}{4m_0^2}\left[m_0^4\log(\beta_2)+m_2^4\log(\beta_0)+\frac{\kappa^3}{6m_1^2}+\frac{\kappa}{4}(3m_0^2+3m_2^2-m_1^2)\right], \tag{D.15}$$

$$I_{11}^{00} = -I_1^0-I_{11}^{02} = \frac{1}{4m_0^2}\left[2m_2^2(m_1^2+m_2^2-m_0^2)\log(\beta_0)+\frac{\kappa^3}{6m_1^2}+2\kappa m_2^2\right], \tag{D.16}$$

$$I_{00}^{11} = -I_0^1-I_{00}^{12} = \frac{1}{4m_0^2}\left[2m_2^2(m_0^2+m_2^2-m_1^2)\log(\beta_1)+\frac{\kappa^3}{6m_0^2}+2\kappa m_2^2\right], \tag{D.17}$$

$$I_{11}^{22} = -I_1^2-I_{11}^{02} = \frac{1}{4m_0^2}\left[2m_0^2(m_0^2+m_1^2-m_2^2)\log(\beta_2)+\frac{\kappa^3}{6m_1^2}+2\kappa m_0^2\right]. \tag{D.18}$$

Note the symmetries in $0 \leftrightarrow 1$ and $0 \leftrightarrow 2$.

References

[1] S. L. GLASHOW, Nucl. Phys. **22** (1961) 579.
[2] S. WEINBERG, Phys. Rev. Lett. **19** (1967) 1264.
[3] A. SALAM, in Elementary Particle Theory, ed. N. Svartholm (Almqvist and Wiksell, Stockholm, 1968), p. 367.
[4] S. L. GLASHOW, J. ILLIOPOULOS, L. MAIANI, Phys. Rev. **D 2** (1970) 1285.
[5] F. DYDAK, in "Proceedings of the 25th International Conference on High Energy Physics", eds. K. K. Phua and Y. Yamaguchi, World Scientific, Singapore (1991), Vol. 1, p. 3.
[6] M. DAVIER et al., in [63], p. 120, Vol. 1.
[7] M. VELTMAN, Nucl. Phys. **B123** (1977) 89.
[8] J. ELLIS and G. L. FOGLI, Phys. Lett. **249 B** (1990) 543.
[9] A. C. K. HSIEH and E. YEHUDAI, SLAC-PUB-5576 (1991).
[10] E. E. BOOS et al.; in "New computing techniques in physics research", eds. D. Perret-Gallix and W. Wojcik, Paris (1990), p. 573; Moscow State University preprint MGU-89-63/140.
[11] J. KÜBLBECK, M. BÖHM and A. DENNER, Comp. Phys. Comm. **60** (1990) 165.
[12] R. MERTIG, M. BÖHM and A. DENNER, Comp. Phys. Comm. **64** (1991) 345.
[13] "Z-physics at LEP", CERN-89-08 eds. G. Altarelli, R. Kleiss and C. Verzegnassi, Vol. 1–3 and references therein.
[14] W. BEENAKKER, F. A. BERENDS and T. SACK, Nucl. Phys. **B367** (1991) 287.
[15] R. KLEISS, in [13], Vol. 3, p. 1 and references therein.
[16] P. W. HIGGS, Phys. Lett. **12** (1964) 132; Phys. Rev. Lett. **13** (1964) 508; Phys. Rev. **145** (1966) 1156;
R. BROUT and F. ENGLERT, Phys. Rev. Lett. **13** (1964) 321;
T. W. B. KIBBLE, Phys. Rev. **155** (1967) 1554.
[17] G. 'T HOOFT, Nucl. Phys. **B33** (1971) 173; **B35** (1971) 167.
[18] G. PASSARINO and M. VELTMAN, Nucl. Phys. **B160** (1979) 151;
M. CONSOLI, Nucl. Phys. **B160** (1979) 208;
M. VELTMAN, Phys. Lett. **91 B** (1980) 95;
M. GREEN and M. VELTMAN, Nucl. Phys. **B169** (1980) 137; E: Nucl. Phys. **B175** (1980) 547.
[19] D. C. KENNEDY and B. W. LYNN, Nucl. Phys. **B322** (1989) 1;
B. W. LYNN, SLAC-PUB 5077 (1989) and SU-ITP-867 (1989);
D. C. KENNEDY, Nucl. Phys. **B351** (1991) 81;
M. KURODA, G. MOULTAKA and D. SCHILDKNECHT, Nucl. Phys. **B350** (1991) 25.
[20] D. A. ROSS and J. C. TAYLOR, Nucl. Phys. **B51** (1979) 25.
[21] D. YU. BARDIN, P. CH. CHRISTOVA and O. M. FEDERENKO, Nucl. Phys. **175** (1980) 435; Nucl. Phys. **197** (1982) 1.
[22] J. FLEISCHER and F. JEGERLEHNER, Phys. Rev. **D 23** (1981) 2001.
[23] S. SAKAKIBARA, Phys. Rev. **D 24** (1981) 1149.
[24] K. I. AOKI, Z. HIOKI, R. KAWABE, M. KONUMA and T. MUTA, Prog. Theor. Phys. **64** (1980) 707; **65** (1981) 1001; Suppl. Prog. Theor. Phys. **73** (1982) 1.
[25] M. BÖHM, W. HOLLIK and H. SPIESBERGER, Fortschr. Phys. **34** (1986) 687.
[26] A. SIRLIN, Phys. Rev. **D 22** (1980) 971;
W. J. MARCIANO and A. SIRLIN, Phys. Rev. **D 22** (1980) 2695;
A. SIRLIN and W. J. MARCIANO, Nucl. Phys. **B189** (1981) 442.
[27] A. DENNER and T. SACK, Nucl. Phys. **B347** (1990) 203.
[28] G. 'T HOOFT and M. VELTMAN, Nucl. Phys. **B153** (1979) 365.
[29] D. B. MELROSE, Nuovo Cimento **XL A** (1965) 181.
[30] R. G. STUART, Comp. Phys. Comm. **48** (1988) 367 and 56 (1990) 337.
[31] G. J. VAN OLDENBORGH and J. A. M. VERMASEREN, Z. Phys. **C46** (1990) 425;
G. J. VAN OLDENBORGH, Ph. D. Thesis, Amsterdam 1990;
G. J. VAN OLDENBORGH, Comp. Phys. Comm. **B66** (1991) 1.
[32] A. DENNER, U. NIERSTE and R. SCHARF, Nucl. Phys. **B367** (1991) 637.
[33] B. GRZADKOWSKI, P. KRAWCZYK, J. H. KÜHN and R. G. STUART, Nucl. Phys. **B281** (1987) 18;
R. J. GUTH and J. H. KÜHN, Nucl. Phys. **B368** (1992) 38.
[34] H. ECK, Diploma thesis, Würzburg (1990).

[35] *SCHOONSHIP* by M. VELTMAN, see H. STRUBBE, Comp. Phys. Comm. **8** (1974) 1;
REDUCE by A. C. HEARN, see *REDUCE* User's Manual, Rand Corporation, 1985;
FORM by J. A. M. VERMASEREN, see *FORM* User's guide, Amsterdam (1990).
[36] F. BLOCH and A. NORDSIECK, Phys. Rev. **52** (1937) 54.
[37] M. GRECO, G. PANCHERI and Y. SRIVASTAVA, Nucl. Phys. **B171** (1980) 118;
E: Nucl. Phys. **B197** (1982) 543.
[38] M. BÖHM and W. HOLLIK, Nucl. Phys. **B204** (1982) 45.
[39] Particle Data Group, Phys. Lett. **239B** (1990) 1.
[40] H. HARARI and M. LEURER, Phys. Lett. **B181** (1986) 123.
[41] H. BURKHARDT, F. JEGERLEHNER, G. PENSO and C. VERZEGNASSI, Z. Phys. **C43** (1989) 497;
G. BURGERS and F. JEGERLEHNER, in [13], Vol. 1, p. 55.
[42] W. J. MARCIANO, Phys. Rev. **D20** (1979) 274;
A. SIRLIN, Phys. Rev. **D29** (1984) 89.
[43] W. BEENAKKER, F. A. BERENDS and W. L. VAN NEERVEN, in "Radiative Corrections for e^+e^--collisions", ed. J. H. Kühn, Springer-Verlag, Berlin, Heidelberg (1989).
[44] M. CONSOLI, W. HOLLIK and F. JEGERLEHNER, Phys. Lett. **227B** (1989) 167;
M. CONSOLI and W. HOLLIK, in [13], Vol. 1, p. 7.
[45] J. J. VAN DER BIJ and F. HOOGEVEEN, Nucl. Phys. **B283** (1987) 477.
[46] E. LONGO et al., in [63], p. 85.
[47] P. ROUDEAU et al., in [63], p. 49.
[48] D. ALBERT, W. J. MARCIANO, D. WYLER and Z. PARSA, Nucl. Phys. **B166** (1980) 460;
K. INOUE, A. KAKUTO, H. KOMATSU and S. TAKESHITA, Prog. Theor. Phys. **64** (1980) 1008;
T. H. CHANG, K. J. F. GAEMERS and W. L. VAN NEERVEN, Nucl. Phys. **B202** (1982) 407.
[49] D. YU. BARDIN, S. RIEMANN and T. RIEMANN, Z. Phys. **C32** (1986) 121.
[50] F. JEGERLEHNER, Z. Phys. **C32** (1986) 425 and in [51].
[51] Proc. of the 11th International School of Theoretical Physics "Testing of the Standard Model", Szczyrk-Bila (Poland) 1987; eds. M. Zrałek and R. Manka, World Scientific, Singapore (1988).
[52] F. A. BERENDS and R. KLEISS, Z. Phys. **C27** (1985) 365.
[53] J. FLEISCHER and F. JEGERLEHNER, Z. Phys. **C26** (1985) 629.
[54] T. ALVAREZ, A. LEITES and J. TERRON, Nucl. Phys. **B301** (1988) 1.
[55] A. DENNER and T. SACK, Z. Phys. **C46** (1990) 653.
[56] T. KINOSHITA, J. Math. Phys. **3** (1962) 650;
T. D. LEE and M. NAUENBERG, Phys. Rev. **133** (1964) 1549.
[57] CDF collaboration, K. Sliwa, in Proceedings of the XXV Rencontres de Moriond, Electroweak and Unified Theories, Les Arcs, March 1990.
[58] M. JEŻABEK and J. H. KÜHN, Nucl. Phys. **B314** (1989) 1.
[59] J. LIU and Y.-P. YAO, Int. J. Mod. Phys. **A6** (1991) 4925.
[60] A. DENNER and T. SACK, Nucl. Phys. **B358** (1991) 46.
[61] G. EILAM, R. R. MENDEL, R. MIGNERON and A. SONI, Phys. Rev. Lett. **66** (1991) 3105.
[62] "Physics at LEP", CERN-86-02, eds. J. Ellis and R. Peccei, Vol. 2.
[63] "ECFA Workshop on LEP200", CERN-87-08, eds. A. Böhm and W. Hoogland, Vol. 1.
[64] M. LEMOINE and M. VELTMAN, Nucl. Phys. **B164** (1980) 445.
[65] R. PHILIPPE, Phys. Rev. **D26** (1982) 1588.
[66] M. BÖHM, A. DENNER, T. SACK, W. BEENAKKER, F. A. BERENDS and H. KUIJF, Nucl. Phys. **B304** (1988) 463.
[67] J. FLEISCHER, F. JEGERLEHNER and M. ZRAŁEK, Z. Phys. **C42** (1989) 409 and in [51].
[68] W. BEENAKKER, K. KOŁODZIEJ and T. SACK, Phys. Lett. **258B** (1991) 469.
[69] K. KOŁODZIEJ and M. ZRAŁEK, Phys. Rev. **D43** (1991) 3619.
[70] H. TANAKA, T. KANEKO and Y. SHIMIZU, Comp. Phys. Comm. **64** (1991) 149.
[71] T. MUTA, R. NAJIMA and S. WAKAIZUMI, Mod. Phys. Lett. **A1** (1986) 203;
G. BARBIELLINI et al. in [62].
[72] B. GRZADKOWSKI and Z. HIOKI, Phys. Lett. **B197** (1987) 213.
[73] A. AEPPLI and D. WYLER, Phys. Lett. **B262** (1991) 125.
[74] T. SACK, Ph. D. Thesis, Würzburg (1987).
[75] K. HAGIWARA and D. ZEPPENFELD, Phys. Lett. **B196** (1987) 97.
[76] B. GRZADKOWSKI, Z. HIOKI and J. H. KÜHN, Phys. Lett. **B205** (1988) 388;
Z. HIOKI, Nucl. Phys. **B316** (1989) 1.

[77] H. NEUFELD, J. D. STROUGHAIR and D. SCHILDKNECHT, Phys. Lett. **B198** (1987) 563;
K. HAGIWARA, R. D. PECCEI, D. ZEPPENFELD and K. HIKASA, Nucl. Phys. **B282** (1987) 253;
P. MERY, M. PEROTTET and F. RENARD, Z. Phys. **C36** (1987) 249.
[78] S. DITTMAIER, M. BÖHM and A. DENNER, Nucl. Phys. **B376** (1992) 29.
[79] C. AHN, B. W. LYNN, M. PESCIN and S. SELIPSKY, Nucl. Phys. **B309** (1988) 221.
[80] F. JEGERLEHNER, in "Radiative Corrections for e^+e^--collisions", ed. J. H. Kühn, Springer-Verlag, Berlin, Heidelberg (1989).
[81] T. SACK, private communication.
[82] A. DENNER and T. SACK, Z. Phys. **C45** (1990) 439.
[83] A. AEPPLI, private communication.